Flood hazard reduction by mangroves

Master Thesis

M.P.J. (Merijn) Janssen

Technische Universiteit Delft

TU Delft

Deltares
Enabling Delta Life

Flood hazard reduction by mangroves

Master Thesis

by

M.P.J. (Merijn) Janssen

to obtain the degree of Master of Science
at the Delft University of Technology,
to be defended publicly on Thursday October 6, 2016 at 1:00 PM.

Student number: 4091949

Thesis committee:		
	Prof. dr. ir. M.J.F. Stive	TU Delft, Chair of committee
	Dr. B.K. van Wesenbeeck	Deltares
	Dr. ir. J.T. Dijkstra	Deltares
	Dr. ir. B. Hofland	TU Delft
	Ir. V. Vuik	TU Delft

.

TU Delft

Deltares
Enabling Delta Life

Abstract

Although mangrove forests have proven to contribute to wave dissipation significantly, these ecosystem are threatened mainly by the expanding aquaculture. International or nationwide applied greenbelt policies are often used for the preservation of the mangroves and hence the flood hazard reduction, without taking local (hydrodynamic) conditions into account. Therefore this research developed insights in the mangrove forests' effect on waves and their contribution to flood hazard reduction as function of forest width. This is done by setting up a globally applicable tool for determining the governing storm wave and water level conditions at the seaward edge of the mangrove forest and the wave attenuation in the forest itself. In contrary to greenbelt policies, the developed method enables the option to locally review on required mangrove forest widths.

The application of the wave transformation model SWAN-2D with offshore global wave data from ERA-Interim significantly increased the prediction accuracy of nearshore wave conditions compared to the direct use of ERA-Interim. This holds mainly for the sheltered and shallow locations like embayments, estuaries and behind barrier islands, in which mangroves are located. For less sheltered and deep conditions, no improvement of the ERA-Interim data with the additional use of SWAN was observed.

The attenuation in the forest depends on the highly varying physical characteristics of dimensions of the mangrove trees. The large variabilities were included in several vegetation sets, prior to their implementation into a 1D stationary XBeach model. From a comparison with wave height measurements, three characteristic mangrove species were selected. By combining these species, typical coastal interspecific patterns were composed, representing a young dense and an old sparse forest. In addition, bathymetric and hydrodynamic conditions, which are common for mangrove forests, were imposed to the model. It appeared that a 100 m dense forest is potentially able to dissipate waves to acceptable levels, while sparser forests might need 450-900 m. The model also indicated that the effect of landward deforestation on a sloped profile results in a higher wave exposure for the area behind a forest than seaward erosion, although it does not take the effect of breaking and uprooting of trees into account.

The method to determine the required forest and evaluate on maintained greenbelt policies was tested on three case study locations, which differ in hydrodynamic conditions and forest characteristics. The policies appeared to result in different levels of hazard for the hinterland, underlining the great uncertainty of acceptable mangrove buffer zones for coastal zone management. The application of global (open source) data, SWAN-2D and XBeach-1D provides the set-up of a (quick) hazard assessment tool. The inclusion of local conditions improved the prediction ability compared to the conservative use of greenbelt policies.

***Keywords**: mangroves, forest width, global application, wave attenuation, hazard reduction, SWAN, XBeach, greenbelt policies*

Preface

This thesis symbolises the final milestone to complete the MSc programme Hydraulic Engineering at the University of Technology Delft. The research has been conducted at Deltares in Delft.

Although I unfortunately have never been able to observe mangroves in real life, this thesis really encouraged my interest in these trees. I am convinced that these ecosystems, if properly maintained, are beneficial solutions for the reduction of flood hazards. With this research, I hope to have contributed to the recognition of the values of mangroves. During my internship I received a lot of support from everyone who stood beside me during the process and I would like to thank all of you, without whom I could not have accomplished this thesis. Your help has been of vital essence.

First of all, I want to thank my thesis committee for their guidance and patience during the coarse of this project. I would like to show my gratitude towards the Chair of my committee, Marcel Stive. For the arrangement before my internship and help scoping this research, I would like to thank Bregje van Wesenbeeck. Furthermore, credits to Jasper Dijkstra who often scheduled time for helping me determining the right direction. I want to thank Bas Hofland for his positive and constructive feedback during the meetings and Vincent Vuik for sharing his knowledge and experience. Finally, thanks to my family and friends I have been able to successfully finalize this research.

M.P.J. (Merijn) Janssen
Delft, October 2016

Summary

Coastal mangrove ecosystems are found in (sub-)tropical, saline, tide-dominated areas. Besides their beneficial role in erosion prevention, carbon sequestration and provision of shelter for a diversity of animals, mangroves have proven to reduce wave heights. Despite that their wave reductive qualities are acknowledged, a quantitative description of the wave height reduction in a mangrove forest is yet lacking. Several governments maintain a greenbelt policy in order to prevent (further) mangrove deforestation and provision of safety for the hinterland. This policy is often assumed to be similar for different mangrove vegetated foreshores, without taking the various local conditions into account. In addition, the knowledge concerning wave propagation into mangrove forests is insufficient due to the trees' large differences in characteristics. A better understanding of the reductive effect of mangrove forests and consequently the required forest width for flood hazard reduction could seriously contribute to the preservation or even realization of mangrove ecosystems. Hence this research has focussed on developing a method for determining the required mangrove forest width under a broad range of (hydraulic) conditions. The method distinguishes an area in front of a mangrove forest, in the forest itself and behind it. In the first zone, the hydrodynamic conditions which are representative for mangrove areas have been determined. Subsequently the attenuation of the forest was quantified and finally an indication for flood hazard has been given.

Mangroves are often located in headland bays, estuaries and behind barrier islands, because the wave conditions in these areas are relatively mild. The extreme storm situations are more relevant for hazard indications. Due to the universal applicability of the method, global wave, water level and bathymetry datasets were used. ERA-Interim provided the wave and wind data on offshore locations in this research. Based on a validation with wave buoys, it appeared that ERA-Interim is unable to accurately represent the nearshore positions in embayments, estuaries and other sheltered positions, while it can be used for deep and exposed locations. Hence, the wave transformation model SWAN was used in combination with ERA-Interim to describe the representative storm conditions at the front edges of mangrove forests. The model significantly improved the wave height and wave period estimations compared to the direct use of ERA-Interim. This validation enabled the option to quantify the wave conditions for hazard estimations in mangrove areas, but can also be applied for engineering practises in data scarce areas. The downside of using ERA-Interim is that it might underestimate the conditions during a tropical cyclone and hence the hazard an area is exposed to. Finally, a simple depth-induced breaking criterion appeared to be unable to represent the nearshore conditions accurately.

Subsequently the wave attenuation in a mangrove forest under different conditions was modelled. According to the vegetation model implementation, the required parameters are the density, diameter, vegetation height and drag coefficient. The large variability in these values and their appearances in the coastal zone were inventoried first. By using various sources, relations between the physical parameters and an empirical relation between drag coefficient, hydrodynamics and density, multiple mangrove vegetation sets were found. Subsequently the wave height was simulated using the found sets and compared with wave height measurements. It appeared that the range in wave attenuation between the different sets was too large. Hence, the mangrove sets were limited to three, which are characterized by root type. These are young dense pioneer trees, well-grown stilt rooted mangroves (Red) and low aerial pencil-shaped rooted mangroves (Black).

By combining the three species, two distinctive forest types were composed. The first modelled forest type is represented by well-grown and large trees, which are often found in Indo-Pacific regions. This category is characterized by Black mangroves at the seaward front and Red mangroves at the back of the forest. The zonation of the trees was considered to be a function of the tidal range, because the mangroves are often found between low and high tide due to their capability to deal with saline and submerged conditions. The other forest type, populated with young pioneer trees in the front and Red mangroves in the back forest, is considered to be very efficient in wave height reduction.

XBeach in stationary mode was the used hydrodynamic numerical model to simulate the wave attenuation in the different forest types, because of its vegetation option and similarities with previous conducted mangrove studies. The forest category appeared to highly influence the wave height reduction. A 100 m dense forest might already be able to reduce wave heights to safe levels, while sparser forests need 450-900 m. Furthermore, a milder slope, higher depth and larger incoming wave height resulted in a larger required forest width. This required forest width is defined as the cross-sectional length of mangroves, which is capable to reduce wave heights to 0.2 m. This is based on the assumption that such waves are able to inflict damage to low-quality walls and houses. Additionally, the effect of a seaward and a landward loss of forest were investigated, which can be related with erosion and deforestation for agriculture and/or aquaculture purposes respectively. The landward loss of forest appeared to result in a higher significant wave height than the seaward loss of forest. However, the model does not take potential damage of trees and consequentially the reduced capability to attenuate waves into account. Therefore it is recommended to improve the model with breaking and uprooting of mangrove trees.

In order to evaluate the combination of ERA-Interim, SWAN and XBeach to come up with the eventual hazard reduction in terms of wave attenuation, the method was applied at three mutually distinctive locations. A case study location in Thailand, in which a large part of the economy relies on the fish industry, is characterized by a wide and well-developed mangrove forest. Good bathymetric data is available, but the ERA-Interim wave database might underestimate the extreme tropical cyclone conditions in the area. This can be the reason that the waves for different storm return periods did not vary significantly. The simulated required forest width ranges between 130-200 m, although it is stated that the wave attenuation is directly related to the limited depth in the area, implying that the reduction is not solely influenced by the mangroves. In case a greenbelt policy of 100 is maintained, allowing the shrimp farms and fish industry to expand at the expense of the mangrove forest, the flood hazard is considered to be too high. A policy which states that the required forest width depends on the present tidal range in the area, might provide sufficient protection for the Thai study location, because it would coincide with a forest width of 400 m.

The second location, a headland bay in Indonesia, differs with the first case study in terms of a smaller but younger forest and a city (Singkawang) directly located behind the forest. According to the model, a one-in-hundred year storm can inflict damage to the city, because insufficient mangroves are in place for protection. The effect of a 100 m long eroding coastline was simulated at this location. It appeared that the disappearance of the very dissipative front mangroves can result in almost 0.4 m high waves in the city of Singkawang.

Finally a location in the Philippines was studied. This country is known to be the most exposed to tropical storms. Hence the extreme wave and water level conditions are large in the area (San Miguel Bay). Despite a 450 m wide forest, the wave conditions during a one-in-ten and one-in-hundred year storm are too large to be dissipated to save levels at the considered location. The greenbelt policies maintained in the Philippines are very low, namely 50-100 m for mangroves facing open sea. This would result in 0.8 to 1.1 m high waves directly behind the forest in case of a one-in-hundred year storm.

The large range in required forests width underlines the great uncertainty of acceptable mangrove buffer zones for coastal management. Only a few greenbelt policies appeared to provide sufficient protection against waves. This is based on the SWAN and XBeach models, the assumptions made considering the bathymetry in a forest and the safely considered wave height of 0.2 m. The developed method of using global (open source) data, SWAN and XBeach seemed to be a viable solution for determining forest widths rather than conservative greenbelt policies. The procedure can be used as a (relatively) quick assessment tool to calculate flood hazard reduction by mangroves. The summarized observations and recommendations for further work are illustrated in Figure 1.

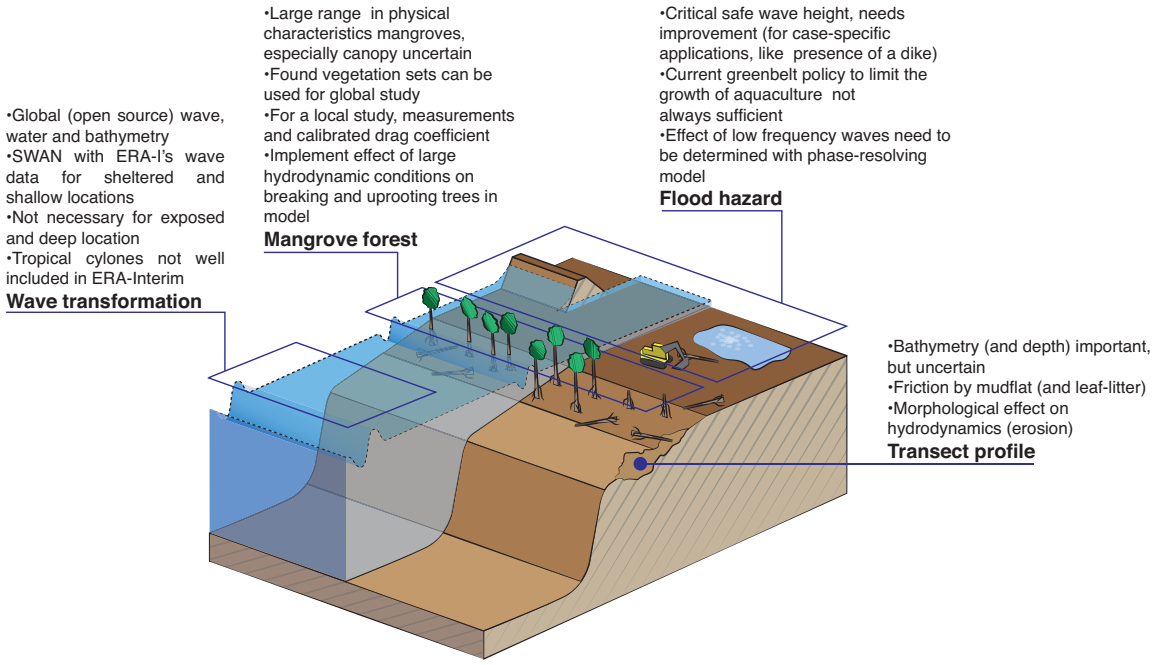

Figure 1: Most important methods, observations and recommendations

List of Figures

List of Tables

Contents

Nomenclature

Abbreviations

DIB	Depth-Induced Breaking
DIVA	Dynamic Interactive Vulnerability Assessment
ERA	European Centre for Medium-range Weather Forecasts (ECMWF) Re-Analysis
EVA	Extreme Value Analysis
FT	Forest Type
GEBCO	General Bathymetric Chart of the Ocean
GLOSSIS	Global Storm Surge System
GTSR	Global Tide and Surge Reanalysis
MSL	Mean Sea Level
ORCA	Ocean data tRansformation Classification and Analysis
POT	Peak-Over-Threshold
RP	Return Period
SRTM	Shuttle Radar Topography Mission
SWAN	Simulating WAves Nearshore
TC	Tropical Cyclone

Symbols

a	Stroke of orbital motion	(m)
α	Relative vegetation height	(-)
A	Wave action	(J Hz^{-1})
A_p	Projected surface area mangroves	(m^2)
b_v	Vegetation diameter of stem or root	(m)
BM_{fac}	Biomass factor	(-)
B_w	Forest width	(m)
$B_{w,f}$	Front forest width	(m)
$B_{w,gb}$	Green belt width	(m)
$B_{w,req}$	Required forest width	(m)
c_g	Group wave velocity	(m s^{-1})
C_D	Drag coefficient	(-)
$\tilde{C}_D$	Bulk drag coefficient	(-)
γ	Breaking parameter	(-)
D_w	Dissipation by wave breaking	(J)
D_f	Dissipation by bottom friction	(J)
D_v	Dissipation by vegetation	(J)
Δh	Surge height	(m)
ε_v	Time-averaged energy dissipation rate by vegetation	(J s^{-1} m^{-1})
F	Horizontal force component acting on vegetation	(N m^{-3})
f_w	Johnson friction factor	(-)
g	Gravitational acceleration	(m s^{-2})
h	Water depth	(m)
h_0	Water depth at x=0	(m)
h_v	Vegetation height	(m)
H_0	Significant wave height at x=0	(m)
H_1	Wave height seaward edge of mangrove forest	(m)
H_2	Wave height landward edge of mangrove forest	(m)
H_{max}	Maximum shallow water wave height	(m)
H_{rms}	Root-mean-square wave height	(m)

i	Vegetation layer number	(-)
i_b	Bed slope	(-)
k	Wave number	(rad m^{-1})
KC	Keulegan-Carpenter number	(-)
KC_M	Keulegan-Carpenter number with Mazda length scale	(-)
L	Wave length	(m)
L_e	Mazda length scale	(m)
L_t	Transect length	(m)
MWD	Mean Wave Direction	(°N)
$MWiD$	Mean Wind Direction	(°N)
n	Number of vegetation layers	(-)
N	Vegetation density	(m^{-2})
PWD	Peak Wave Direction	(°N)
$RMSE$	Root Mean Square Error (for wave height or period)	(m) or (s)
ρ	Water density	(kg m^{-3})
S	Distance between (vegetation) cylinders	(m)
S_j	Scaling factor tropical cyclone for parameter j	(-)
T	Wave period	(s)
T_p	Peak wave period	(s)
T_{m02}	Mean zero crossing wave period	(s)
TR	Tidal range	(m)
σ	Wave frequency	(rad s^{-1})
u	Horizontal velocity	(m s^{-1})
$\hat{u}$	Wave orbital velocity	(m s^{-1})
V	Control volume	(m^3)
V_m	Control volume mangroves	(m^3)
V_{fac}	Vegetation factor	(m^{-1})
WS	Wind speed	(m s^{-1})
x	Position in transect	(m)
z	Position above the bed	(m+MSL)

1

Introduction

1.1. Problem description

Mangroves are tidal forest ecosystems, populating the low-latitude coastlines, where a tropical or sub-tropical climate is present (Figure 1.1). Because of their salt tolerant trees and shrubs, mangrove ecosystems are able to thrive in sheltered intertidal areas, where a subtle combination of salt sea water and fresh river water is present. More than 68 species are known, which are often distinguished by their root system (Kauffman and Donato, 2012). The mangrove ecosystem is unfortunately highly threatened. Already one third of the world's mangrove population disappeared the past 50 years for aqua or agricultural purposes (Alongi, 2002), despite their many beneficial features.

Figure 1.1: Global distribution of mangroves (Giri et al., 2011)

Mangroves have proven to play an important role in flood defence by dissipating wave energy (Kathiresan and Rajendran, 2005; Mazda et al., 1997a). Their system of aboveground roots and trunks are able to reduce wave heights and tidal currents. Additionally, the roots are capable of reducing erosion rates. Next to these physical benefits, mangroves provide the habitat for different species of insects, birds, fish, reptiles and mammals. Finally, mangroves have shown to have high rates of carbon sequestration due to their large aboveground biomass and productivity, contributing to less atmospheric CO_2 (Hutchison et al., 2014).

The developing countries whose foreshores are vegetated by mangroves, are prone to flooding due to a lack of resilient measures and frequently occurring tropical storms. Instead of or in addition to applying 'hard' measures as dams or dikes, people in the mentioned areas can also preserve, restore or plant mangroves. This would not only increase the safety, but also the biodiversity and ecological value of the area. Additionally, erosion rates of coasts are likely to reduce. Finally, flood defence by vegetation requires low initial and maintenance cost, because they are able to grow if the right conditions are met.

Numerous studies conclude that mangroves do contribute to wave attenuation. The measurements conducted in these studies include different locations, differing the hydrodynamic conditions and mangrove species between them (Bao, 2011; Brinkman, 2006; Horstman et al., 2014; Mazda et al., 1997a, 2006; Quartel et al., 2007). Therefore there is not a one-to-one relation for input parameters for the quantitative description of wave reduction by mangroves. However, Mendez and Losada (2004) presented a general formulation of waves over a vegetation field, which is also applicable for mangrove trees. Yet the behaviour of this model for the variable mangrove parameters is uncertain. Due to this lack of qualitative knowledge of wave reduction by mangroves, governments often maintain an international or national imposed greenbelt policy. This implies that a certain generalised width of mangroves provides sufficient protection at various coastal locations, while this policy lacks background theory and is not adapted to local conditions.

1.2. Research objective

A better understanding of the reductive effect of mangroves on hydrodynamic conditions could seriously contribute to the preservation or even the realization of mangrove ecosystems, suppressing costs and improving ecological value and safety. A tool, often used in engineering practise, to indicate the effectiveness of certain flood reductive defences, is risk. Flood risk estimations can serve in the determination of optimal solutions for defensive measures.

Risk: combination of the consequences of an event and the associated likelihood/probability of its occurrence (ISO, 2009).

Hazard: a dangerous phenomenon, substance, human activity or condition that may cause loss of life, injury or other health impacts, property damage, loss of livelihoods and services, social and economic disruption, or environmental damage. *Comment: In technical settings, hazards are described quantitatively by the likely frequency of occurrence of different intensities for different areas, as determined from historical data or scientific analysis.* (UNISDR, 2009)

Risk is often confused with hazard in case these terms are used in different backgrounds. Hazard is the source, whereas risk gives the likelihood of the damaging effect of this source. An area can be exposed to a hazard, but is not necessarily at risk if resilient measures are in place. A correct quantified risk assessment requires locally accurate data of failure probabilities and damage value estimations, which is not always available for the concerned countries, making a risk assessment difficult to perform. Therefore the estimation of the effectiveness of mangroves in this research is presented as hazard reduction. This estimation can potentially serve as a safety policy tool for the countries in which these policies are often absent or not well adapted to local conditions. Next to that, insights are gained into the wave attenuation qualities of mangroves. Accordingly, the main research question in this thesis is defined as:

"How wide should mangrove areas be to contribute to flood hazard reduction under diverging boundary conditions?"

The acquisition of hazard reduction requires several steps to be taken, illustrated in Figure 1.2. At first the nearshore wave and water level conditions need to be determined (area I), because these dictate the initial level of hazard. The waves subsequently propagate into the mangrove forest (area II), resulting in wave height reduction (area III). Finally, the resulting wave conditions cause a certain risk of flooding (area IV). As stated, the translation to risk depends on local conditions, which are not always available. Hence and due to the global focus in this study, the risk quantification in area IV is outside the scope of this research. Additionally, no water level reduction by mangroves is taken into account. Partly because the effect is negligible under the many made assumptions and due to the focus on purely wave attenuation. The same holds for morphodynamics, which is not included in this study either.

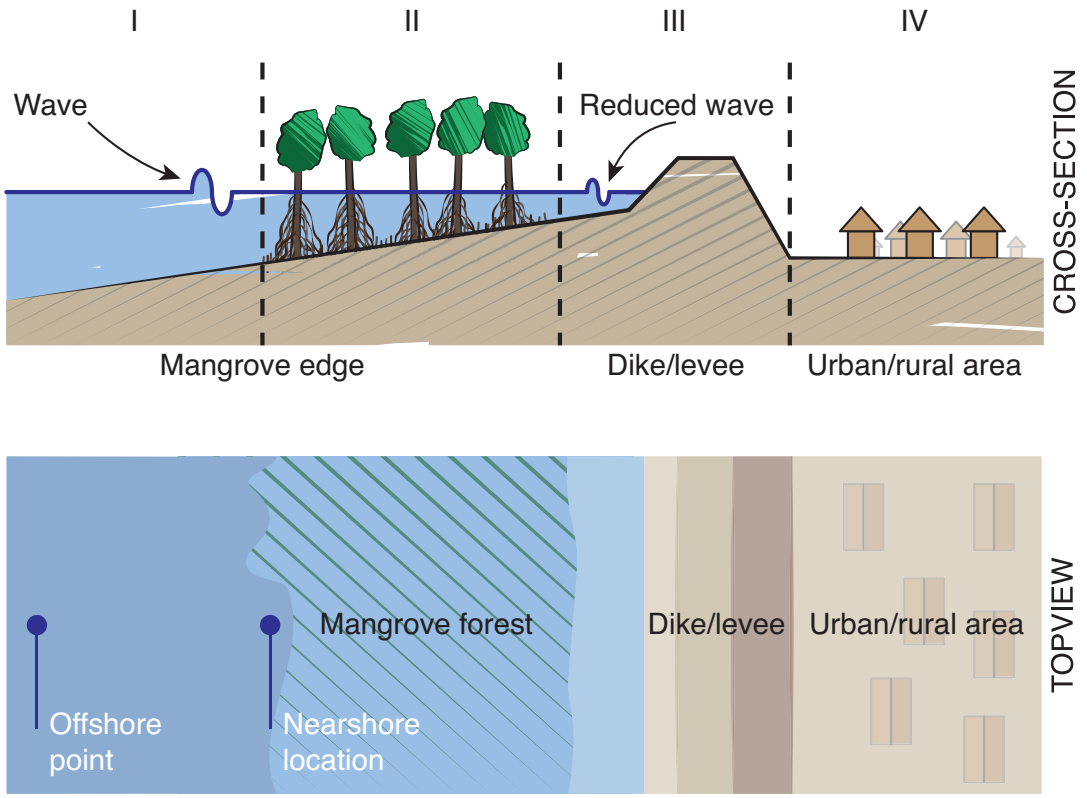

Figure 1.2: Mangrove vegetated foreshore, divided into areas, which represent the steps to be taken for hazard assessment.

Based on the distinct areas, the following sub-questions are presented:

Area I How can global representative hydrodynamic conditions for mangrove areas be determined?
Area II: What is the magnitude of wave related mangrove parameters, are there relations between them and what is their influence on wave attenuation?
Area III: How does the mangrove forest, as function of its width, contribute to flood hazard reduction?

1.3. Methodology

Each area is characterized by its occurring distinctive processes. In the first, most offshore zone, the water level and wave conditions are determined. These are extreme conditions, due to the focus on flood hazard, at the seaward edge of a mangrove forest. In the interest of a global applicable model, also global wave and water level databases are used (Figure 1.3). Due to the combination of offshore output of these databases and the significance of representing nearshore conditions, a wave transformation procedure is applied. The method, validated for several locations, transforms offshore extreme conditions to the representative conditions at a mangrove forest boundary (see topview in Figure 1.2).

The current predictions on wave height reduction in a mangrove forest (area II) are highly uncertain and hence this needs improvement. The high level of unpredictability is mainly due to the mangrove's large variability in physical characteristics. Accordingly, a mangrove analysis on its physical (density, diameter, height) and wave force related (drag coefficient) parameters is performed. The resulting mangrove vegetation sets are reviewed and subsequently applied in the flood hazard model. Additionally, the model's sensitivity for diverging parameters is tested in order to understand its behaviour on wave height reduction.

After obtaining knowledge concerning hydrodynamics and wave attenuation by mangroves, the results are used to indicate the level of flood hazard reduction. This is expressed as function of mangrove forest width. Namely, a larger 'greenbelt zone' results in more dissipation and hence hazard reduction. Finally, the effect of deforestation at the landward edge and erosion at the seaward edge, on flood hazard are reviewed. The method of obtaining nearshore wave conditions and wave attenuation in the forest is finally applied at three case study locations. Also the effect of forest loss elaborated at these locations.

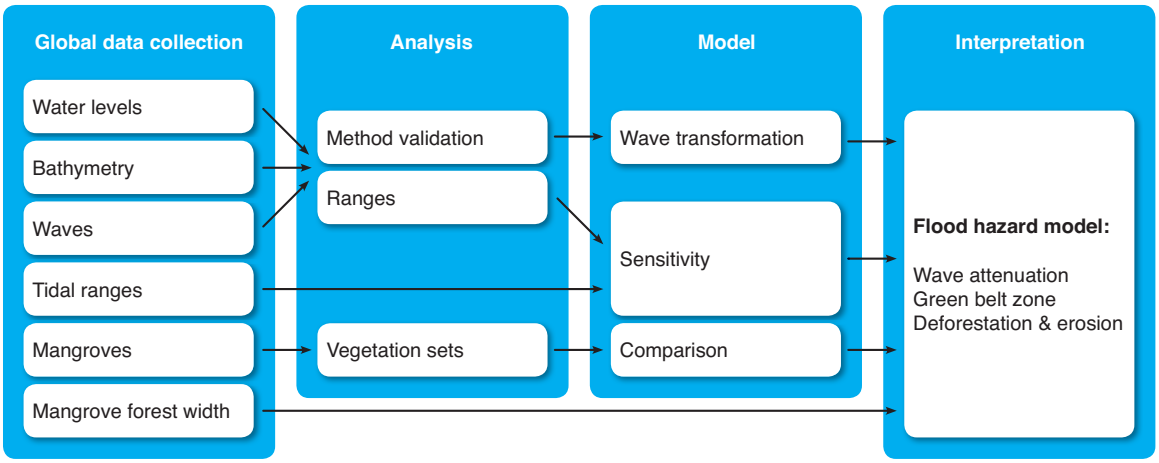

Figure 1.3: Research methodology

1.4. Report outline

The global applicability of the wave attenuation model requires additional information about mangroves, hydrodynamics and vegetation studies, which are presented in Chapter 2. Thereafter, this collected global data has been analysed. For the representative hydrodynamic conditions, this means a validation of a wave transformation method (Chapter 3). The wave related properties of mangroves have been reviewed to eventually come up with representative vegetation sets, which have been used in the flood hazard model. This is presented in Chapter 4. Subsequently, these values and other model settings have been compared with measurements in Chapter 5, in which also the sensitivity of water levels, bathymetry (slope), wave height and tidal ranges has been analysed. Additionally, the initial set-up of the flood hazard model is presented in this chapter. Whether the method of wave transformation and attenuation due to mangroves is globally applicable has been tested in Chapter 6. Finally, the discussion and conclusions are presented in Chapters 7 and 8.

2

Literature review

Due to the mangrove's many benefits, numerous studies have been conducted regarding their diverging features. These studies vary from relating mangroves with attenuation to linking biological and hydrodynamic conditions with the mangrove dominance along a coast. Namely, the adaptations of mangroves to (a)biotic conditions, dictates their coastal position, root structure and therefore the capability of reducing wave heights. Hence, the different types of mangroves, their zonation and current mangrove policies are reviewed. Due to the strong dependency of the waves and water levels on attenuation, an introduction to the global hydrodynamic databases is subsequently given. Finally, the conducted studies and simulated models on wave attenuation by vegetation (mainly mangroves) is elaborated.

2.1. Mangroves

Mangroves refer to tree structures typically found in saline coastal environments in the tropics and subtropics, primarily between 25° north and 25° south. The conditions for the mangroves to grow in, seem to meet in Asia (42%), Africa (20%) and North and Central America (15%) according to Table 2.1.

Table 2.1: The 15 most mangrove-rich countries (Giri et al., 2011)

Country	Area (ha)	Global (%)	Cumulative (%)	Region
Indonesia	3,112,989	22.6	22.6	Asia
Australia	977,975	7.1	29.7	Oceania
Brazil	962,683	7	36.7	South America
Mexico	741,917	5.4	42.1	North and Central America
Nigeria	653,669	4.7	46.8	Africa
Malaysia	505,386	3.7	50.5	Asia
Myanmar (Burma)	494,584	3.6	54.1	Asia
Papua New Guinea	480,121	3.5	57.6	Oceania
Bangladesh	436,570	3.2	60.8	Asia
Cuba	421,538	3.1	63.9	North and Central America
India	368,276	2.7	66.6	Asia
Guinea Bissau	338,652	2.5	69.1	Africa
Mozambique	318,851	2.3	71.4	Africa
Madagascar	278,078	2	73.4	Africa
Philippines	263,137	1.9	75.3	Asia

The mangroves are able to populate these areas, because they adapted to the present abiotic, i.e. non-living conditions:

- **Temperature**. By orienting its leaves to reduce excessive sunlight and heat. Next to that, these leaves are able to grow tiny hairs to reflect sunlight or produce pigments to absorb it. Mangroves grow the best under high temperatures, which is the reason they are exclusively found in the (sub-)tropics.
- **Salinity**. Excessive salt concentrations reduce the vitality and growing process of a plant. The mangrove copes with this by developing salt-excreting leaves and/or excluding salt during the intake of water as a result of saltproof membranes on the roots. (Tomlinson, 1986)
- The **tide** causes the submergence of the soil and its pores twice a day. Plant roots are not able to extract oxygen, when these pores are filled with water instead of air. The important processes in the plant shift from aerobic to anaerobic, i.e. without oxygen, which is accompanied with the production of toxins. Mangroves are able to grow aerial roots, allowing the trees to extract oxygen even during submerged conditions.
- **Nutrients** are crucial for the growing process of the plants. Trees can grow less roots in case of lacking nutrients. Hence, larger and thicker trees are found near nutrient-rich areas.

Due to the difficulties for competitive plants to thrive in saline, tide-dominated environments, the mangroves have a strategic advantage in occupying these coastal areas. Mainly the roots are responsible for this areal dominance. These roots have proven to be very efficient in reducing wave heights and (tidal) currents. The amount of roots, their strength and their complex common structure makes the mangrove a good dissipator of wave energy. Also the canopy can contribute to the attenuation if it is sufficiently submerged (Mazda et al., 2006). Next to that, sediments in mangrove areas have the tendency to settle during slack water, giving the mangroves the feature of accretion enhancing. Additionally, mangroves are an excellent habitat for different kind of animals, which increases the biodiversity in these ecosystems. On a global scale, they have a large part in the sequestration of carbon dioxide due to their large biomass.

2.1.1. Types

There is a large diversity in mangrove types, often divided into three dominant categories: the Red, Black and White types. They among others differ in chemical composition, like the carbon and chlorofyll content, and appearance of roots and leaves. The main parts of the mangrove are classified as roots, stem and canopy.

Red mangroves or Rhizophora mangle can be distinguished by its long prop roots. These roots originate from the trunk, diverging in many roots towards the bottom (Figure 2.1 left). The dimensions of these prop roots vary with tidal range, type and height of the mangrove tree. They enable both the stability of the tree and the exposure to oxygen. Next to that, they provide a great habitat for different kind of animals. The Red mangroves thrive in brackish water and swampy salt areas. They can be submerged for a long time, which determines their seaward position in the coastal zone and the length of their roots. The Red mangrove produces a sapling, called the propagule. These pencil shaped fruits can sprout roots right away or after it has been moved away due to the tide. The Rhizophora mucronata, Rhizophora apiculata, Bruguiera, Lumnitzera and Kandelia Kandel is considered to be in the same category as the Red mangrove due to their family classification or prop rooted structure (Table A.1).

The Black mangrove type, also identified as the Avicennia germinans, is characterized by its black vertical cone roots, also known as pneumatophores (Figure 2.1). These roots are able to trap oxygen, even in (partially) submerged conditions, in habitats that have a waterlogged soil. The Black mangrove is commonly found on the sandy and muddy shores that seawater reaches. It can reach heights of 15 to 20 m and often grow in isolated groups. In contrary to the Red mangrove, Black mangroves produces oval shaped seeds, which can also float for long periods prior to rooting. Sonneratia alba, Avicennia marina and Xylocarpus are in this research identified as the Black mangrove category due to their distinct pneumatophores.

The Laguncularia racemosa or White mangroves often dominates the higher coastal areas. It grows on land and is found in tidal areas, around lagoons and ponds. Depending on the tidal range and the surface elevation on which the White mangrove is located, this tree can grow both prop roots as pneumatophores.

Finally the pioneer trees are mentioned. Although these trees are often scaled to the Red mangroves, they are considered individually here. The reason is that their appearance significantly differs with a developed Red mangrove tree. Because these trees are mainly found at the seaward edges of a mangrove forest, they need to be able to resist the harshest conditions, resulting in a very dense root layer. These roots are underdeveloped in diameter, but can grow to considerable heights (Figure 2.1). The area of the canopy, stem diameter and root size increases when the tree grows. Concerning exposure to waves, the young trees are likely to uprooting while the older trees are vulnerable to breaking (Husrin et al., 2012).

Figure 2.1: Typical root structures mangroves: dense stilt roots of Red mangrove (left), pneumatophores of Black mangrove (middle) and young dense pioneer trees (right)

2.1.2. Zonation

The adaptations to (a)biotic conditions among mangroves itself are also diverse and therefore different mangroves dominate various coastal zones. Accordingly, patterns in coastal cross-sections in which certain species are likely to grow, often referred as zonation, are present. Similarly as in the mangrove dimensions, the variability in the zonation is large and depends on several factors. For the Indo-Pacific region, the Black mangrove is often dominant in both lowest and highest intertidal zones and rare or absent in the middle. This middle area is often dominated by Red mangroves.

The other, most occurring zonation, is where the young Red mangrove (pioneers) dominate the lower intertidal areas and Black mangroves covers higher grounds. This zonation is in agreement with the theory that stilt roots are able to resist the harshest conditions and pneumatophores can extract oxygen from the more inland muddy marshlands. However, also factors based on land building and plant succession, geomorphological processes, differential dispersal of propagules due to tidal action, differential predation of propagules, physiological specialization and interspecific competition influence the zonation of the mangrove forest, resulting in the large variation (Feller and Sitnik, 1996).

2.1.3. Greenbelt policies

The coastal zone is an area of basic, social, economic and public function. Space is claimed for the production of food, supply of water and energy, housing, transport and flood protection. The many needs of humans puts a large pressure on the subtle ecosystem conditions in which mangroves thrive. Namely, agriculture and economy often develops at the expense of mangrove forests in the countries where proper spatial coastal zone management is lacking. The influence of these functions can negatively influence the mangrove forests widths.

Most common example of mangrove deforestation is for the purposes of the aquaculture industry. The rapidly expanding shrimp farms and fish ponds poses a large treat to the mangroves. The mangrove areas are perfect for transforming into shrimp farms, because shrimps thrive the early stages of their lives in mangroves. The use of antibiotics in shrimps causes the ponds to be abandoned after the water becomes too toxic. Thereafter, more mangrove areas are deforested for new shrimp farms.

Based on the abovementioned functions, mangrove areas can be designated into four zones (Primavera, 2005):

1. Preservation for coastal protection, biodiversity and ecotourism
2. Sustained yield of forestry and fisheries products
3. Conversion to aquaculture, salt beds and other uses
4. Rehabilitation or reforestation

The area preserved for the protection of coastal hinterland are also called greenbelt zones. The policy behind these zones differs for the countries which maintain such greenbelt policies. Indonesia maintained from 1984 to 1990 a width of 200 m, with a minimum of 100 m (Brown et al., 2007). This provided a nation-wide guideline, but was also applied in other countries. In 'Presidential Decree 32' (1990), this greenbelt width $B_{w,gb}$ was adjusted based on an ecological study to (Soerianegara, 1986) and considered to be a fucntion of the tidal range TR:

$$B_{w,gb} = 130 \cdot TR \tag{2.1}$$

For typical tidal ranges in Indonesia, this means that buffer zones of 200-550 m should be applied. In the Philippines and many other South-East Asian countries a buffer zone of 50-100 m coastal mangroves is considered to be sufficient.

Spalding et al. (2014) provided a guideline for coastal protection in mangrove areas. Besides flood hazard by waves, also tsunami impact, erosion and sea-level rise are mentioned as potential risks for coastal areas and the potential added value of mangroves in reducing these risks. As guidance it is stated that a dense forest is already able to reduce wave heights to half its initial height in 100 m forest. For sparse forests a 500 m belt width to reduce the initial wave height twice, is recommended in these guidelines. Although this is not considered to be an official greenbelt policy, coastal engineers might use these criteria as guidance.

2.2. Hydrodynamics

Mangroves are often located in the more sheltered areas, where roots and stems are able to grow in mild wave conditions. The daily recurring rising water of salt water regulates the habitat for mangroves, resulting in the distinct roots. On the other hand determines less mild conditions, i.e. storm, typhoon or cyclone, the governing situation for flood hazard.

Due to the global character of this research, this section includes the different global hydrodynamic sources for both waves as surges. Additionally, hydrodynamic numerical models are presented. Finally, the phenomenon of tropical cyclones (TC's) is briefly introduced.

2.2.1. DIVA

The need for consistent national- to global scale assessment of potential impacts on coastal zones accelerated through the 21st century due to rise of sea level. The lack of available data in terms of resolution, coverage, parameter availability and outdated sources led to the DINAS-COAST project, which developed the Dynamic Interactive Vulnerability Assessment (DIVA) database. This global coastal database was founded to address the needs of vulnerability assessment of coastal zones. It enables users to analyse mitigation and adaptation policies by presenting a range of coastal and socio-economic scenarios at different scales (Vafeidis et al., 2008). The data in DIVA is expressed into linear coastal segments, which differs from other common raster based data structures. This linear decomposition of the world's coastline has been based on physical, administrative and socio-economic criteria. This resulted in 12,148 coastal segments, representing homogeneous units based on the impact and vulnerability to sea-level rise (Hinkel and Klein, 2009).

Different research institutes and universities are working on supporting policy tools for governmental agencies, industry consultants, NGO's and citizens to assess the effectiveness of (vegetated) foreshores in reducing floods and erosion[1,2]. Afar offshore wave data (Section 2.2) is currently projected on DIVA segments in such tools in order to describe nearshore conditions.

2.2.2. ERA-Interim

Comparable with DIVA, the need for data increased substantially, because of the growing awareness of vulnerability of coastal zones. Around the same time numerical models improved and data sets were extended. The European Centre for Medium-Range Weather Forecasts (ECMWF), a research institute, produces numerical weather predictions and provides forecast data that can be purchased by businesses and commercial customers worldwide. Data is assimilated from satellites, numerical models provide weather forecasts and global data sets, describing recent history of atmosphere, land and oceans, are created. ERA-Interim (ERA-I) is one of the data atmospheric reanalysis projects of ECMWF. It calculates wave and wind characteristics based on a wave prediction model with a global grid resolution of $0.75 \times 0.75^{\circ}$ and a time interval of 6 hours (Komen et al., 1996). This means that the resolution in kilometres differs between various global locations.

Shanas and Kumar (2015) analysed the ERA-Interim data from 1979 till 2012 for the Bay of Bengal and concluded that for high waves ERA-I under-predicts measured buoy data with 15%. They also found that the highest waves (significant wave height>5 m) are caused by tropical cyclones (TC). Kumar and Naseef (2015) compared the significant wave height of a buoy during a TC with the ERA-I data and found an underestimation of 33% by ERA-I, caused by the the low resolution of the ERA-I grid. Caires et al. (2006) conducted an analysis of nearshore locations by using the ERA-40 data, the atmospheric model predecessor of ERA-Interim. The wind data in the research is assumed to underestimate 10% from the actual wind data, without giving a reasoned argumentation for that. The analysis was conducted to describe nearshore wave conditions accurately, because ERA-40 was unable to give sufficient accuracy. Muis et al. (2007) confirmed that ERA-I is unable to represent TC's properly by comparing model outputted surge levels using ERA-I as input, with 260 tide gauge stations (see also Section 2.2.5.

[1] The Foreshore Assessment using Space Technology project: http://fast.openearth.eu/
[2] Coastal Hazard Wheel (Appelquist and Halsnæs, 2015):http://chw.openearth.eu/

The use of global databases to represent wave conditions is apparently at the expense of the accuracy. Although there is also some imprecision in ERA-I for non-storm conditions, its result is considered to be usable in this research, partly because ERA-I has similarities with previous conducted studies (Section 2.2.1). Additionally, the uncertainty with respect to mangrove variability is rather low. Downside of ERA-I is its incapability to properly describe tropical cyclones due to its large grid size. In TC susceptible areas, this have to be kept in mind. Next to that, the database is unable to represent nearshore conditions accurately. However, these conditions matter the most for determining wave attenuation by mangroves.

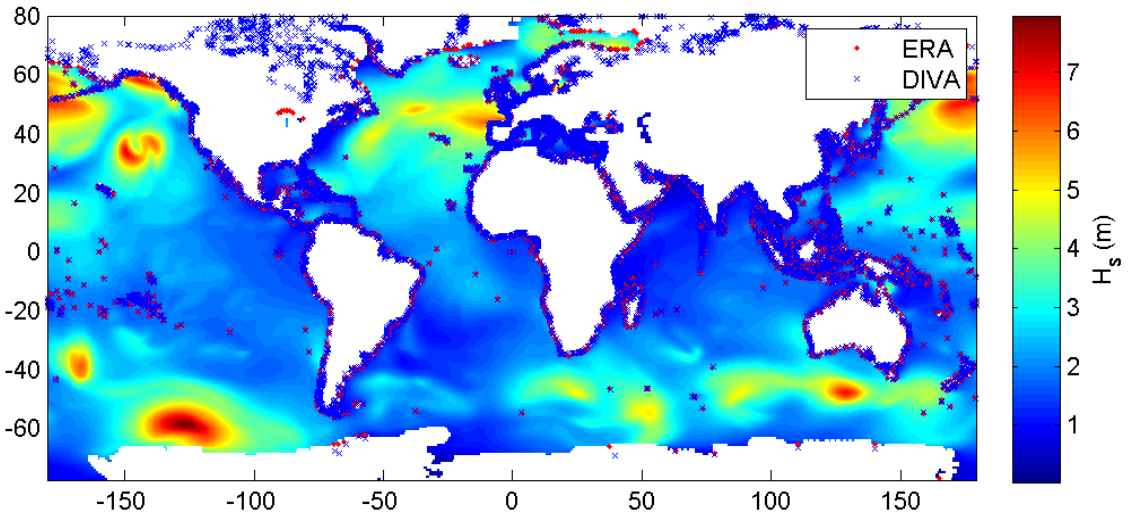

Figure 2.2: Global ERA dataset for the year 1979. Blue crosses are DIVA segments and red dots are their nearest ERA points.

2.2.3. SWAN

As mentioned above, the ERA-I still has some inaccuracies concerning wind and wave data. Especially in the more sheltered areas as headland bays, estuaries and basins behind barrier islands, ERA-I probably provides insufficient accuracy to describe the governing wave conditions accurately. The magnitude of nearshore wave parameters is of importance for engineering purposes, like constructing sea defences or land acquisition. The description of offshore wave data towards more nearshore areas of interest is a regularly conducted exercise in these type of branches. A numerical model which can transform this offshore data towards coastal locations is SWAN (Simulating Waves Nearshore). This third-generation spectral wave model, accounts for among others wave propagation in time and space, shoaling, refraction, wave generation by wind, whitecapping, bottom friction and depth-induced breaking (Booij et al., 2004). SWAN is able to run stationary, in which the wave statistical properties do not change in time, and a non-stationary mode. The former is useful when simulating fixed sets of extreme values (Caires et al., 2006). In contrary, the non-stationairy mode can be used to produce a time series of nearshore wave parameters (Booij et al., 2004).

Caires et al. (2006) reviewed on a situation in the North Sea (Netherlands) concerning the applicability of SWAN with ERA-40 data to describe locations along the coast by comparing it with wave buoy data. Initially, a storm in non-stationary mode was simulated and calibrated by adjusting model properties and ERA-I data. An increase of the ERA-I wind data and a modification of the directional spreading of the waves influenced the model the most. Subsequently, the model adjustments were used to run a 44 year non-stationary model and a stationary run by using fixed sets of wave conditions related to its representative storm return period. The latter means that an extreme value analysis (EVA) was conducted for the wave boundary conditions and thereafter applied on the SWAN model. The EVA for the non-stationary run was executed for the nearshore conditions, after they had been transformed by SWAN. The stationary approach is conservative when compared with the non-stationary, but has a significant smaller computation time.

2.2.4. ORCA

In long-term statistics the conditions are not stationary and therefore different to describe in comparison with short-term statistics, which are based on a stationary period of a few minutes (Holthuijsen, 2010). An EVA provides a solution for obtaining representative wave conditions. This is usually limited to significant wave height and its return period (RP), e.g. a 100-yr significant wave height. The most important condition for an EVA is that the values, storm events in this case, need to be statistically independent. They also need to be identically distributed, implying that each value should be from the same population (Caires and van Os, 2012). This might include that sea and swell waves have to be separated. The most applied method of EVA is the peak-over-threshold method (POT). A certain wave height in a POT is considered to be generated by a storm, if this value exceeds a threshold value.

The POT option in the ORCA tool is used in Caires et al. (2006). ORCA (met Ocean data t Ransformation Classification and Analysis) is used for the analysis, classification and transformation of metocean data. In the POT analysis a threshold value is determined first and subsequently the peaks over this threshold are used to determine the relation between RP and significant wave height. Representative wave period, wave direction and wind variables can be found by formulating relations between wave heights and these respective parameters.

2.2.5. Water levels

The water levels in this research are important for several reasons. First, the daily rising and falling water determines the zonation of mangroves (Section 2.1.2). Hence are larger tidal ranges often related with larger mangrove coasts. A global coverage of this parameter[3] enables the estimation of species dependant coastal zones. Secondly, the depth often determines whether a wave breaks in case of shallow water. A storm can produce significant water level set-up due to the strong winds, especially in estuarine-like regions. This increased water depth enables higher waves to exist, which are also likely to occur during a storm. Also does the rate of submergence of a mangrove tree determines which parts of the tree contribute to the dissipation of wave energy. Additionally, the depth influences the distribution of the wave orbital velocity over the depth profile. In general holds that higher water depths causes smaller wave orbital velocities at the bottom.

Muis et al. (2007) developed a global surge level model, which provides water levels for a storm RP. The Global Tide and Surge Reanalysis (GTSR) uses a global unstructured grid and the ERA-Interim database to simulate the representative surge levels according to a return period, projected on DIVA segments too. It appears that the accuracy of the model is good for time series, but the relative error for extremes is rather large. GTSR uses ERA-I as boundary conditions, implying that also this model underestimates tropical cyclones (Section 2.2.2). This error is 11-14% for return periods ranging from 5-100 years and larger for higher return periods (Muis et al., 2016).

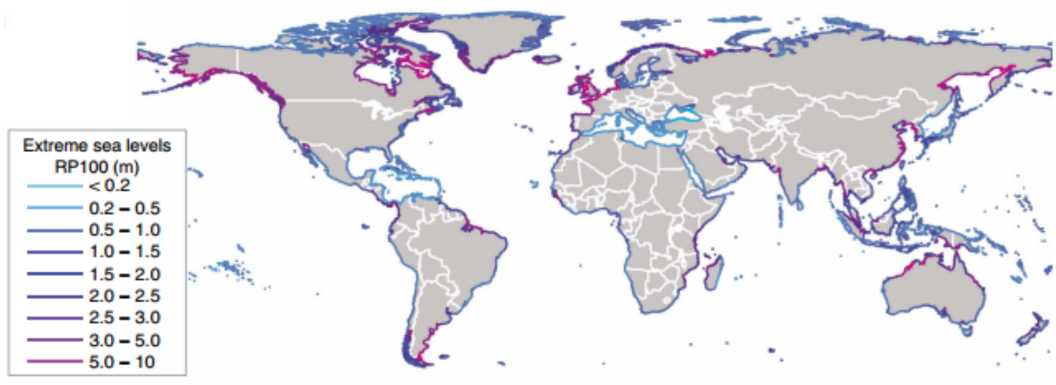

Figure 2.3: Height of extreme sea levels with a return period of 100 years around the world's coastline, projected on DIVA segments (Muis et al., 2016)

[3]AVISO, Satellite Altimetry Data

2.3. Vegetation studies and models

In many field researches it is concluded that vegetation contribute to the reduction of waves. However, the capability of vegetated foreshores as buffer zones is not well understood yet, although some vegetation formulations for wave reduction have been presented. In this chapter the most common models for mangroves is presented. Also the conducted research in the field concerning wave attenuation and the application in numerical models is elaborated.

2.3.1. Theoretical and empirical studies

The damping of wave heights due to vegetation is widely recognized. The opinions about involved processes, influence of different conditions and model approaches is less unanimous in the research community. Some studies uses an increased bottom friction approach to include the effect of vegetation, while other studies include the effect of physical characteristics of vegetation. Additionally, the various researches were conducted in different conditions and often are the uncertainties included in calibration parameters. Mazda et al. (1997a) gave an approximation of wave attenuation by mangroves, expressed as an increased bottom friction parameter. The expression, which is only valid for non-shoaling waves, is given by:

$$C_D = \frac{32\sqrt{2}}{\pi}\frac{h^2}{H_1 \Delta x}\left(\frac{H_1}{H_2} - 1\right) \tag{2.2}$$

This C_D thus represents both bottom friction as drag due to vegetation. The water depth is defined as h and H_1 and H_2 are the wave heights at a mangrove edge location and a more onshore position respectively, seperated by a distance Δx. Quartel et al. (2007) also uses Eq. 2.2 to find C_D values under different hydrodynamic conditions and for several cross-shore transects. In these transects different species, densities and mangrove dimensions were found, allowing to determine a formulation for the resistance coefficient as function of the projected mangrove area. Disadvantage of the approach is that it is only valid for a location specific and thus no mangrove characteristics can be included.

The cylindrical approach does include the effect of different vegetation characteristics, by representing a tree as multiple vertical cylinders (Figure 2.5). Dalrymple et al. (1984) made the first theoretical energy dissipation model for this approach in which normally incident waves are assumed and wave growth, refraction and dissipation due to friction and wave breaking are neglected:

$$\frac{\partial E c_g}{\partial x} = -\varepsilon_v \tag{2.3}$$

where E is wave energy density, c_g wave group velocity and ε_v time-averaged vegetation-induced rate of energy dissipation per unit horizontal area. The rate of energy dissipation is commonly used as a function of the time-averaged wave-induced drag force. When the inertial forces and the relative motion between plant and fluid are neglected, the plant-induced force can be expressed as a Morison equation, in which vegetation is assumed to compose of several cylindrical units:

$$F = \frac{1}{2}\rho C_D b_v N u\,|u| \tag{2.4}$$

where ρ is the water density, C_D the drag coefficient (does not include bottom friction, see Eq. 2.2), b_v the vegetation stem diameter, N the vegetation density and u the horizontal velocity. Mendez and Losada (2004) used the method of Dalrymple to include the propagation of random breaking and non-breaking waves over vegetation fields. Finally, Suzuki et al. (2012) adjusted the formulation to include vertical layering of vegetation, which is useful for mangroves because of its strong vertical variation. The Mendez and Losada (2004) formulation is given by:

$$< \varepsilon_v >= \frac{1}{2\sqrt{\pi}}\rho \tilde{C}_D b_v N \left(\frac{kg}{2\sigma}\right)^3 \frac{\sinh^3 k\alpha h + 3\sinh k\alpha h}{3k\cosh^3 kh} H_{rms}^3 \tag{2.5}$$

in which k, defined as $2\pi/L$ (L is wave length), σ, defined as $2\pi/T$ (T is wave period) and H_{rms} are respectively the wave number, wave frequency and root mean square wave height. The additional vegetation parameter is α, which represent the relative vegetation height h_v/h, where h_v resembles the vegetation height. $\tilde{C}_D$ is an average drag coefficient (bulk drag coefficient), because C_D might depend on the wave height, while it is not considered in Eq. 2.3.

In the formulation exists uncertainty concerning the drag coefficient. The drag coefficient of an isolated element is usually affected by the wake structure, and thus the Reynolds number. The C_D for rigid cylinders is often assumed to be 1.0 (Narayan, 2009). The bulk drag coefficient is used for cases with multiple elements. It varies among others with the dimensions of the object, wave orbital velocity, flexibility, depth and row spacing. Kobayashi et al. (1993) determined the drag coefficient for artificial kelp with a calibration procedure of the normalized decay coefficient k_i, by comparing an exponential wave decay model and an analytic solution, based on linear wave theory for small amplitude waves. A relation for the drag coefficient as function of the Reynolds number was found. Méndez et al. (1999) extended the calibration model to include vegetation motion. A few years later C_D was attempted to be parametrized for the artificial kelp and instead of the Reynolds number, the drag coefficient number was presented as a function of both the Keulegan-Carpenter (*KC*) number as the relative vegetation height (Mendez and Losada, 2004). For this flexible vegetation, the bulk drag coefficient varied between 0 and 0.6. The *KC* number, which describes the relative importance of drag forces over inertia by reviewing the ratio between wave related parameters and object dimensions, is defined as:

$$KC = \frac{\hat{u}T_p}{b_v} \tag{2.6}$$

in which $\hat{u}$ is the oscillating velocity amplitude. This is the orbital velocity in case of waves. This velocity is largely determined by the depth, where its amplitude as function of the depth is given by:

$$\hat{u}(z) = \frac{\pi H_{rms} \cosh k(h+z)}{T_p \sinh kh} \tag{2.7}$$

Nepf (1999) looked into the drag of rigid cylinders in different formations and found an increasing bulk drag coefficient as a result of decreasing element spacing i.e. higher densities. Suzuki and Arikawa (2010) studied the physical relationship between bulk drag coefficient and density of multiple cylinders to obtain an estimation for wave dissipation. They found a dependency between relative spacing of rigid cylinders, wave orbital velocity and drag coefficient (Figure 2.4). In the research, an immersed boundary model and a large eddy simulation turbulence model were used to determine the bulk drag coefficient values of rigid dense vegetation. Based on the rigidity of stems and roots and dense structure of the roots, the model can be used for mangroves.

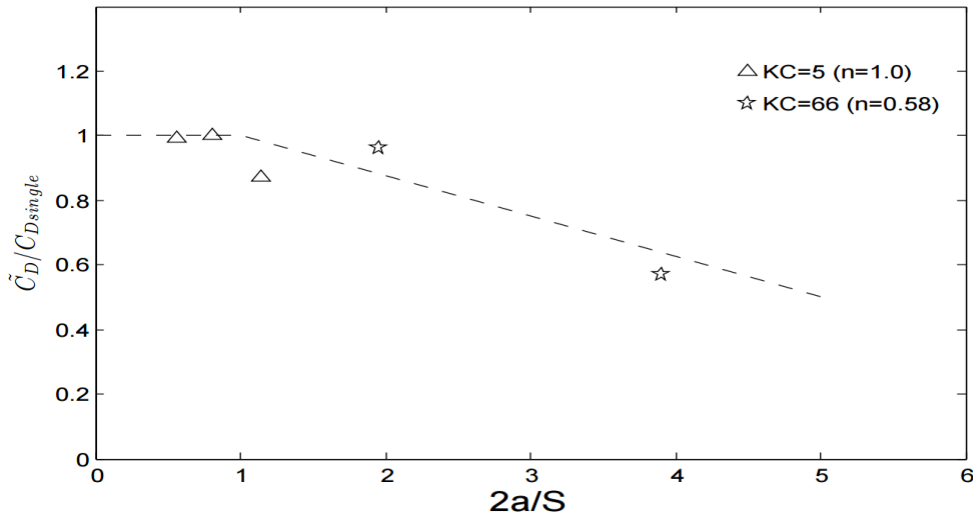

Figure 2.4: Drag coefficient as function of the non-dimensional parameter *2a/S* (Suzuki and Arikawa, 2010)

In Figure 2.4, $C_{Dsingle}$ the drag coefficient of one cylinder. The stroke of the motion of a particle and the distance between each cylinder are respectively defined as:

$$2a = \frac{KC}{\pi} b_v \tag{2.8}$$

$$S = \sqrt{\frac{2}{N\sqrt{3}}} \tag{2.9}$$

2.3.2. Field studies in mangrove areas

Several studies have been conducted regarding wave attenuation by mangroves. In these researches the quantitative or qualitative relation between hydrodynamics or mangrove characteristics and wave attenuation is explored. The studies are not directly comparable due to differing local conditions like wave characteristics, bottom slope and water depth. Also the measurements done in these studies were during mild conditions, implying that the quantified effect of mangrove attenuation during extreme conditions is still unknown. Mazda et al. (2006) measured during a typhoon, where he found that due the large water level set-up, the canopy of mangroves also plays a significant role in wave height reduction. Also Horstman et al. (2014) measured during a storm, though the wave heights measured were not significantly high. Other factors influencing the wave attenuation in a mangrove area are the forest band width (Bao, 2011), shore slope, wave height, period (Brinkman, 2006; Mazda et al., 2006) and the (physical) characteristics of mangroves. The latter can be divided in type of roots (Brinkman, 2006; Horstman et al., 2014; Quartel et al., 2007) and age of trees (Mazda et al., 1997a).

Table 2.2: Studies on wave attenuation by mangroves. VN = Vietnam, AU = Australia, JP = Japan, TH = Thailand and *r* = wave reduction factor (Eq. 2.10)

Source	Location	Vegetation	*H* (10^{-2} m) and *T* (s)	Wave attenuation
Mazda et al. (1997b)	Tong King Delta, VN	Sparse Kandelia candel seedlings (1/2 year-old),	*H* = - , *T* = 5-8	*r* = 0.01-0.10 per 100 m
		Dense 2–3 year-old Kandelia candel,up to 0.5 m high	*H* = - , *T* = 5-8	*r* = 0.08-0.15 per 100 m
		Dense 5–6 year-old Kandelia candel, up to 1 m high	*H* = -, *T* = 5-8	*r* = 0.15-0.22 per 100 m
Mazda et al. (2006)	Vinh Quang, VN	Sonneratia sp., 20 cm high pneumatophores,canopy starts 60 cm above bed	*H* = 11-16 , *T* = 8-10	*r* = 0.002-0.006 m^{-1}
		No vegetation	*H* = 11-16 , *T* = 8-10	*r* = 0.001-0.002 m^{-1}
Vo-Luong and Massel (2008)	Can Gio, VN	Mixed Avicennia sp. and Rhizophora sp.	*H* = 35-40, *T* = -	Energy red. factor = 0.50-0.70 over 20 m (including cliff)
Quartel et al. (2007)	Do Son, VN	Mainly Kandelia candel bushes and small trees	*H* = 15-25 , *T* = 4-6	*r* = 0.004-0.012 m^{-1}
		Non-vegetated beach plain	*H* = 15-25 , *T* = 4-6	*r* = 0.0005-0.002 m^{-1}
Bao (2011)	Red River Delta, VN	Mixed vegetation	*H* = 15-27 , *T* = -	*r* = 0.0055-0.01 m^{-1}
Bao (2011)	Can Gio, VN	Mixed vegetation	*H* = ±55 , *T* = -s	*r* = 0.017 m^{-1}
Brinkman et al. (1997) Brinkman (2006)	Cocoa Creek, AU	Zonation:Rhizophora sp. (front), Aegiceras sp., Ceriops sp. (back)	*H* = 1-7 , *T* 2	Energy trans. factor = 0.45-0.80 over 160 m
Brinkman et al. (1997) Brinkman (2006)	Iriomote, JP	Bruguiera sp., 20–30 cm high knee root	*H* = 8-15 , *T* ± 2	Energy trans. factor = 0.15-0.75 over 40 m
Brinkman (2006)	Oonoonba, AU	Zonation: Sonneratia sp. (front) and Rhizophora sp. (back)	*H* = 4-25 , *T* ± 6	Energy trans. factor = 0.9-1.0 over 40 m
Horstman et al. (2014)	Kantang, TH	Zonation: sparse Avicennia and Sonneratia (front), Rhizophora (back)	*H* = 5.5-10.6 , *T* = 6-11 (normal) *H* = 15.3 , *T* = 4 (storm)	*r* = 0.0024 m^{-1} Avi. zone *r* = 0.061 m^{-1} Rhiz. zone
	Palian, TH	Zonation: sparse Avicennia and Sonneratia (front), Rhizophora (back)	*H* = 4.4-11.3 , *T* = 10-20	*r*=0.0032 m^{-1} Avi. zone *r* = 0.012 m^{-1} Rhiz.zone

Most researches express the rate of wave attenuation into the wave reduction factor (Table 2.2), defined as:

$$r = \frac{\Delta H}{H \Delta x} \tag{2.10}$$

where ΔH is the difference in wave height between initial wave height *H* and the wave height at the end of the mangrove forest transect. Δx refers to the distance over which this distance is measured, often expressed in 1 or 100 m.

From Table 2.2 it becomes clear that the hydrodynamic conditions and mangrove characteristics are diverging. Next to that, most researches do not give a complete overview of all relevant parameters. The research of Horstman et al. (2014) does give accurate data in terms of bathymetry, mangrove zonation, governing water depths and wave heights at different transects in the mangrove forest. The findings in the study emphasizes the coastal defence function of mangroves and provides the starting point for modelling studies like this research. Disadvantage are the small wave heights measured, which might enlarge the influence of capillary waves and thus a simple short wave model does not apply any more. Additionally, a model output can significantly change if the input is slightly adjusted. A continuation of the research was done by Hendriks (2014) in which the bulk drag coefficient was determined by calibration.

Non-wave attenuating related researches on mangroves include mainly the sediment trapping capabilities of the roots and mangrove biomass (and carbon) mapping. Concerning the erosion reductive qualifications, Furukawa and Wolanski (1996) concludes that mangroves are an important sink for sediments. Next to that, he addresses that mangroves are responsible for lowering turbidity in coastal waters and hence increase productivity of planktonic algae, increasing the biodiversity. While the influence of counter erosive and carbon sequestration features of mangroves is outside the scope of this thesis, the measurements conducted in these researches can be beneficial. For instance, measuring mangroves in order to obtain knowledge about typical dimensions for different type of mangroves, have shown to link biomass with carbon content, but can also be used to link with wave and water level attenuation. Cole et al. (1999), Dahdouh-Guebas et al. (2007) and Kauffman and Donato (2012) provide mangrove dimensions in order to describe carbon content estimations.

2.3.3. Numerical models

The full description of transforming waves in nearshore vegetated areas not only depends on the vegetation. Multiple processes as wave transformation and wave dissipation by friction and breaking determine the wave conditions at the end of a mangrove forest. Modelling wave heights for mangrove vegetated coast can eventually contribute to coastal implementations, like mangrove preservations programs, dike realisations or beach nourishments in order to protect hinterland and coast.

XBeach is a numerical model developed to simulate hydro and morphodynamic processes on different kind of coasts. It includes the hydrodynamic processes of short wave transformation, long wave transformation and wave-induced setup and unsteady currents, as well as overwash and inundation. XBeach is based on solving the short wave action balance, which is for a 1D simulation with normal incident waves:

$$\frac{\partial A}{\partial t} + \frac{\partial c_g A}{\partial x} = -(D_w + D_f + D_v) \tag{2.11}$$

where A is the wave action, c_g is the group celerity and the right hand side represents the dissipation for respectively waves, bottom friction and vegetation. It can work in three model options, allowing the choice on which time-scale the waves are resolved (Deltares, 2015):

1. Stationary wave model: by imposing a constant incoming wave energy at the boundary, Eq. 2.11 is efficiently solved, but infragravity, i.e. long, waves are neglected.
2. Surfbeat (instationary): short wave variation on the wave group scale (envelope) and their associated long waves are resolved.
3. Non-hydrostatic mode: calculated non-linear shallow water equation with a pressure correction term, allowing to simulate propagation and decay of individual waves. Computationally expensive mode.

In order to solve short wave amplitude variation separately from the long waves, currents and morphological change in a limited computation time, the surfbeat mode is recommended. The phase of the short waves is not simulated in this case, in contrast to the non-hydrostatic mode, which solves all the processes at the expense of the computation time.

The model of Mendez and Losada (2004) is commonly used in hydrodynamic models, like SWAN and the tree modes of XBeach (Figure 2.5). The expression is added to the short wave action balance to take wave attenuation by vegetation into account. Also, the vegetation effect on infragravity waves and mean flow is included in XBeach, again by using a Morison type of equation (Eq. 2.4). Shortcomings of the model implementation is the uncertainty of the bulk drag coefficient, damping effect of infragravity waves and mean flow and the effect of emerged vegetation and nonlinear wave effects.

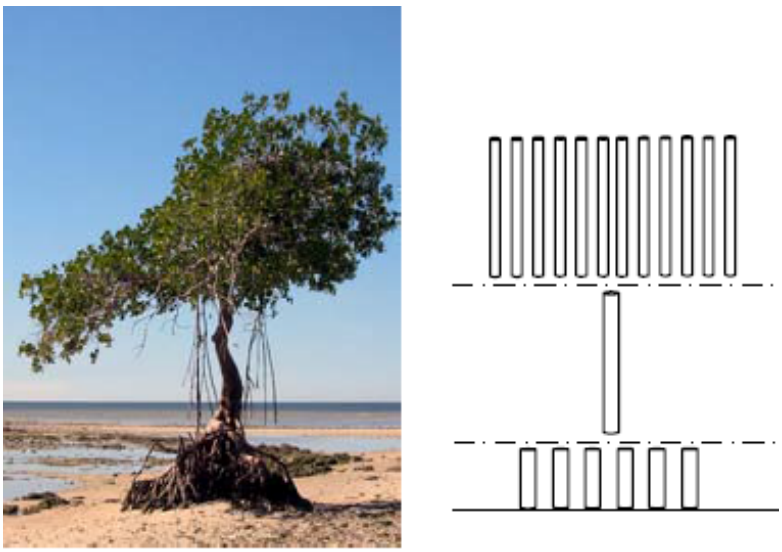

Figure 2.5: Mangrove schematization according to the cylindrical approach, implemented in Xbeach and SWAN (Burger, 2005)

Studies concerning the modelling of mangroves in XBeach have among others been conducted by Phan et al. (2014). Despite the research involved a study location in the Mekong Delta (Vietnam), the model was generic, implying that input parameters were based on likely values instead of measurements. Conclusion drawn from the analysis is that the long waves cannot be neglected in understanding mangrove hydrodynamics. Other mangrove modelling studies were conducted by de Vos (2004), Burger (2005), Narayan (2009), Tusinski (2012) and Suzuki et al. (2012). However, none of the models were validated, compared or calibrated with measurements.

3

Hydrodynamics

The wave dissipation highly depends on the governing wave conditions according to Eq. 2.5, because both wave period and height appear to the power three in the formulation. Next to that, the water depth determines which part of the mangrove tree is submerged and therefore contribute to the wave dissipation. Hence, obtaining accurate hydrodynamic conditions is paramount.

The focus of this research is presenting a method in which mangrove effectiveness in dissipating wave energy can be determined globally. Therefore, global wave and water level databases are used in order to determine representative conditions. Due to the global character of ERA-Interim and GTSR (Sections 2.2.2 and 2.2.5), these databases are used. ERA-I has already proven to be quite accurate for deep areas, but not for sheltered areas yet. The grid size of this database is fairly rough, implying that a potential large inaccuracy in more sheltered coastal waters can exist. Especially because ERA-I was not designed with an initial focus on presenting nearshore conditions very well. Assuming that nearshore conditions are thus represented by offshore ERA-I points can be too rough. Therefore the ERA-I data might need to be adjusted for certain locations. In addition to the rough grid size of ERA-I, tropical cyclones (TC's) are not accurately included in this database. This means that ERA-I most likely underestimates wave and wind conditions for the tropical areas.

In this chapter the wave transformation of ERA-I towards nearshore coastal zones is presented. First, the different transformation methods are elaborated and a substantiation for the choice of the final method is given, which eventually is validated. A method to deal with TC's is left out this analysis, but a possible approach is given in Appendix B.2.

3.1. Wave transformation

The character of the transformation of a wave when it propagates towards shore depends on both local conditions as the wave conditions itself. Especially in shallow and sheltered areas, the local conditions are able to significantly influence the shape, height and period of the resulting wave. Gradual sloping zones can increase wave heights as a result of shoaling processes, shallow waters decrease wave heights due to bottom friction and very limited depth even forces the waves to break. Next to that, depth variation along the wave crest with a corresponding variation in phase speed along that crest, causes the wave slowly changing direction as it approaches the coast. Other processes as diffraction, white-capping, triad interactions, quadruplets and wind-induced wave growth also play a role in coastal waters. Each of the mentioned processes has its relative influence on the wave height, depending on especially the bathymetry (Table 3.1).

Table 3.1: Relative importance of processes on waves in different oceanic and coastal regions (Holthuijsen, 2010). +++=very important, ++=important, +=weakly important and 0=unimportant.

	Oceanic waters	Coastal waters	
		Shelf seas	Nearshore
Wind generation	+++	+++	+
Quadruplet wave-wave interactions	+++	+++	+
White-capping	+++	+++	+
Bottom friction	0	++	++
Bottom refraction/shoaling	0	++	+++
Depth-induced breaking	0	+	+++
Triad wave-wave interactions	0	0	++
Diffraction	0	0	+

The translation from ERA-I towards shore takes place in all three categories. The accuracy of ERA-I in deep oceanic waters is rather good. Therefore the processes in the coastal waters are more interesting. It can be seen that in relatively shallow seas processes as wind generation, quadruplets, white-capping, bottom friction, shoaling and refraction are important. In order to describe the nearshore processes, the three possible methods are given.

In the first method the resulting wave height nearshore is assumed to completely depend on breaking due to limited depth. It would therefore only need the local depth as input. The maximum shallow water wave height which can exist is based on the following criterion:

$$\frac{H_{max}}{h} = \gamma \tag{3.1}$$

in which γ represents the breaking parameter. The opinions on this parameter differs: for regular waves this varies between 0.78 and 0.88 and for irregular waves γ=0.4. The criterion for irregular waves is used in the depth-induced breaking method (DIB). Equation 3.1 is used for sheltered areas, where the depth most likely limits the wave height ($h/L \leq 0.05$). The method is very simplified, which can both be considered as an advantage and disadvantage. It is namely computation inexpensive, but might be inaccurate due to the many neglected processes. Next to that, the method does not describe wave periods and directions. Despite this method is considered to be inaccurate, the calculated values of Eq. 3.1 are given in the analysis. This is only done for shallow water wave buoys.

The second option is a numerical model. A commonly used model for these kind of applications is SWAN (Section 2.2.3). It is able to describe the required processes in both longitudinal and lateral direction for among others wave height, period and direction. In the following sections the SWAN procedure is presented for 4 hydrodynamic study locations.

3.1.1. Model set-up

Whether SWAN, with the ERA-Interim data as input, describes the sheltered nearshore wave conditions accurately, needs to be validated in advance. In order to do so, measurements are required for the period 1979-2014, the years which the ERA-I database covers. Accurate and available buoy data is difficult to obtain for mangrove vegetated countries due to financial insufficiency, inaccurate measurements and non-public access. Therefore the locations to validate the method are also non-mangrove vegetated areas. Additionally, the locations are selected based on different degrees of shelter in order to get insights into the validity of the method for different kind of coasts. The validation method is conducted by simulating a historical storm, because extreme values are interesting for flood hazard indications and in this way the importance of bottom induced processes are simulated. This means that SWAN non-stationary is used, with a time interval of 2 hour. The included processes are the most relevant ones presented in Table 3.1. These are wave generation by wind, quadruplet wave-wave interactions, white-capping, bottom friction, refraction, shoaling and depth-induced breaking.

The study locations are among others determined based on the degree of shelter in which the buoys are located. Next to that, also the character of the continental shelf is varied among the different hydrodynamic study locations. In this way the method is checked for varying kind of coasts in order to give a substantiation for global use. The functionalities from Delft Dashboard are used to create a grid and depth profile. The bathymetry used to set up this profile are from various sources, which can be loaded into Delft Dashboard. The grid size in the models are relatively rough, because the research is focussing on quick assessments rather than accurately validate wave conditions.

ERA-I provides the boundary conditions of the model in terms of a time-series of wave height, wave period, wave direction, wind speed and wind direction at certain points along the study areas. The conditions in the area between the points are determined based on linear interpolation. The hydrodynamic study locations are presented in Table 3.2.

Table 3.2: Hydrodynamic study locations with features. NLD=Netherlands, IE=Ireland and US=United States

	Degree of shelter	Bathymetry	Grid (km)	ERA-I	Buoy(s)
North Sea (NLD)	Exposed	GEBCO[1]+Vak.[2]	2x3	10	5
Wadden Sea (NLD)	Barrier islands	GEBCO+Vak.	0.7x1	5	4
Galway Bay (IE)	Barrier island	CS[3]	0.4x0.5	3	1
Monterey Bay (US)	Headland bay	GEBCO	1.1x1	1	2

3.1.2. North Sea

The North Sea is a marginal sea of the Atlantic Ocean, located between Great-Britain and the Netherlands. It is part of the European continental shelf, consisting of sandy beaches and wide mudflats (Figure 3.1). This makes the North Sea a relatively shallow sea, implying that bottom effects are important. The heaviest storms come from the north-east, accompanied with strong winds, causing large surges and wave heights.

The Dutch have been measuring wave parameters extensively for years[4]. The buoys can be considered as 'exposed', because they are not located behind barrier islands nor in a headland bay. Next to good buoy data, also accurate near-coastal bathymetry data, the Vaklodingen measurements, is present. This database does however not cover the entire North Sea. Therefore GEBCO completes the bathymetry map. The 10 ERA-Interim points provide the boundary conditions for the SWAN model. Finally, the grid is around $0.03 \times 0.03°$, which is around 2×3 km, for longitude and latitude respectively.

The performance of SWAN is checked for the IJmuiden buoy, which is located in front of the Dutch coast (see Figures 3.1 and 3.2). Between the nearest ERA-I point (point 2) and the buoy, no obstacles in terms of barrier islands are present. This causes the shape of the SWAN simulation to be similar with the ERA-I data. Apparently also the depth at the buoy location is not small enough to induce breaking, because hardly any wave height reduction is present. Another explanation for the similar wave height output of ERA-I and SWAN is the compensation of the ERA-I overestimation by dissipating processes between the ERA-I point and wave buoy IJmuiden. The depth at IJmuiden buoy is however around 20 m, so limited bottom induced dissipation is present. Also other exposed wave buoys show similar results (Appendix B). Next to that, the SWAN simulation seems to underestimate the wave period instead of the overestimation of ERA-I. Also hardly any improvement for the wave direction is observed.

[1] General Bathymetric Chart of the Ocean, Intergovernmental Oceanographic Commission and International Hydrographic Organization
[2] Vaklodingen Kustmetingen, Rijkswaterstaat
[3] Celtic Seas Bathymetry from British Oceanographic Data Centre
[4] Multifunctional Access Tool foR Operational Oceandata Services (Matroos)

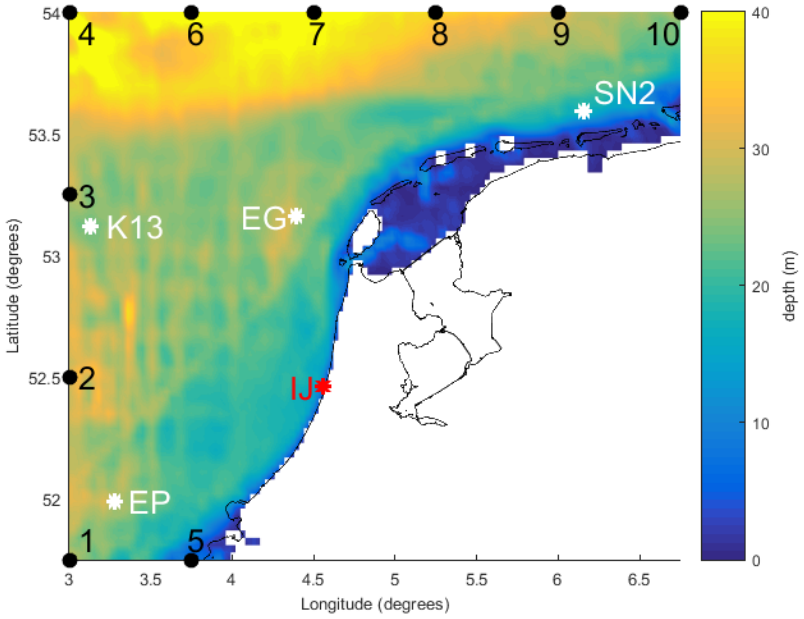

Figure 3.1: SWAN model area North Sea. Black dots represent ERA-I boundary points, stars are wave buoys (red is the analysed buoy).

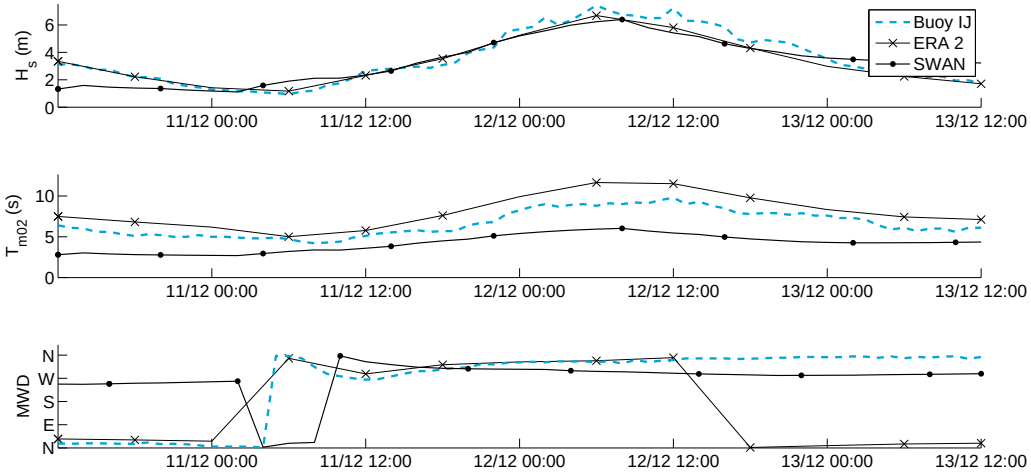

Figure 3.2: SWAN validation for IJmuiden buoy. ERA-I point 2 is the closest boundary point to IJmuiden.

3.1.3. Wadden Sea

The Wadden Sea is an intertidal zone in the north of the Netherlands (Figure 3.1). It is known for its tidal flats, wetlands and rich biological diversity. Due to the barrier islands and its shallow bottom, the Wadden Sea is comparable with a mangrove area. An improvement of wave conditions for this location would support a SWAN procedure for the mangrove areas. The waves need to penetrate between the islands, causing 2D processes to be more significant. The grid is three times more refined compared ($0.01\times0.01°$) with the North Sea model and the bathymetry is again a combination of Vaklodingen and GEBCO. The three Amelander Zeegat buoys (AZ numbers in Figure 3.3) are located around the shallow region of the island Ameland.

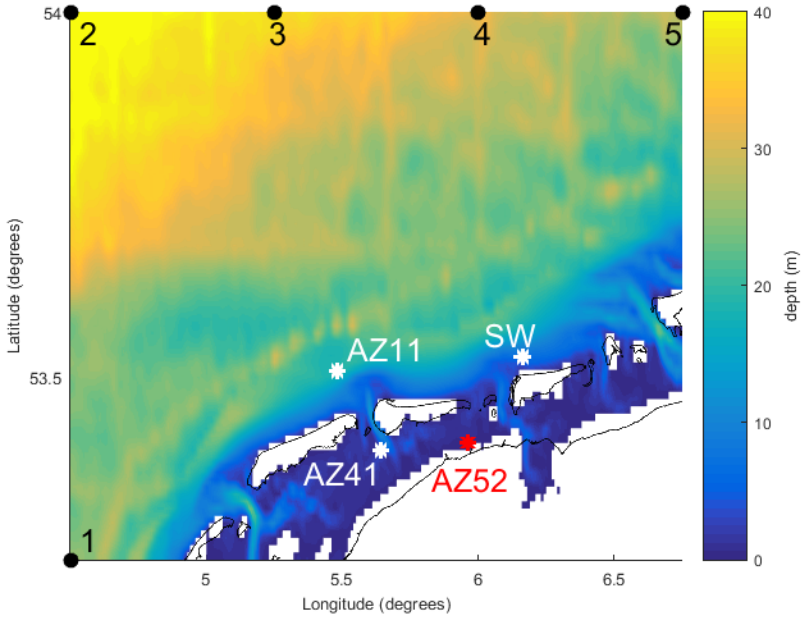

Figure 3.3: SWAN model area Wadden Sea. Black dots represent ERA-I boundary points and the blue/white stars are wave buoys

SWAN significantly improves the result in comparison with ERA-I for the sheltered Wadden Sea for wave height and period (Figure 3.4). Relatively small disturbances in these parameters are not observed by ERA-I due to its 6 hour interval. Therefore SWAN also does not produce these peaks. Despite these peak, the buoy data seem to coincide well with the SWAN output. No wave direction measurements were conducted by wave buoy AZ52.

The water depth at AZ52 is around 10 meter and the peak wave period during the storm around 4-5 sec (Figure 3.4). This would mean that a DIB approach (Section 3.1) can not be applied, because h/L=0.2-0.3. However, a DIB approach would satisfy at an depth of around 2.5 m. In this case it would result in a maximum wave height of 1.0 m.

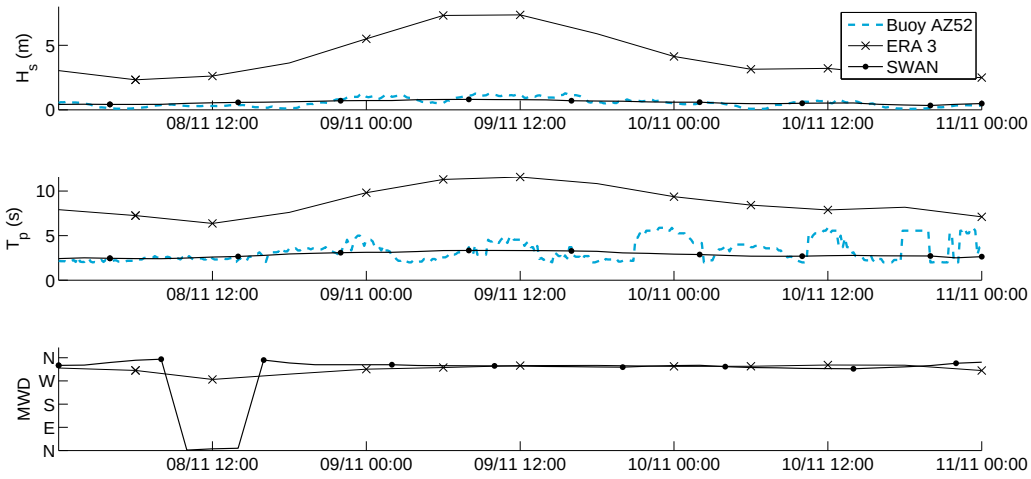

Figure 3.4: SWAN validation for Amelander Zeegat 5.2 buoy. ERA-I point 3 is the closest boundary point to AZ52.

3.1.4. Galway Bay

This bay is a large bay on the west coast of Ireland. A buoy[5] is located behind the Inishmore island (53.1°N 53.1°W in Figure 3.5), making the situation at this location interesting to investigate for the sheltered wave transformation. Namely, the waves need to bend around the island and therefore a difference between ERA-I and the buoy data is expected. This is also confirmed by Figure 3.6, where both wave height as period for the Galway Bay buoy (GB3) has a similar shape as the output of ERA-I point 3, but significantly lower. SWAN improves the governing wave height and wave period for the nearshore location. There still is some deviation between measured and simulated output. This can be caused by the excluded diffraction from the model or inaccurate measurement of the buoy. The DIB approach would result in wave heights of around 8 m, but it can be observed in Figure 3.6 that this would result in a significant overestimation of the wave height.

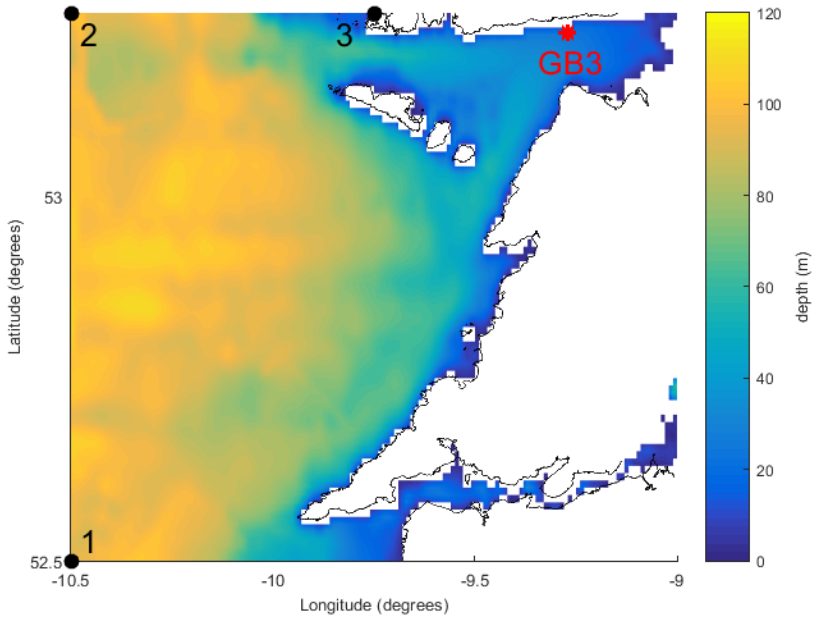

Figure 3.5: SWAN model area Galway Bay. Black dots represent ERA-I boundary points and the white star is a wave buoy.

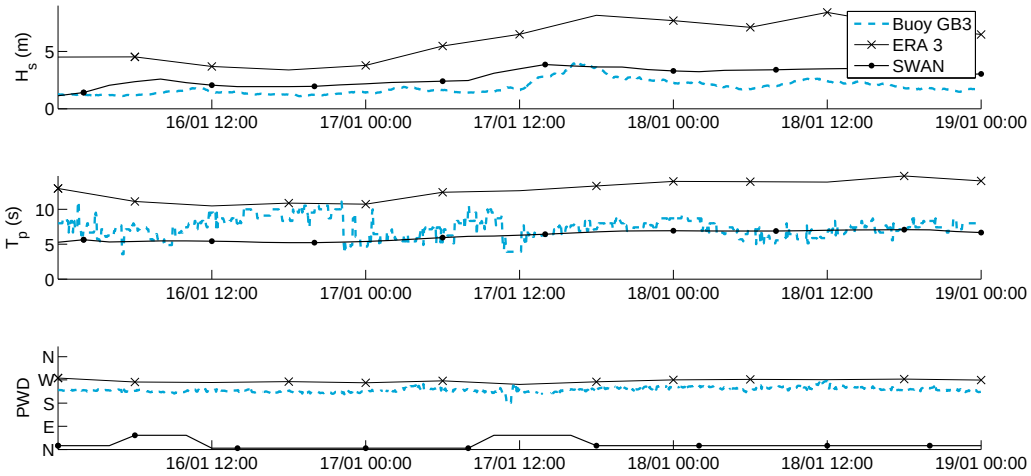

Figure 3.6: SWAN validation for Galway Bay 3 buoy. Red line represents nearest ERA-I output.

[5]Marine Institute Ireland, Wave buoy data

3.1.5. Monterey Bay

The final hydrodynamic study location is an embayment at the Californian coast. This federal protected bay inhabits a large diversity of animals and sea life, making it the largest Marine Reserve in the US. The US west coast is known for its deep continental shelf and abrupt depth changes (Figure 3.7). Additionally, the bathymetry around embayments is often such, that waves refract towards the headlands. These observations distinguishes this area from the others hydrodynamic study location and is thus interesting to investigate. The bathymetry map is from GEBCO.

There are two useful buoys located in Monterey Bay. The first is Canyon Outer (CO), an exposed buoy, and the second one is Cabrillo Point (CP), which is located just behind the land in the south [6]. This latter buoy measures among others the waves which refract around the small headland.

As expected from previous hydrodynamic study locations, SWAN produces a better result compared to ERA-I for CP than for CO. Only the wave period does not give a satisfying result, but this can be explained by the fact that ERA-I does not as well. The match of ERA-I and SWAN for CO can be explained by the fact that the buoy CO is located in very deep water, especially compared to the other hydrodynamic study locations. This implies that almost one dissipation from the bottom is generated.

The combination of the 10 m depth around CPO and the peak wave period of 10-14 s, enables a DIB approach. This results in a maximum wave height of around 4 m. In Figure 3.9 wave heights between 1-3 were measured. A DIB would perform better here, than at the other hydrodynamic study locations. However, apparently other dissipative processes also reduced the wave height, because DIB overestimates the wave height. Hence, the DIB approach is considered to be too inaccurate for this situation. Additionally, it would not describe the (small) disturbances in wave height.

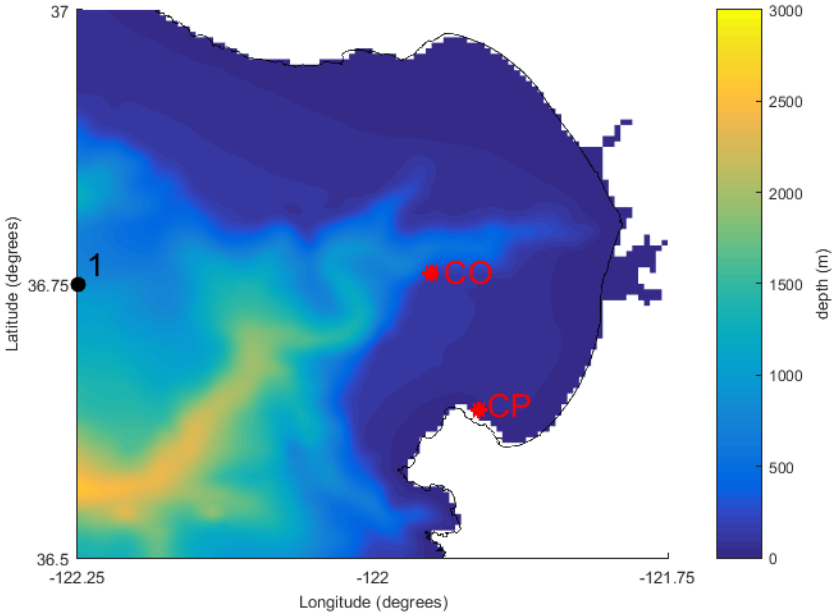

Figure 3.7: SWAN model area Monterey Bay. Black dot represents ERA-I boundary point and white stars are wave buoy.

[6]The Coastal Data Information Program, Scripps,Scripps Institution of Oceanography. Wave buoy data

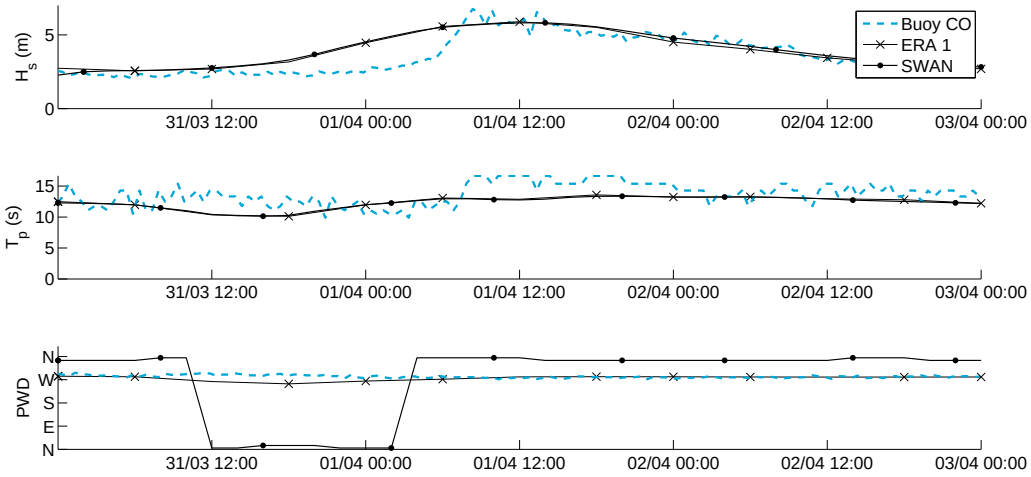

Figure 3.8: SWAN validation for Canyon Outer buoy. Red line represents nearest ERA-I output.

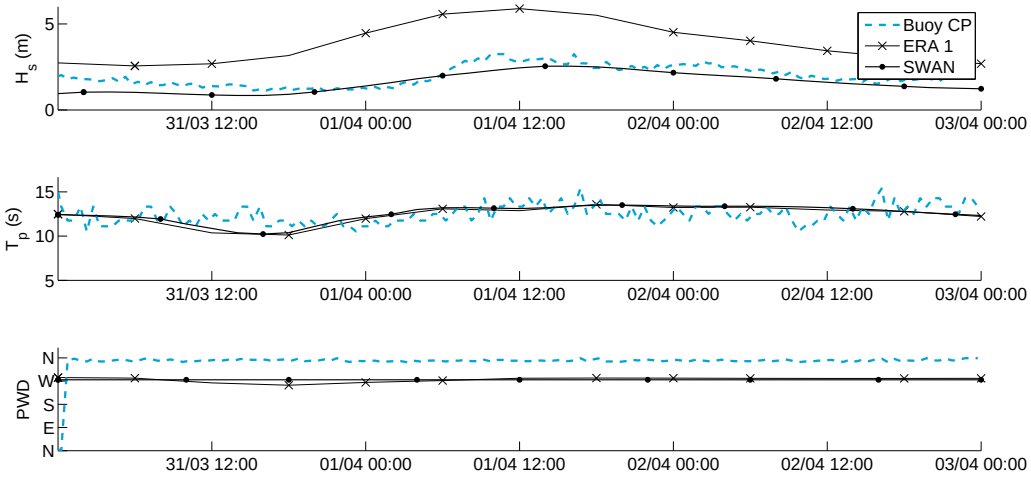

Figure 3.9: SWAN validation for Cabrillo Point buoy. Red line represents nearest ERA-I output.

3.1.6. Comparison

This section (quantitatively) describes the difference in wave height and period between the ERA-I data and the use of SWAN in combination with this ERA-I. In order to do so, buoy data is averaged over both the ERA-I and SWAN time-interval, which are six and two hours respectively. Due to the different intervals, more points for SWAN are obtained than for ERA-I. Subsequently, the obtained wave heights and periods are compared with the ERA-I and SWAN outputs. These are presented as 'simulated' in the figures. Next, the correlation coefficient (ρ) and root mean square deviation (*RMSE*) are calculated. The first-mentioned quantifies the statistical relationship between two variables and the second parameter the difference between predicted and observed values. The RMSE is considered to be the most relevant, because the representation of observed data is attempted to be simulated.

The comparisons for the North Sea (IJmuiden buoy) and Wadden Sea (Amelander Zeegat 52 buoy) are given in order to give the difference for different degrees of shelter (Figures 3.10 and 3.11). The comparison of the other buoys can be found in Appendix B.1.3.

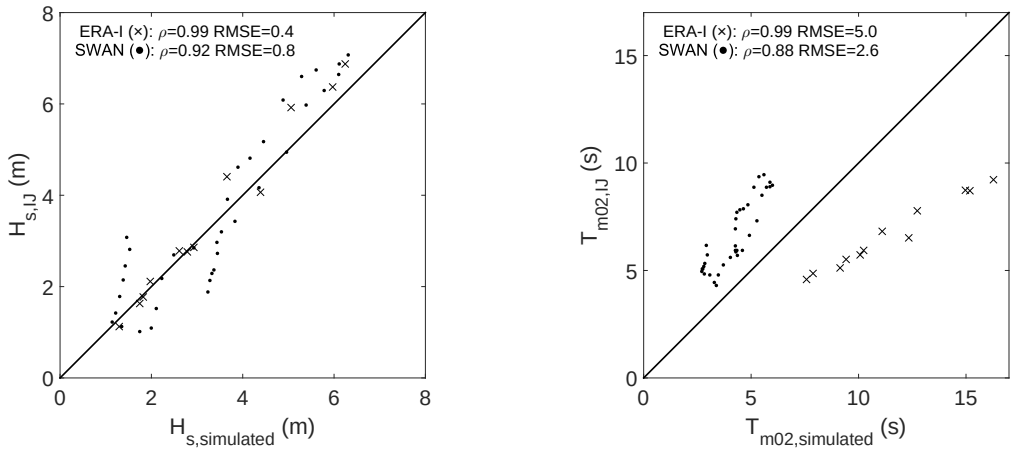

Figure 3.10: Comparison of the IJmuiden buoy with simulated wave heights (left) and periods (right) of ERA-I and SWAN.

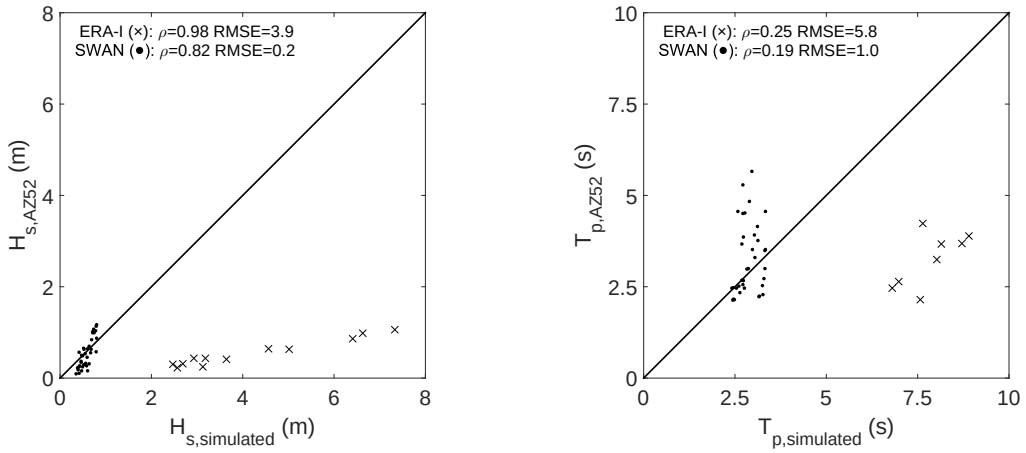

Figure 3.11: Comparison of the Amelander Zeegat 5.2 buoy with simulated wave heights (left) and periods (right) of ERA-I and SWAN.

It can be observed that SWAN even reduces the accuracy of the description of the nearshore wave height for the IJmuiden buoy. In contrary, the wave heights and periods estimations for the Wadden Sea buoy significantly improved. The correlation coefficient of the wave period in Figure 3.11 shows a decline. This can be explained by the fact that the wave period in SWAN significantly is reduced, while the wave buoy data more or less remains the same (for both averaging of ERA-I and SWAN). The difference in RMSE, presented in Table 3.3, is calculated as follows:

$$\Delta RMSE = RMSE_{ERA-I} - RMSE_{SWAN} \tag{3.2}$$

Table 3.3: Difference in *RMSE* (Eq. 3.2) for wave height *H* and period *T*. E=exposed and S=sheltered

			$\Delta RMSE_H$ (m)	$\Delta RMSE_T$ (s)
North Sea	IJ	E	-0.4	2.4
Wadden Sea	AZ 5.2	S	3.7	4.8
Galway Bay	GB3	S	3.3	3.6
Monterey Bay	CO	E	0	0.2
	CP	S	1.7	-0.1

4

Mangrove analysis

The quality of mangroves is directly linked with their effectiveness in reducing wave heights. The abiotic factors discussed in Chapter 2 largely determine the type, appearance and zonation of mangroves. The large variabilities in mangroves, requires a data analysis in order to assess their contribution to flood hazard reduction. The varying vertical profile of the tree (Figure 2.1), makes it difficult to quantify wave height reduction by mangroves. The variable mangrove characteristics which influence wave height reduction are:

- Root structure: pneumatophores, prop roots, buttress roots and knee roots.
- Wood quality: flexibility and canopy type/density.
- Dimensions: height and diameter of roots, stems and canopy.
- Forest characteristics: width, density, zonation.

This chapter is focussing on the range of mangroves parameters. This is done for two method, which are both based on the Mendez and Losada (2004) formulation (Section 2.3).

4.1. Method 1 - General mangrove description

The model of Mendez and Losada (2004) enables the possibility to include physical characteristics (dimensions and densities) in its formulation. Next to that, rigidity and shape of the vegetation are expressed in the drag coefficient. The parameter evidently does have a physical meaning, both as function of tree characteristics as hydrodynamic conditions (Section 2.3.1). Hence this method uses the formulation of Suzuki and Arikawa (2010), in which the drag coefficient is determined based on the waves, depth and density. Additionally, this method focusses on global applicable physical characteristics by reviewing different kind of literature. It is mentioned that the analysis is associated with assumptions, which limits the confidence of the result validity. However, the assumptions are thought-out (see Appendix A) and taken into consideration when reviewing the results.

The steps of this method are:

1. Determine representative densities for different mangrove species and forest qualities.
2. Find relations between the physical characteristics (diameter, density and height) of non-canopy parts of the mangrove trees for these subdivisions.
3. Use a biomass relationship to determine representative canopy characteristics.
4. Calculate the bulk drag coefficient for the non-canopy parts based on Suzuki and Arikawa (2010) and assumptions for canopy parts.

In this approach, global applicable sets of mangrove characteristics are found. Due to the varying characteristics of mangrove trees, a subdivision for distinct mangrove species is made. Additionally, the quantity of trees in a forest are varied, which can be considered as the difference between a young pioneer mangrove population and an old well-grown forest.

4.1.1. Red and Black mangroves

The vertical layering of vegetation proposed by Suzuki et al. (2012) is convenient for describing the different parts of a mangrove tree. The main parts of a mangrove tree are roots, stem and canopy, i.e. layer 1, layer 2 and layer 3 (Figure 2.5). Conducted studies on mangrove dimensions are mainly focussing on large stilt- and pencil shaped (pneumatophores) roots. Due to the significant and distinct differences in these root types, the mangrove characteristics in this analysis are based on the division of stilt roots and pneumatophores. These are referred as 'Red mangroves' and 'Black mangroves' respectively. Only values for the canopy i.e. layer 3 are reviewed separately due to lacking data. The range of parameters for the different sources is presented in Figure 4.1.

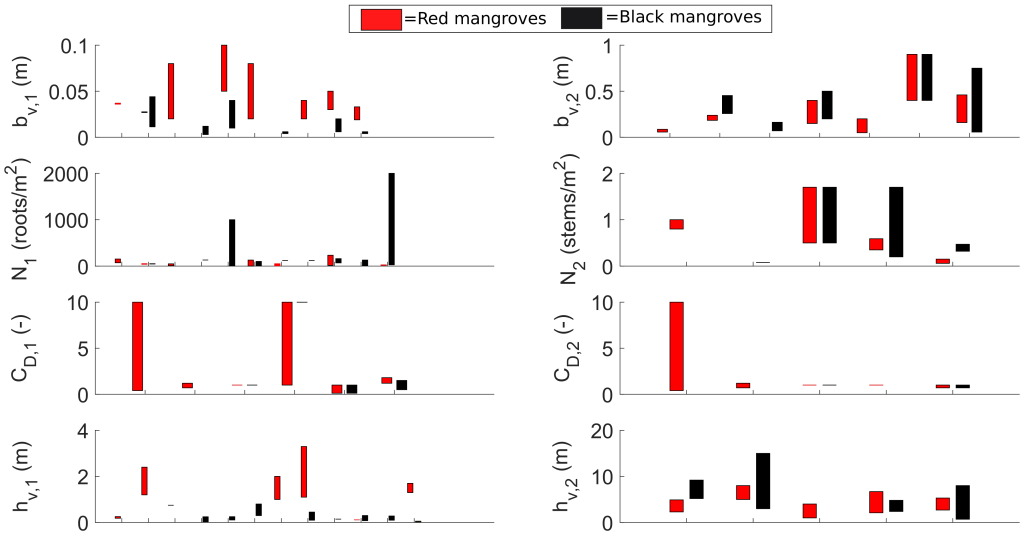

Figure 4.1: Large parameter range in mangrove characteristics according to different literature. (see Table A.2 for values). Index 1 refers to the root layer and 2 to the stems.

From this figure, the large range in mangrove characteristics is confirmed. Next to the natural variability, also other causes for the large spread are present. First are not all measurements conducted according to standard procedures given in Kauffman and Donato (2012). Secondly, some data from literature is based on assumptions or derived from other sources, which cannot be reviewed or accessed any more (see Appendix A.1.1). It can also be seen that the drag coefficient is included. This is to give an indication of its large range used in the different literature. Explanation for this spread is given in Section 2.3.1. It is however not considered as a physical parameter and is therefore reviewed individually in Section 4.1.4.

In order to exclude outliers, the data is analysed using boxplots. These statistical figures are useful when comparing different datasets which are not correlated to each other. In this way a range of parameters is presented in a statistical justified manner. The boxplots are reviewed in order to find a representative sparse, medium and densely vegetated forest.

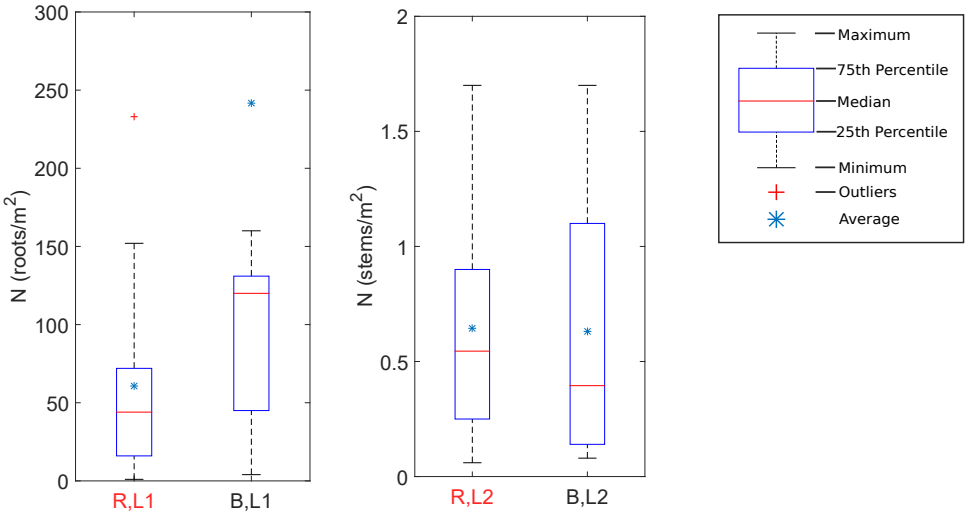

Figure 4.2: Boxplot for the root densities (left;L1) and for the stems (right;L2) for Red and Black mangroves

From the result in Figure 4.2, the following can be concluded:

- The number of pneumathophores per m^2 is higher than the stilt roots of the Red mangrove type.
- The Black mangrove type needs more space than the Red mangrove, based on the number of trees (stems). This was already confirmed in Section 2.1.1 and can be observed in Figure 2.1.
- There exists a large difference between roots and stems, implying that a vertical layering proposed by Suzuki et al. (2012) seems to be required. However, in Eq. 2.5 the dissipation is a multiplication of multiple factors and hence diameter or bulk drag coefficient can compensate for low densities.

Relations between certain physical characteristics of trees seem to exist. A high tree has a large diameter to maintain its stability and a well-grown mangrove forest is likely to have more and larger trees. On the other hand can too many large trees limit the development of young pioneer trees. Based on the data available, relations between the different parameters are found (Tables 4.1 and 4.2). It is noted that the relations are not necessarily true and, for simplicity, are assumed to be linear.

Table 4.1: Diameter in relation to density

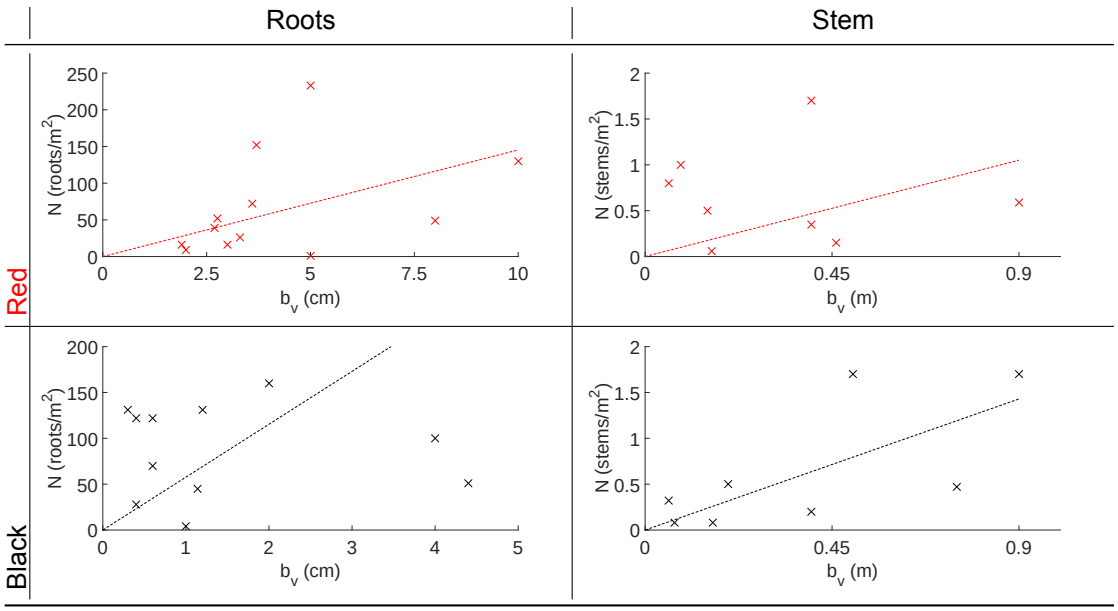

Both root and stem diameters are likely to be larger if there are also more roots or stems respectively. This is in accordance with earlier theories. Another increasing trend is visible in Table 4.2, where thicker roots and stems correspond with higher branches. Based on these figures, the diameter and vegetation height of root and stem layer are determined for the two mangrove types and the three vegetation densities (Table 4.3).

Table 4.2: Diameter in relation to vegetation height

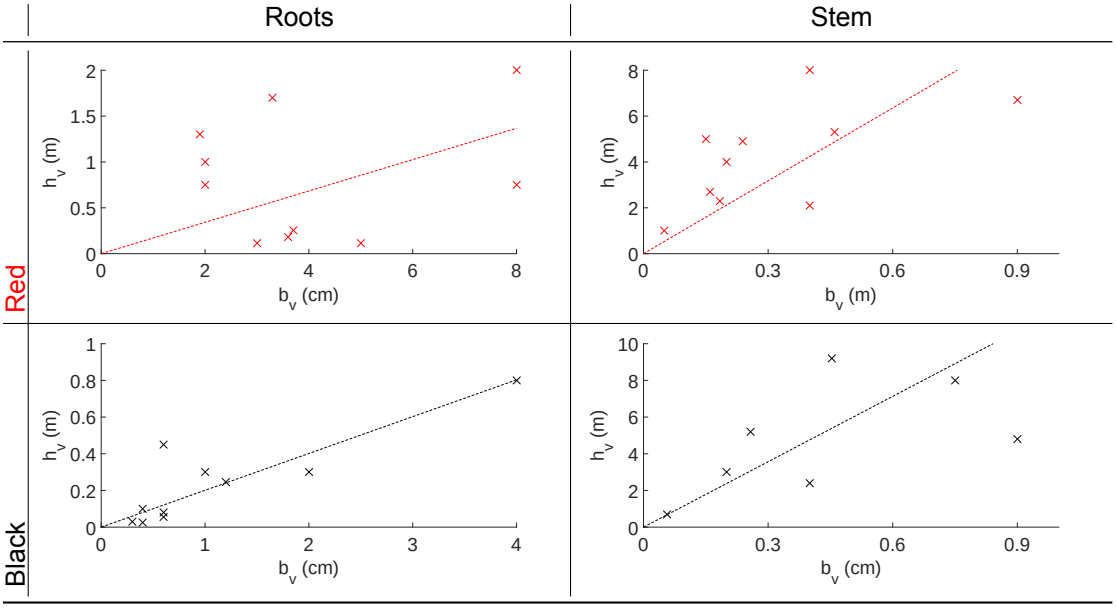

Depending on the local depth, root- and stem height, the canopy can contribute significantly to the dissipation of wave energy (Mazda et al., 2006). A considerable submerged canopy is able to attenuate waves more than in case the surge level does not fully reach the canopy. Unfortunately, mangrove canopy data is scarce. In order to determine canopy characteristics, the biomass factor is introduced, which represent the total amount of 'blocking surface' per m^2 for an incoming wave:

$$BM_{fac,i} = b_{v,i} N_i h_{v,i} \tag{4.1}$$

in which *i* is the layer number. $BM_{fac,3}$ is estimated by scaling it with the maximum found biomass factor from the analysis of layer 1 and 2. The reasoning behind this is that a larger root system and thicker stem is correlated with a large canopy too. A maximum biomass factor for layer 3 is based on the assumption of Narayan (2009), where $BM_{fac,3,max}$=100. This can be considered as a 10 m high canopy, consisting of 1,000 branches per m^2 with a diameter of 1 cm each.

The Mendez and Losada (2004) equation requires the input of a bulk drag coefficient, density, diameter and height. The first three parameters appear as a multiplication in the formulation and can be seen as one factor. Suzuki et al. (2012) uses this multiplied factor to indicate the relative dissipation. The bulk drag coefficient is determined individually in Section 4.1.4, because it is less directly measurable compared to the other factors. Hence the Suzuki-factor without bulk drag coefficient is introduced:

$$V_{fac,i} = b_{v,i} N_i \tag{4.2}$$

For $V_{fac,3}$ this means the number of twigs times its respective diameter. By determining a vegetation factor, the uncertainty of both parameters is combined in one factor, which also appears in Eq. 2.5. This equation corresponds with 4.1 divided by the height, which is convenient because of the absence of this height in the multiplication of the model. The vegetation factor is used to study the different mangrove types. A boxplot analysis of this factor can be found in Appendix A.1.1.

The determination of the canopy height is conducted using Cole et al. (1999). In here relations between diameter and tree height for different mangroves are investigated. By using the found diameters for the stem ($b_{v,2}$), the total tree heights can be determined. Subtracting the already found root and stem height from these values, gives the canopy height ($h_{v,3}$). Subsequently the found biomass factor can be divided by this tree height in order to obtain $V_{fac,3}$. The result of the physical relationships is given in Table 4.3.

Table 4.3: Physical mangrove parameter result. S = sparse, M=medium, D=dense, r=roots and s=stems

		Roots				Stem				Canopy	
		N (r/m^2)	b_v (cm)	V_{fac} (m^{-1})	h_v (m)	N (s/m^2)	b_v (cm)	V_{fac} (m^{-1})	h_v (m)	V_{fac} (m^{-1})	h_v (m)
Red	S	15	1	0.2	0.30	0.3	20	0.06	2	0.1	10
	M	45	2	0.9	0.50	0.6	45	0.27	5	1.1	12
	D	70	3	2.1	1.00	0.9	75	0.68	8	4.5	12
Black	S	45	0.5	0.2	0.15	0.1	10	0.01	1	0.5	9
	M	120	1	1.2	0.40	0.4	25	0.10	3	0.5	11
	D	240	4	9.6	0.80	1.1	70	0.77	8	7.7	13

4.1.2. Pioneer trees

Horstman et al. (2014) measured developed and relatively large mangrove trees till 2 meter height (see Section 4.2), while Narayan (2009) came up with multiple 3-layered mangrove trees. By integrating the vegetation factors of both studies and those in Table 4.3 over the first two meter, Figure 4.3 is obtained. It illustrates the large differences in imposed vegetation sets. Especially the found dense variants are out of range with Horstman et al. (2014). Therefore these variants are not considered to represent the developed mangroves well.

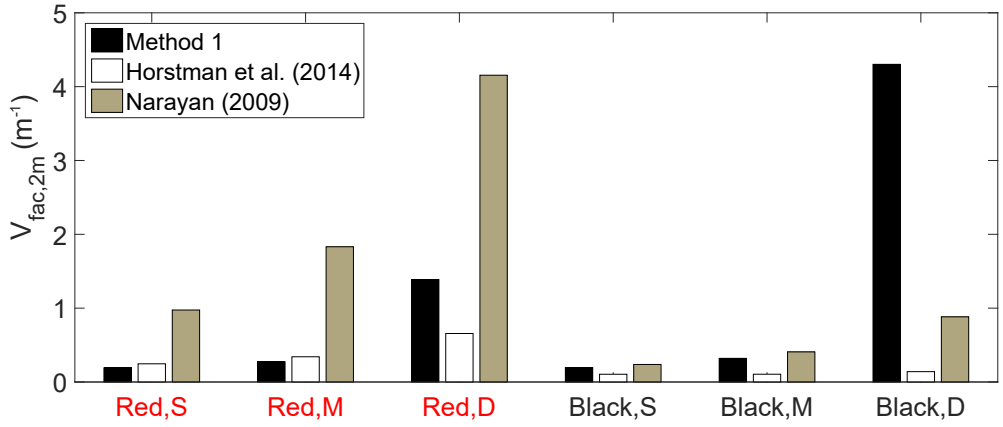

Figure 4.3: Vegetation factor integrated over the lower 2 meter according to Table 4.3 and Narayan (2009). Horstman et al. (2014) is after adjustment by Hendriks (2014)

Whether the used values in Method 1 hold for coastal or riverine mangroves is often not described in the literature. These types of mangroves can significantly deviate in dimensions. Namely, coastal (pioneer) mangroves are exposed to harsher conditions and are therefore not always able to grow to considerable heights. This in contrary to the more land-inward mangroves, where the conditions are milder and sufficient nutrients from rivers are supplied to grow extensively.

The pioneer mangroves can be very dense, but their height remains limited (Figure 2.1). Therefore the characteristics of the dense, Red mangrove is used to represent young pioneer trees. In here the vegetation height is adjusted to a 1 m root layer and 2 m canopy layer (Brunt and Davies, 2012). This means that no stem layer is applied.

4.1.3. Vertical layering

As can be observed in Figure 2.1, the vertical variability of a mangrove tree can be very high. This hold especially for developed Red mangrove trees. The current schematization of a mangrove tree consists of three layers. This implies that the depth can greatly influence the wave dissipation:

1. A larger depth is accompanied with more submergence of a certain layer, which means that more tree surface contributes to the dissipation.
2. The wave orbital velocity at a certain vertical location *z* decreases for increasing water depth (Eq. 2.7), implying that less dissipation occurs at *z*.

The calculation of dissipation in XBeach is implicitly based on a wave orbital velocity calculated from linear wave theory. This means that the orbital velocity at the water surface is high and decreases towards the bottom according to a hyperbolic function (Eq. 2.7). In XBeach is no distinction made for different layers. In reality it is expected that the wave orbital velocity profile depends on the dissipative qualities of the mangrove parts (see Figure 4.4). This might cause a deviation between simulation and reality.

In order to represent the vertical variation of a mangrove tree better, more than three layers are imposed. This is done by gradually increasing the vegetation factor. The method of vertical layering is presented in Appendix A.1.2.

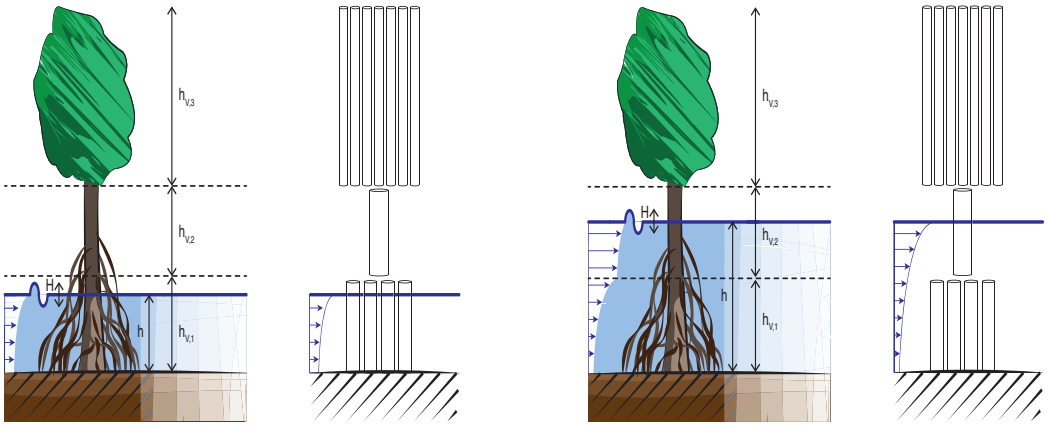

Figure 4.4: Difference in wave orbital velocity as function of depth between reality and XBeach model for only root submergence (left) and partially stem submergence (right)

4.1.4. Bulk drag coefficient

The method to describe the bulk drag coefficient is different for varying studies (2.3.1). Suzuki et al. (2012) did an attempt to parametrise the drag coefficient for rigid cylinders and found a relation between bulk drag coefficient, relative spacing and wave orbital velocity. Combining equations 2.6, 2.8 and 2.9 results in the dimensionless parameter, given in Figure 2.4, as:.

$$\frac{2a}{S} = 0.3\hat{u}T\sqrt{N} \tag{4.3}$$

Equation 4.3 is considered only to be valid for (mostly) rigid layers, i.e. roots and stems. Based on the inputs, $\tilde{C}_D$ of these layers will be variable for both different hydrodynamic conditions as mangrove characteristics. This approach is assumed to apply for $0.6 \leq \tilde{C}_D/C_D \leq 1.0$, implying that values lower are set to 0.6. Additionally, C_D=1.0 (presented as $C_{Dsingle}$ in Figure 2.4), which is accurate enough for a single rigid cylinder.

The bulk drag coefficient of the canopy is determined under the assumption that this value should be lower than those of the root and stem layer, due to its flexible branches. For the sake of simplicity $\tilde{C}_{D,canopy}$=0.5.

4.1.5. Final vegetation sets

The applied analysis to determine representative vegetation sets for Red, Black and pioneer mangroves, appears to result in a high accuracy of mangrove dimensions. However, this 'apparent accuracy' does not necessarily describe wave attenuation correctly. The dimensions and bulk drag coefficients can still deviate significantly and in order to exclude this apparent accuracy, the numbers are rounded and the amount of vegetation sets are limited to 3 sets of typical mangroves. Additionally, the sparse variants in Table 4.3 are considered to be too low, which is confirmed with wave attenuation simulations in Section 5.1.2. Finally, due to lacking valid canopy data, this layer has the same vegetation factor and height for all variants in order to avoid differences in wave attenuation. The final vegetation sets are (see also Figure 2.1):

1. Large Red mangroves, characterized by a strong vertical variation due to their stilt roots.
2. Large Black mangrove, presented as a low pneumatophores layer, but well developed stem and canopy.
3. Young pioneer trees, determined by the dense red mangrove values from Table 4.3, with adjusted height.

The classification of three representative mangrove types is assumed to cover the diverging densities of mangrove trees. The eventual, vertical layered mangrove trees are presented in Figure 4.5.

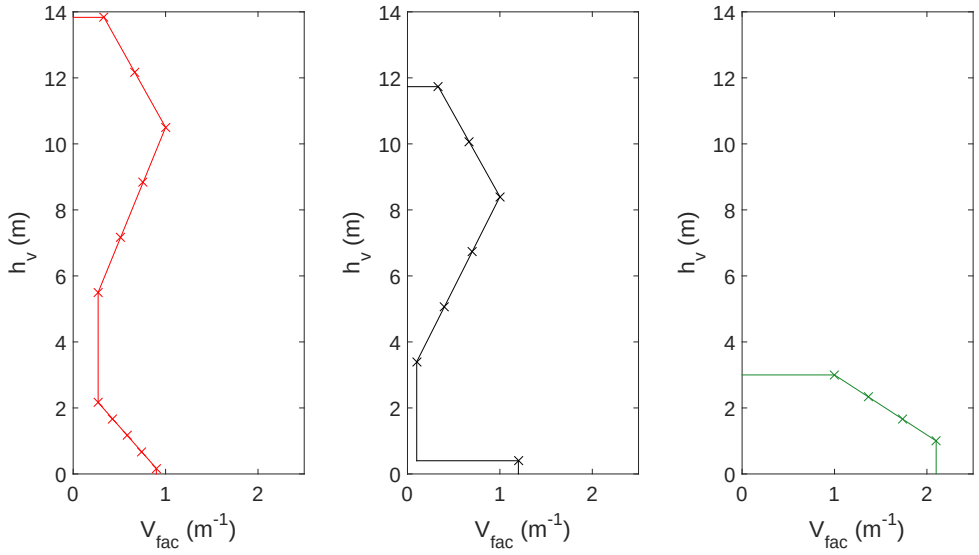

Figure 4.5: Eventual implementation of mangrove tree types. From left to right: Red mangroves, Black mangroves, pioneer trees. Crosses represent the layers

4.2. Method 2 - Calibrated bulk drag coefficient

In Method 1 multiple studies are used, global representative mangrove sets are found and the bulk drag coefficient is calculated in advance. In Method 2 this is the opposite: study location specific mangrove data is used, locally applicable mangrove sets are found and the drag coefficient is determined by calibration. Horstman et al. (2014) measured both mangrove dimensions as wave heights at different locations in a mangrove forest. He did this for two locations in Thailand: Kantang and Palian. At these locations sparse Avicennia and Sonneratia populations were found at the seaward side of the mangrove forest and dense Rhizophora at the landward side. This is assumed to represent Black and Red mangroves respectively. The zonation in Kantang and Palian coincides with the pattern presented in Section 2.1.2 for Indo-Pacific regions. Hendriks (2014) subsequently calibrated the bulk drag coefficient with this data.

4.2.1. Physical parameters

Horstman et al. (2014) measured at five different heights from the bed. Therefore, Hendriks (2014) came up with a 5 layer schematization, given in Table 4.4. This layer schematization does not distinguish the distinct vertical layers (roots, stems and canopy) in a mangrove tree. Instead it focusses on the found dimensions at the different heights. It can be observed that at higher locations above the bed the Rhizophora tree has more roots than the Avicennia, because stilt roots usually reach higher than pneumatophores. However, more pneumatophores were found than stilt roots at the bottom. Disadvantage of the data is that it reaches till a height of 2 m and no canopy data is included. This is not a problem if the depth does not exceed this limit, but can significantly underestimate wave height reduction in extreme situations. The values are considerable lower than those in Table 4.3

Table 4.4: Mangrove layer model implemented by Hendriks (2014) for six distinct mangrove areas.

		Avicennia			Rhizophora		
		TIa	TIb	TPI	TIIa	TIIb	TPII
h_v = 0.05 m	b_v (cm)	0.5	0.6	0.5	0.6	1.3	2.9
	N (m^{-2})	947	451	747	252	70	55
h_v = 0.30 m	b_v (cm)	4.3	4.8	66.0	2.7	2.4	2.9
	N (m^{-2})	0.48	0.49	0.01	15.10	25.59	54.92
h_v = 0.75 m	b_v (cm)	3.7	3.7	57.0	2.3	2.6	2.7
	N (m^{-2})	0.48	0.58	0.01	6.65	9.96	15.98
h_v = 1.50 m	b_v (cm)	3.1	4.0	66.0	3.1	2.7	3.6
	N (m^{-2})	0.48	0.43	0.0075	2.65	4.44	5.41
h_v = 2.00 m	b_v (cm)	2.1	2.8	61.0	5.1	4.4	2.1
	N (m^{-2})	0.05	0.47	0.0075	0.56	0.90	3.34

4.2.2. Bulk drag coefficient

Hendriks (2014) analysed the data, fitted multiple distribution types and finally found a relation for the bulk drag coefficient. The importance of the Keulegan-Carpenter number is mentioned, but instead of the diameter (Eq.2.6), the Mazda length scale (Mazda et al., 2006) L_e is used:

$$KC_M = \frac{\hat{u}(0)T_p}{Le} = \frac{\hat{u}(0)T_p A_p}{V - V_M} \tag{4.4}$$

The parameter A_p is the projected surface area of the vegetation within the control volume V. The volume of mangroves within the control volume is V_M. For smaller depths these values decrease, because the number of submerged layers reduce and/or the submerged vegetation height $h_{v,i}$ declines. Evidently, the control volume V also decreases for smaller depths.

Hendriks (2014) assumes the bulk drag coefficient to be the same for all layers. This implies that no distinction need to made for the orbital velocity at different layers and hence the orbital velocity at the bed is used (z=0 in Eq. 2.7):

$$\hat{u}(0) = \frac{\pi H_{rms}}{T_p \sinh kh} \tag{4.5}$$

Using the vegetation data, the model of Mendez and Losada (2004) and the wave height measurements, Hendriks (2014) determined the bulk drag coefficient by means of calibration. This implies that the found relation most likely only holds for Kantang and Palian. The parametrisation is given as:

$$\tilde{C}_D = 0.24 KC_M^{0.78} \tag{4.6}$$

The exponential trend in this relation causes a high sensitivity for low KC_M values, resulting in high bulk drag coefficients. However, the relation seems to fit the data quite well (see Appendix A.2).

5

XBeach

The wave attenuation due to the mangroves are simulated in XBeach. Main reason for using this numerical model is the inclusion of the Mendez and Losada (2004) formulation, which enables the option to add a multi-layered dissipation term. In using this model, the wave attenuation with different settings and mangrove types can be simulated. The goal of this chapter is to introduce the model set-up, map out the important parameters and check the model behaviour. Two different models are distinguished here. The first model compares different input options with measured data in order to come up with final model settings (Section 5.1). These settings are subsequently applied in the second model (Section 3.1.1), which simulates the eventual wave attenuation in different mangrove forests. The results of this model is presented in Section 5.3.2.

5.1. Model variables

Whether the found mangrove parameters match with actual measurements is compared here. Although this procedure seems to coincide with a calibration or validation, the model is considered to be a comparison of model settings. The term calibration would refer to fine-tuning of a parameter is order to match simulation with measurements. In this model does the lack of accurate data, the many made assumptions and the resulting high model uncertainty, resemble a good combination of parameters rather than an actual calibration. Namely, model inputs are compared with measurements conducted by Horstman et al. (2014), in which the wave heights are extremely low (order of centimetres). Additionally, the range of mangrove parameters is high (Chapter 4) and accurate spatial data is not present. Therefore the model is simplified to a 1D hydrodynamic simulation, meaning that also morphodynamics are not included. Because this research focusses on efficiently model wave attenuation in mangrove forests, XBeach stationary is used as default mode.

The comparison model elaborates on the validity of the vegetation sets, XBeach model modes and bottom friction. The final settings are subsequently applied in the second model. Horstman et al. (2014) measured fringing mangroves in Thailand, at two locations along the Andaman Sea: Kantang and Palian. Only the comparison with Kantang is presented in this chapter, whereas simulations in Palian can be found in Appendix C.1.1. Both study locations are also used in the case study (Chapter 6).

The two areas consist of a gradual sloping mudflat between the Andaman Sea and begin of the mangrove forest. In the forest itself, the slopes are relatively steep. In Kantang this is around 1:200 (see Figure 5.1). The measured waves are at five locations in Kantang. During the measurement campaign some sensors failed and are therefore left out of the comparison procedure. Kantang is composed of four distinct mangrove areas. In the front forest (TKIa and TKIb), Avicennia and Sonneratia species is dominantly present, while in the back (TKIIa and TKIIb) this is Rhizophora sp. According to the mangrove analysis in Section 4.1, this corresponds with Black and Red mangroves respectively.

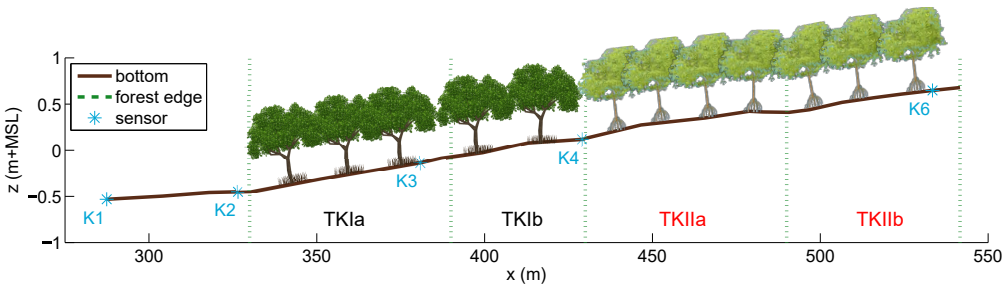

Figure 5.1: Bathymetry and sensor locations in Kantang.

5.1.1. Initial settings

The grid set-up is conducted based on the CFL-condition, which results in a non-equidistant grid. The number of grid cells for Kantang is 255. Five sensors are located here, where the wave boundary condition is provided by the most offshore sensor K1. The measurements of these pressure sensors resulted in wave heights, periods and water depths for burst lengths of around 7 min at intervals of 20 min. In the end 331 were gathered for Kantang. In this analysis 30 bursts for each location is used and subsequently averaged in order to compare the model output. As already mentioned in Section 2.3.2, the wave heights and measured in both transects are very low. For small waves, the water surface can impose a force normal to the surface due to surface tension. This would enable capillary waves to exist, which are not included in XBeach. This effect is negligible if the following holds (Holthuijsen, 2010):

$$\frac{\tau_s k^2}{\rho} < 0.0003g \tag{5.1}$$

in which τ_s is the surface-tension coefficient, k the wave number, ρ the water density and g the gravitational acceleration. Waves with a wave period of around 3 sec are measured in 1.5 m deep water, resulting in $k \approx 0.6$. For this wave number, $\tau_s \approx 0.073$ N/m, ρ=1025 kg/m^3 and g=9.81 m/s^2, this requirement is satisfied. Hence it is allowed to use XBeach, although the exact values of the wave height measurements and model results are not strictly validated.

In the initial model settings, the stationary mode is used (Section 2.3.3), no short wave friction is applied and no wave breaking is included, because Horstman et al. (2014) also did not observe breaking waves. A simulation time of 1000 sec is used, including 500 sec spin-up. Additionally, only Black mangroves are used in TKIa and TKIb and Red mangroves in TKIIa and TKIIb. This means that the pioneer mangroves from Subsection 4.1.2 cannot be compared. At first the vegetation sets are tested, both for Method 1 and 2 (Chapter 4). Next, the XBeach mode stationary and surfbeat are compared. Subsequently, the results are adjusted with the wave friction coefficient. Finally, the eventual settings presented, which are used in the representing wave attenuation model.

5.1.2. Vegetation sets

In Chapter 4 two methods are presented, which elaborate on determining representative vegetation sets. The first method uses the physical parameters from various literature and the bulk drag formulation from Suzuki and Arikawa (2010) to eventually come up with vegetation sets for Red, Black and pioneer mangroves. Because no pioneer trees were found in Kantang (nor Palian), only the first two tree types are considered. The result of the initial 3-layered sparse, medium and dense values from this analysis (Table 4.3) is presented in Figure 5.2. This means that for the sparse variant both sparse Red and Black mangroves are applied. The same holds for the medium and dense variants. Additional settings can be found in Appendix..

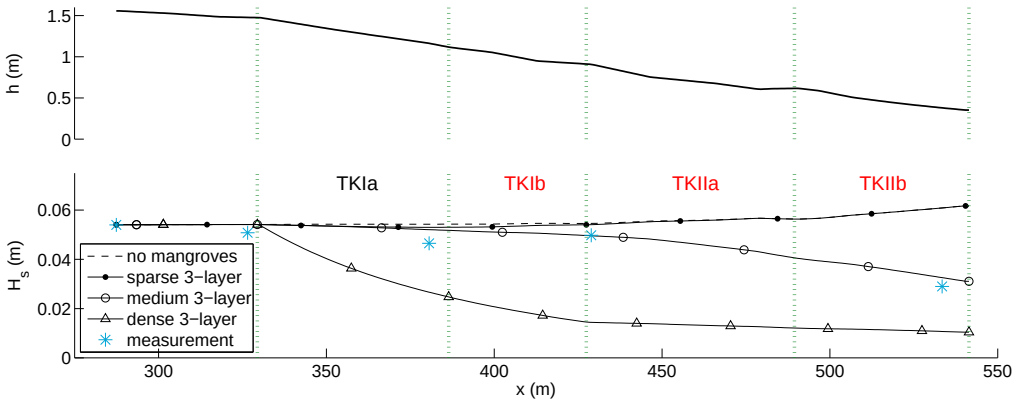

Figure 5.2: Water depth (top) and wave height](bottom) over Kantang transect with initial vegetation sets.

The measurements (blue stars) reveal that there is shoaling present. This most likely compensates for the dissipation is some areas. Especially in TKIb shoaling is present, resulting in even an increase of the wave height. XBeach also takes the shoaling into account, as can be observed from the no-mangrove simulation (dotted line). The relative dissipation in the Red mangrove area is evidently present, which confirms the theory that the stilt roots are better in dissipating waves than the small pneumatophores. The XBeach simulations (black lines) for different densities clearly differ significantly in this dissipation. As Figure 4.3 already suggested, it appears that the simulated sparse variant is too small (almost the same as no mangroves) and the dense variant too large. The medium variant seems to match the measurements quite well. However, it is expected that the water depth is favourable for this vegetation set. This implies that a small depth change, which causes the dissipation to take place in a different layer, can give a different result. Therefore more than 3 layers vegetations are simulated (Subsection A.1.2). Additionally, the vertical adjustment to the vegetation sets is assumed to represent the vertical variation better. Namely, the Red mangrove is characterized by a decreasing density of roots from bottom to top, while the Black mangrove mainly has pneumatophores, reaching to a certain height. It is noted that a better match with measurements does not directly mean an improvement of the model, because of the many uncertainties. Main reason for the vertical layering is decreasing the dependency on water depth, which might mean an improvement for other locations, where the depth is different than this location.

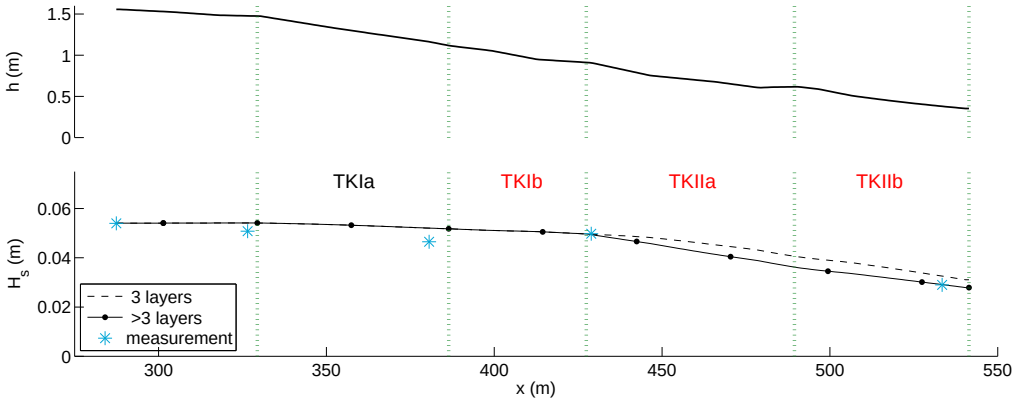

Figure 5.3: Water depth (top) and wave height (bottom) over Kantang transect with initial medium vegetation set and layered set.

The vertical layering in this simulation only affects the dissipation in the Red mangrove area. This can be explained by the depth of 1-1.5 m in which the mangroves are located. The layering at this height is unchanged for Black mangroves, while it is certainly different than the initial set for Red mangroves (Figure 4.5). Although more than 3 layers improves the comparison between measurements and XBeach simulation, this is not directly considered as an improvement (see above). However, at other depths this might be different.

Final comparison is made for Method 2 (Section 4.2). This approach makes use of the actual present mangrove data in Kantang. Subsequently the relation for the bulk drag coefficient is used. Due to the significant smaller physical characteristics of the mangroves used in this method, the $\tilde{C}_D$ is much higher than in Method 1. No bottom friction is applied in the model of Hendriks (2014), implying that the calibration of the bulk drag coefficient also include the dissipation by the bottom.

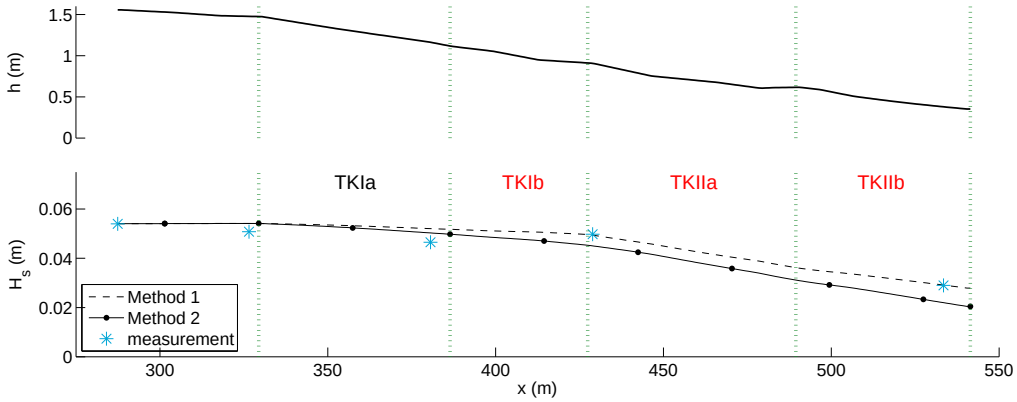

Figure 5.4: Water depth (top) and wave height (bottom) over Kantang transect with layered medium vegetation set (Method 1) and Method 2

Method 2 gives slightly lower results over the mangrove areas than Method 2. A reason might be the inclusion of bottom friction, but it is again mentioned that this argumentation might be too rough for the large uncertainty in this comparison study. Although Method 2 gives reasonable results, Method 1 is used in further calculations, because the focus is on developing a global applicable method rather than a calibration study. Additionally, it is considered that Method 2 is performing less in case of higher hydrodynamic conditions, because of the exclusion of canopy data. Additionally, the performance of the bulk drag coefficient relation to other areas is not tested yet. Nonetheless, the approach can be used for local studies.

5.1.3. Stationary and Surfbeat

In Section 2.3.3, XBeach's stationary and surfbeat modes are presented. In the former mode, the incoming wave at the boundary is stationary, implying that over time no difference occurs in the condition at this location. Due to the absence of shorter high-frequency waves, the long wave generation is not involved in the calculation. However, Phan et al. (2014) found that the long waves are able to penetrate a mangrove forest more easily than the short waves. Also Horstman et al. (2014) found an increase in wave periods along the transect, implying that the short waves are filtered out and long waves can still exist after a few meter mangrove forest. The long wave periods of these waves contribute significantly to the flood hazard of the hinterland. Hence, the determination of long waves in flood hazard calculations for vegetated foreshores is interesting. However, due to the limited amount of useful data, only the short waves are determined in this research. Additionally, this research focusses on efficiently determining the wave attenuation in a mangrove forest as part of a quick assessment tool, implying that XBeach stationary is more convenient. Nonetheless, the model modes are compared to illustrate the difference.

Surfbeat is able to calculate the long waves, due to the imposition of a spectral wave boundary condition. The difference in stationary and surfbeat mode in XBeach concerning wave heights is that the former uses the root-mean-square and latter the significant wave height, H_{rms} and H_{S} respectively. For a Rayleigh distribution, these values are related as follows:

$$H_S = H_{rms}\sqrt{2} \tag{5.2}$$

Besides the description of the wave boundary condition, all settings are the same for both simulations. This means that no friction is (yet) included and the same vertical varying vegetation sets are used. Goal of the comparison is purely to map out the difference in wave heights between both modes.

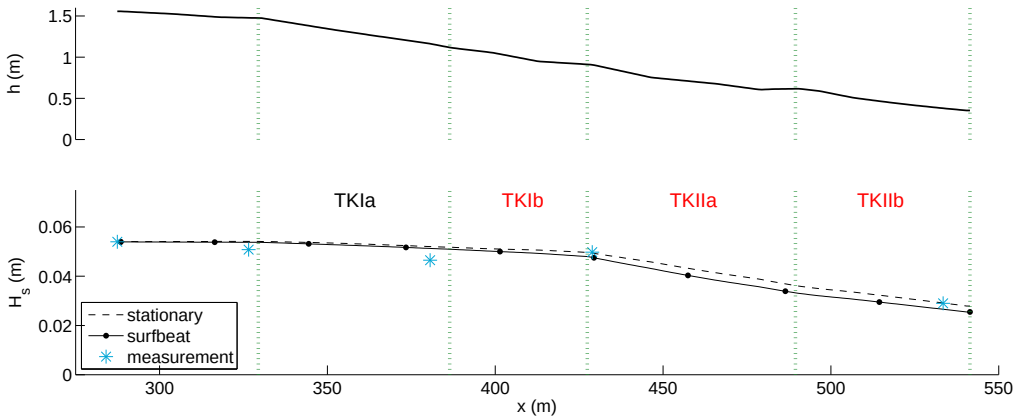

Figure 5.5: Water depth (top) and wave height (bottom) over Kantang transect for stationary and surfbeat modes.

Figure 5.7 illustrates the wave heights along the Kantang transect for the two XBeach modes. Surfbeat mode results in lower wave height for the dissipated simulation. A reason could be that the included longer and higher waves are dissipated more by the vegetation. Due to the non-linearity of the wave height in relation to dissipation (Eq. 2.5), these waves are dissipated more. Overall are the differences between both modes not significant and or of minor importance relative to the other many made assumptions in this research.

Stationary mode efficiently solves the short wave action balance (Eq. 2.11) for one wave intrinsic frequency. In surfbeat, in which the calculation time is a larger, an energy density spectrum is imposed, which eventually is represented by one spectral frequency. This means that no spatial variation of the wave period is calculated (Figure 5.6). These wave periods are interesting for flood hazard calculations (for example wave overtopping). Knowledge about the behaviour of wave period under the presence of vegetation is not well understood yet. Hence, wave period evolution are not considered in this research. Nonetheless, XBeach non-hydrostatic mode (Section 2.3.3) can be used if this parameter is important for a research.

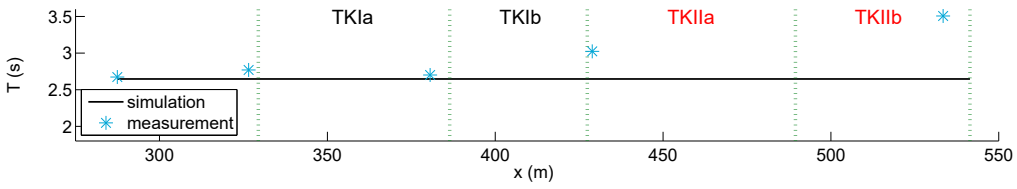

Figure 5.6: Wave period over Kantang transect.

5.1.4. Friction coefficient

Next to the dissipation of wave energy due to mangrove vegetation, also the friction exerted by the bottom is able to decrease wave heights. This contribution is most likely lower than the mangrove's, but may not be neglected in further calculations. The dissipation due to bottom friction on short waves for stationary simulations is formulated as follows in XBeach (see also Eq. 2.11):

$$\langle \tilde{D}_f \rangle = 0.28 \rho f_w \hat{u}_0^3 \tag{5.3}$$

in which f_w represents the Johnson friction factor of the bed shear stress (Deltares, 2015). Due to the inclusion of the wave orbital velocity $\hat{u}_0$ in this formulation, the bottom friction is also influenced by the height above the bed (z in Eq. 2.7). In Figure 5.7 it can be observed that there exists some wave attenuation in the section in front of the forest (before x=330 m). This is probably caused by the bottom friction, although there might be some vegetation present too. The uncertainty of the properties of this area can be covered by increasing the friction factor (Figure 5.7).

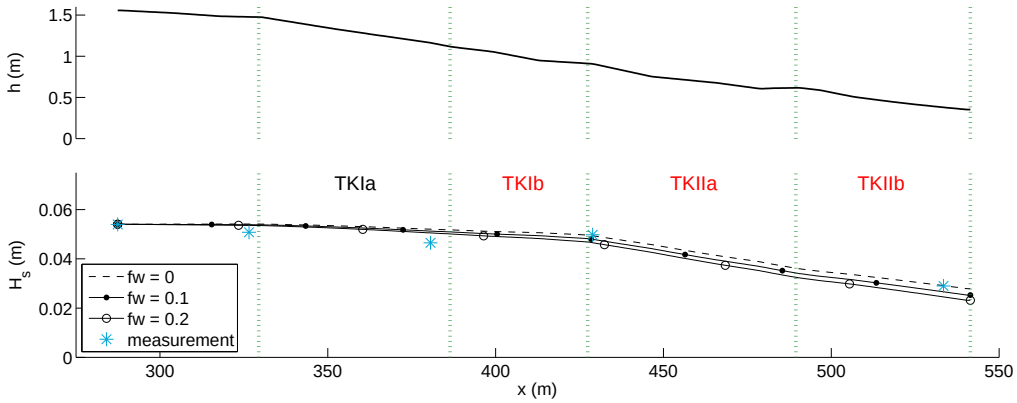

Figure 5.7: Water depth (top) and wave height (bottom) over Kantang transect with different bottom friction coefficients.

It can be observed that a friction factor causes a better match for some measurements, but also decrease for other measurements. Because it is expected that some friction is present due to bottom friction and leaf litter, a friction factor f_w=0.1 is applied in further calculations. As reference, a friction factor of 0.06 was applied for sandy beaches in Van Dongeren et al. (2012).

5.2. Model set-up

This research merely focuses on the short wave attenuation. Hence the hazard reduction due to mangroves is directly linked with the dissipation of short waves. This means that the quantified decrease of waves in a mangrove forest is a measure for hazard reduction. Goal of the model is to give an indication of the influential factors for wave attenuation in a mangrove forest and map out the effectiveness of certain forest types. The factors which are expected to influence wave attenuation the most, are slope, tidal range, depth, wave height and forest type. The settings from the previous section are used as default values. This means that XBeach stationary (simulation time 1000 sec, spin-up 500 sec) with the layered medium mangrove variants are used. Additionally, a friction factor fw=0.1 is used.

In this section the model settings of the profile (grid), forest types and hydrodynamics are given for:

1. Parameter sensitivity (PS). One value is changed each simulation in order to see its influence on wave attenuation. This means that some values are larger than they in reality would be, solely to determine their effect.
2. Hazard model (HM), which is similar to the sensitivity model except more realistic values and relations are used in order to come up with a required forest width.

5.2.1. Profile

Often the slope in front of a mangrove coast is relatively mild. In the forest itself the slope i_b increases. This slope can deviate from coast to coast and largely determines the type of mangrove forest. Horstman et al. (2014) found a slope of 1:200 and 1:150 in Kantang and Palian respectively and Das et al. (2011) assumes an upper limit of 1:500. The forest width at which this slope is present is called the front forest $B_{w,f}$. It is also determined by the tidal range (*TR*) in the area. Namely, as presented in Subsection 2.1.2, the typical mangrove trees exists at elevations between low and high tide. The front forest width is considered to be a function of tidal range and slope:

$$B_{w,f} = TR \cdot i_b \tag{5.4}$$

This means that a maximum front width of approximately 1.5 km (*TR* 3 m, 1:500 slope) can be found. However, larger forest widths are also observed, reaching over more than 5 km. The trees in such back forests are less frequently submerged. The presence of a river or a seaward expansion of the coast might be the cause of their existence. Hence it is expected that the trees in this area are already more developed (see Section 5.2.2). The slope in this area is assumed to be horizontal. In the hazard model a total transect width of 2 km respectively is used. This thus consists of a front forest (Eq. 5.4) and back forest (2 km-$B_{w,f}$), illustrated in Figures 5.8 and 5.9. The length of the transect in the sensitivity analysis is set to 1 km. An equidistant grid with steps of 1 m is applied.

5.2.2. Forest types

In Subsection 2.1.2 the different zonation types of mangroves are presented. It appears that this zonation depends on many factors, which cannot all be included in this research. Hence this zonation is simplified and assumed to only be influenced by tidal range and bottom slope. The abbreviation FT refers to the forest type from now on. The different mangrove forests are presented below.

Young pioneer forest (FT1)
This forest is represented by pioneer trees half way the front forest and larger Red mangroves on the other half. In the back forest are (less dissipative) Black mangroves located, illustrated in Figure 5.8. This zonation often agrees with the typical mangrove patterns in Florida and the Caribbean (Feller and Sitnik, 1996). It is noted that the height of the trees in the figure do not necessarily coincide with the tidal levels and water depth.

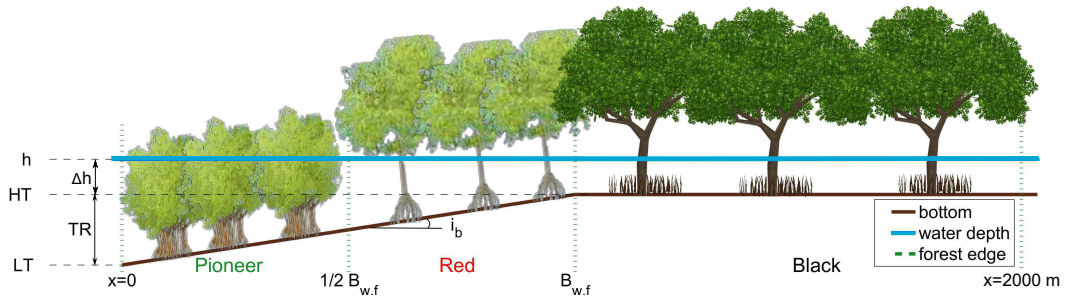

Figure 5.8: Young pioneer model transect. h=water depth, HT=high tide and LT=low tide

Old mangrove forest (FT2)
Examples of this type of forests are Kantang and Palian. Black mangroves cover the first half of the front forest and Red mangroves dominate the other part of the sloped transect. Also here are Black mangroves placed in the back forest.

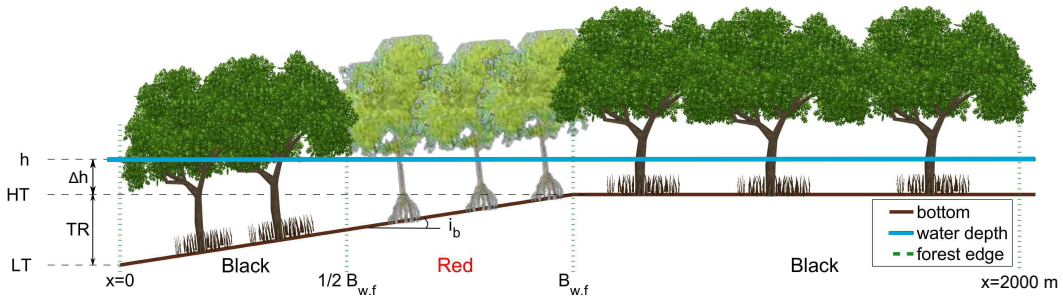

Figure 5.9: Old mangrove forest model transect. h=water depth, HT=high tide and LT=low tide

5.2.3. Hydrodynamics

The field studies which have been conducted in mangrove areas, measured no waves higher than 40 cm. The effect under more extreme conditions is therefore not clearly understood yet. Hence the hydrodynamic conditions in the simulations are considered to be extreme for the sheltered mangrove areas. That is the reason that the water depth, presented in Figures 5.8 and 5.9, exceeds the tidal range in the concerned model area. In the hazard model the following relation is assumed for the depth at x=0:

$$h_0 = TR + \Delta h \tag{5.5}$$

in which Δh is the surge on top of high tide. This surge is assumed to be around 0.5-1.0 m. Additionally, a tidal range of 1-2 m is applied (see Appendix B.4), resulting in a maximum depth of 3 m. In the sensitivity analysis this maximum depth is 4.5, because the influence of the depth is simulated. Incoming wave heights H_0 are larger than 40 cm, because extreme situations are modelled. The corresponding wave period is determined according to Journèe and Massie (2001):

$$T_p = 5.946 \cdot \sqrt{H_{rms}} \tag{5.6}$$

Table 5.1: Model settings for various parameter sensitivity (PS) runs (slope, tidal range, depth and wave height) and for the hazard model (HM). L_t=length of transect

		$1/i_b$	TR (m)	$B_{w,f}$ (km)	L_t (km)	h_0 (m)	H_0 (m)
PS	slope	200,300,500	2	0.4	1	3.5	0.5
	TR	250	2,2.5,3	0.75	1	3.5	0.5
	depth	250	2	0.5	1	3.5,4,4.5	0.5
	wave height	250	2	0.5	1	3.5	0.5,1,1.5
HM	-	250,500	1.5,2.5	Eq. 5.4	2	Eq.5.5: Δh=1, 1.5	0.5,1

5.3. Model results

The model results for the settings presented in Table 5.1 are presented in this section. First the parameter sensitivity gives the influence of the each settings. Furthermore, the final hazard model is elaborated along with the influence of potential forest width changes.

5.3.1. Parameter sensitivity

This section elaborates on the influence of input parameters on wave attenuation. Equations 5.4 and 5.5 do not hold in these models, because in this case two different parameters are changed, while the influence of individual inputs is researched. However, it is used in Subsection 5.3.2, where the eventual contribution to hazard reduction is determined. It is noted here that water depth changes due to set-up and set-down are negligible in these simulations and hence only one water depth simulation is given for the two forest types. The input parameters can be found in Table 5.1.

Slope
Only the slope of the front forest is varied here. A sloped profile of 1:200 and *TR*=2 m determine the $B_{w,f}$ (=400 m). This width is subsequently applied in the other slope simulations in order to exclude a comparison with different front forest widths. The result is given in Figure 5.10.

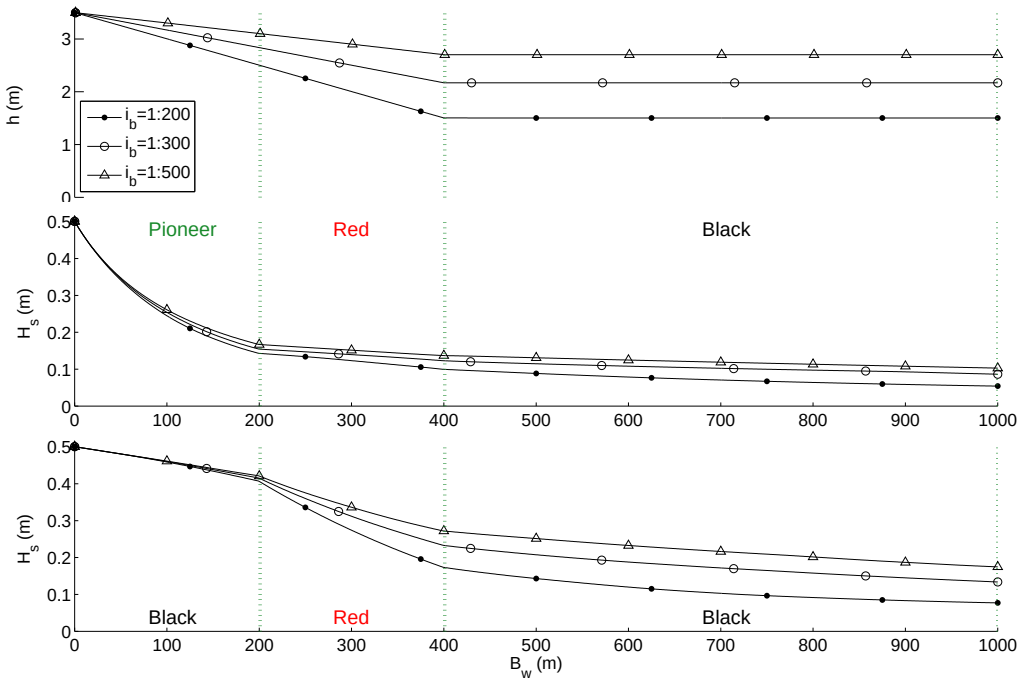

Figure 5.10: Water depth (top), wave height FT1 (middle) and FT2 (bottom) as function of forest width for different front slopes

Varying the slope affects the depth and thus the wave attenuation. This effect is clearly more visible for the Red mangroves due to their vertical varying structure. The opposite holds for the pioneer type and Black mangroves. The reason is that the former does not vary significantly over its vertical and the latter only has an dissipative root layer, which is located much lower (0.4 m) than in the simulations.

Tidal range
The effect of the tidal range is visible in the dominant presence of certain mangrove types in the coastal zone. Evidently some types appear to be more resistant against the salty rising water during flood periods than other types. A default profile is assumed based on the slope and the maximum tidal range (*TR*=3 m, so $B_{w,f}$=750 m). Subsequently the different tidal ranges determine which species populates which part of the front slope. In this way, not different front forest widths are reviewed, but only the

effect of *TR* on zonation. The result is presented in Figure 5.11. For the sake of clarity, the forest edges are left out of the figure.

The effect of different tidal ranges becomes clear after the first mangrove type changes (x= $\frac{1}{2}TR \cdot i_b$=250 m). For forest type 1 this means that the waves are attenuated less because pioneer trees dissipated more than the Red mangroves. For FT2 the opposite holds, in which the Red mangroves dissipate more than the Black mangroves. Overall the effect of changing tidal range is not significant.

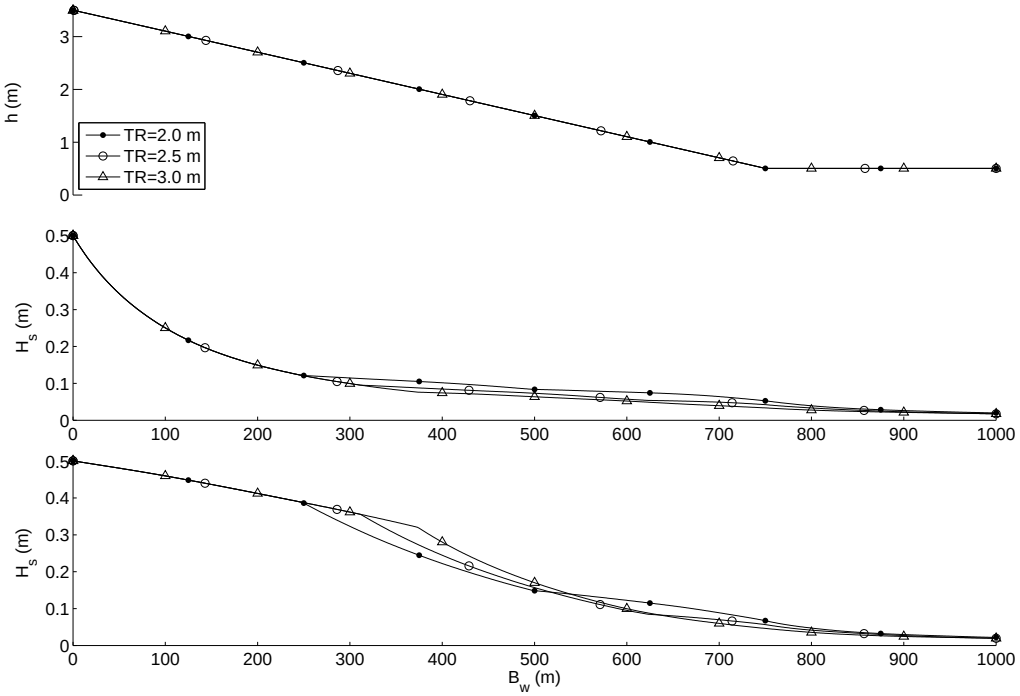

Figure 5.11: Water depth (top), wave height FT1 (middle) and FT2 (bottom) as function of forest width for different tidal ranges

Water depth

The largest difference between FT1 and FT2 is clearly visible in the pioneer area (Figure 5.12). These mangroves are already submerged at *h*=3 m and hence an increase of water depth results in a decrease of relative attenuation. It can also be observed that hardly any reduction takes place for FT1 in the Red mangrove area and higher waves do not cause more dissipation. Apparently the larger water depth compensates for increasing wave attenuation. This underlines the importance of the water depth. Finally, the effect of sudden wave height changes for different water depths is excluded by imposing the vertical layering (for Red mangroves especially).

Wave height

The initial wave height (H_0) is interesting to investigate because in the field studies no extreme wave heights were observed. Hence the ranges of the wave attenuation rate *r* (Eq. 2.10) varies between 0.004 m^{-1} and 0.02 m^{-1} for H_0=1.5 m in the pioneer transect (Figure 5.13). This is high, but not unrealistic (see Table 2.2). Due to the strong decreased wave heights in the pioneer area, the Red and Black mangroves can hardly contribute to wave attenuation. This in contrary to FT2, in which the front forest Black mangroves dissipate much less wave energy and therefore the Red mangroves behind the Black mangroves also contribute to the dissipation. In the lower figure, the larger dissipating effect of the Red mangroves is clearly visible. The initial wave height largely influences the wave dissipation, which can be explained non-linear relation between both (Eq. 2.5).

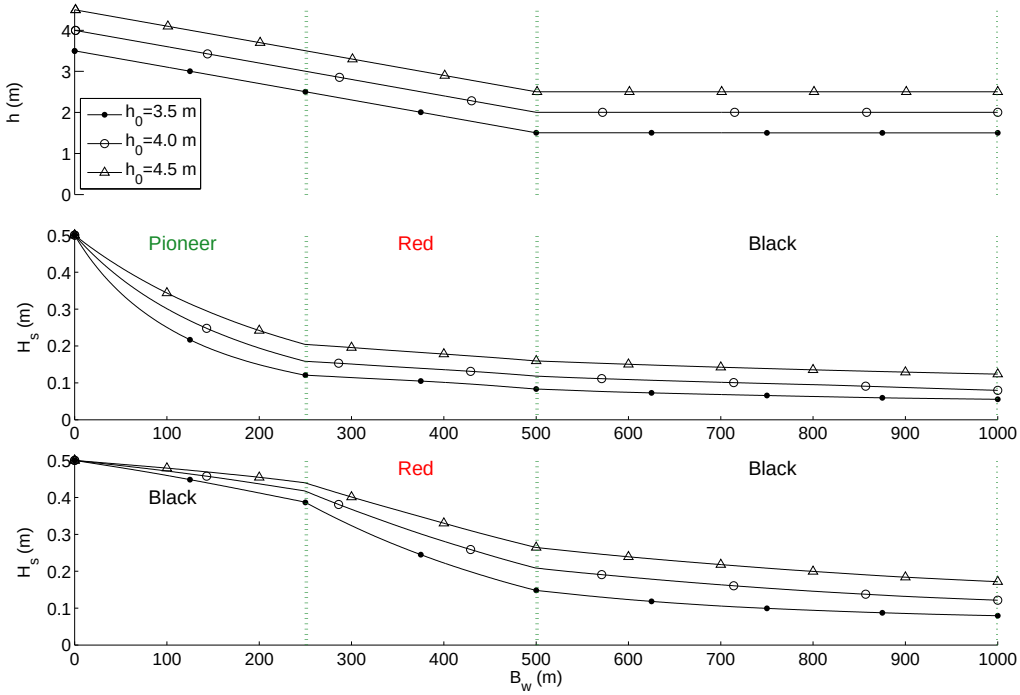

Figure 5.12: Water depth (top), wave height FT1 (middle) and FT2 (bottom) as function of forest width for different water depths.

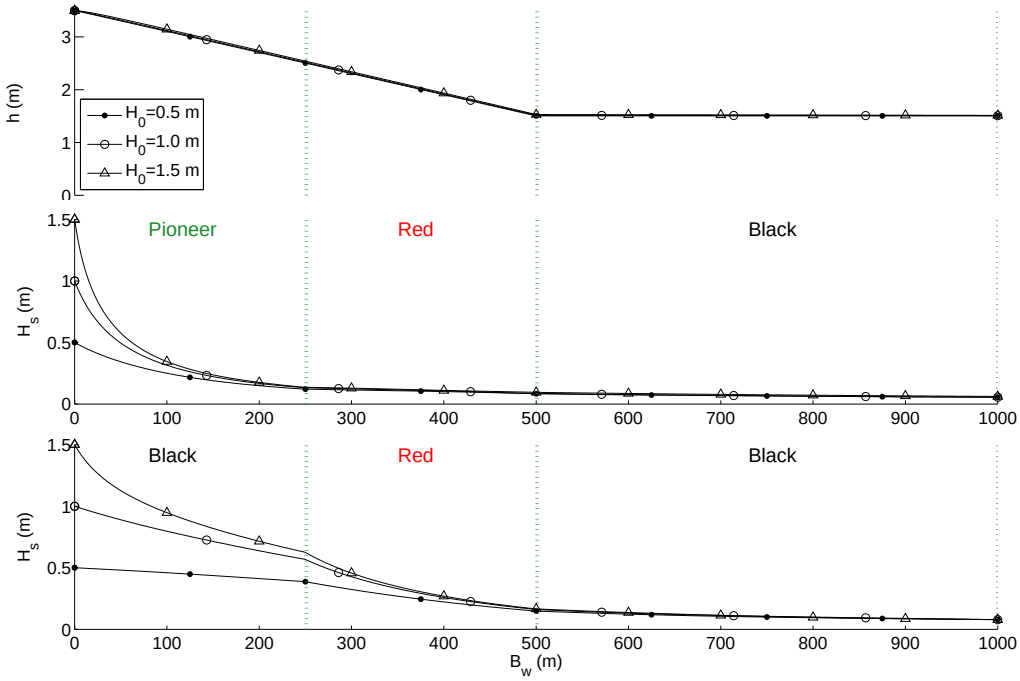

Figure 5.13: Water depth (top), wave height FT1 (middle) and FT2 (bottom) as function of forest width for different initial wave heights.

5.3.2. Hazard model

As stated in Chapter 1, the hazard solely depends on the wave height attenuation in this research and is expressed in forest width. This means that a level of hazard need to be imposed at the landward edge of a mangrove forest. Tung et al. (1999) found a collapse of breakaway walls at wave heights between 0.3 and 0.6 m. This is according to relatively high standards applied in the US. Hence, H_s=0.2 m is used here, under the assumption that the houses in the areas concerned are of less quality. It is noted that this is a very low wave height and can almost be considered to be zero. In case a levee or different kind of flood protection is in place, the wave height that leads to a hazard can be determined from a wave overtopping calculation. Goal of this section is to estimates required forest widths (default case) and to evaluate on the effect of changes in width.

Required forest width: the required cross-sectional mangrove vegetated coastal zone in which the wave height at the end of the forest is reduced to 0.2 m. *Comment: this value is an assumption and an acceptable wave height should be determined locally.*

Default case

In Section 5.3.1 the effect of slope, tidal range, water depth, wave height and forest type are discussed. Every parameters is varied twice in order to come up with a required forest width (Table 5.2). In contrary to the simulations conducted in the sensitivity analysis, Eq. 5.4 is used here, implying that different profiles are compared with each other. Equation 5.5 is used to obtain representative water depths.

Table 5.2: Required forest width $B_{w,req}$ in meters for different parameters and forest types for a reduced wave height of 0.2 m. i_b=slope, TR=tidal range, Δh=surge height, H_0=wave height at x=0, FT1=young pioneer forest type and FT2=old forest type

i_b (-)	1:250								1:500							
TR (m)	1.5				2.5				1.5				2.5			
Δh (m)	1		1.5		1		1.5		1		1.5		1		1.5	
H_0 (m)	0.5	1	0.5	1	0.5	1	0.5	1	0.5	1	0.5	1	0.5	1	0.5	1
$B_{w,req}$ FT1 (m)	78	99	103	129	140	168	193	219	82	104	109	137	156	186	222	248
$B_{w,req}$ FT2 (m)	262	280	331	355	446	472	527	556	415	436	500	530	719	750	832	864

In Section 5.3 it was already confirmed that a steeper slope, smaller tidal range, depth and initial wave height results in smaller wave heights at the end of the mangrove forest. This is confirmed by Table 5.2 in which smaller reduced heights coincide with narrowed required forest heights. For most conditions, the forest width is around 100-450 m, although for very unfavourable conditions a width of 900 m is required to attenuate waves to 0.2 m height.

Forest loss

The mangrove forests are one of the world's most threatened tropical ecosystems. Human activities are most often the cause of these treats. Direct examples are the deforestations for tourist, aquaculture and agriculture purposes. River dams, climate change, overfishing and pollution are indirect triggers for the rapid degradation of the global mangrove population.

The effect of losing 20% of the required forest width is simulated here for a default case. A 1:250 profile, TR=2.5 m, Δh=1 m and H_0=0.5 m are used. This means that a 140 m and 446 m (Table 5.2) required forest width is losing 30 m and 90 m respectively. The forest loss types are (Figure 5.14):

- Deforestation caused by expansion of agricultural and/or aquacultural terrain or other land use planning. Some countries maintain a greenbelt policy, implying that ongoing deforestation is limited by minimum remaining width (Section 2.1.3). This type means a landward loss of forest.
- Erosion, which can be the consequence of changing hydrodynamic conditions (climate change) or human activity. It is mentioned that possible changing hydrodynamics are not considered, only the loss of forest. This type means a seaward loss of forest.

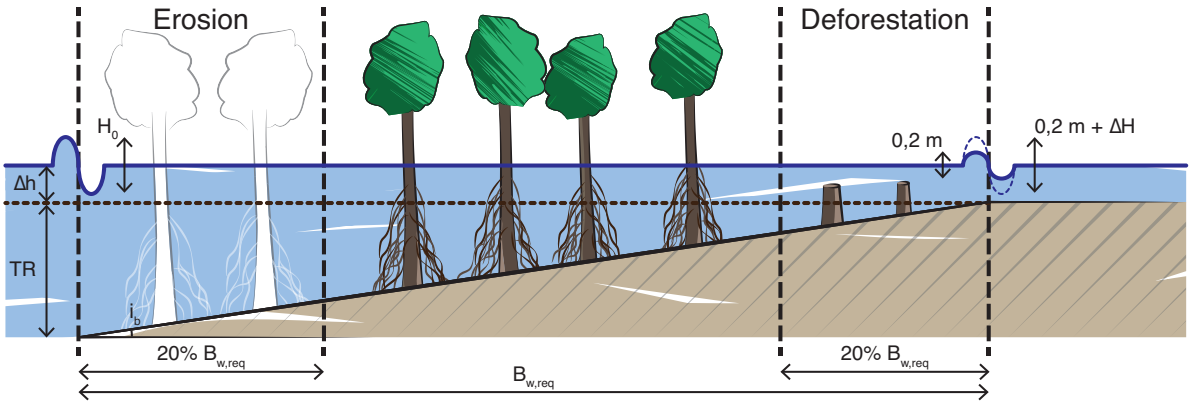

Figure 5.14: Considered types of forest loss.

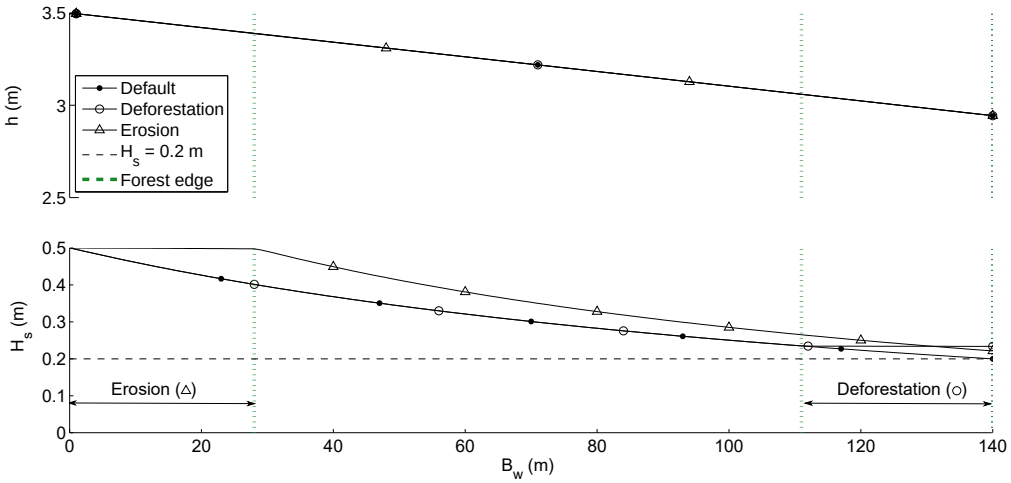

Figure 5.15: Water depth (top) and wave height (bottom) FT1 as function of forest width for the base, 20% deforestation and 20% erosion cases.

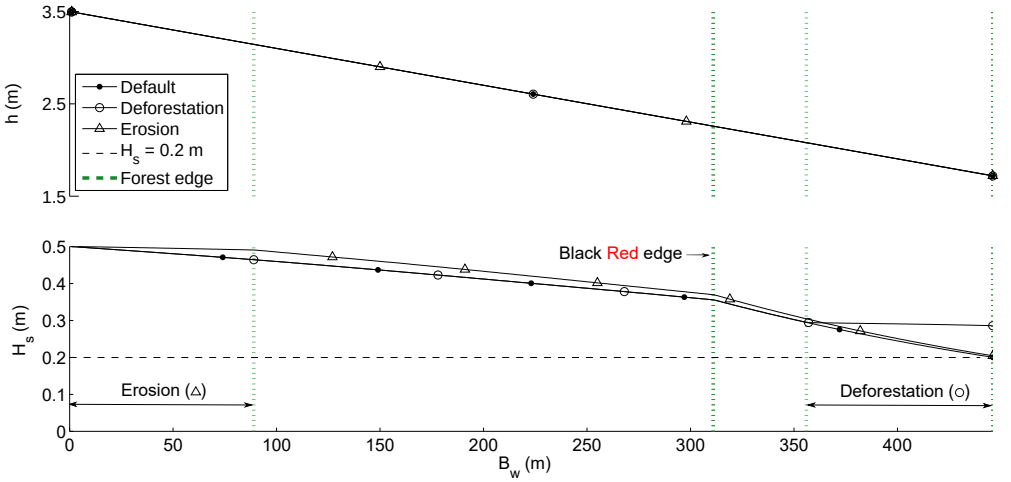

Figure 5.16: Water depth (top) and wave height (bottom) FT2 as function of forest width for the base, 20% deforestation and 20% erosion cases.

From Figures 5.15 and 5.16 it can be observed that the wave height increase is larger for deforestation than for erosion. For a non-sloping frictionless profile the wave height would exactly be the same for erosion and deforestation. However, due to the imposed slope, the wave heights also reduce by breaking and friction. Hence the waves are higher at the begin of the transect than at the end of the forest. Due to the strong dissipation for higher waves, the loss of forest is compensated after a certain distance. If this distance, i.e. loss of forest is longer, also the difference between deforestation and erosion increases. The wave height increase for the other simulations can be found in Appendix C.2

6

Case studies

In the previous chapters are the separate steps to determine the wave height reduction by mangroves elaborated. SWAN can be used to increase the accuracy of nearshore conditions and XBeach to simulate the dissipation in the mangrove forest. The reduced wave height would represent the hazard, which is assumed to be present for significant wave heights higher than 0.2 m (see Section 5.3.2). This assumption is based on the critical wave height for low-quality breakaway walls.

In this chapter, this procedure is the other way around. The current forest width is reviewed and used in XBeach. The positions in or behind the forest where the wave height is 0.2 m, is compared with the location in the case study. Goal of the chapter is to indicate whether the combination of SWAN and XBeach for mangrove areas can be applied for flood hazard determination in real situations. Additionally, the different case study locations are selected such that the hydrodynamics, mangrove forest types and potential danger for hinterland, deviate among those areas. Hence, a locations with a large range in hydrodynamic conditions between storm return periods, an area with distinct mangrove zonation and a case study with a populated region directly behind the forest are chosen. The sequence of determining the wave height reduction by mangroves for the concerning study locations is as follows:

1. The model area, respective ERA-Interim boundary conditions, forest width[1], bathymetry[2], surge levels[3] and tidal range[4] are determined.
2. A peak-over-threshold method is applied in order to calculate wind and wave conditions accompanied to a return period (Section B.3).
3. SWAN is used in 2D mode to simulate nearshore hydrodynamic conditions for a certain return period.
4. A 1D stationary XBeach model is set up using the simulated nearshore conditions in order to determine the wave attenuation.
5. Concluding remarks concerning hazard reduction are given.

First the hydrodynamics are discussed for every case study. Subsequently, the wave height attenuation and accompanied hazard reduction are determined. Additionally, as discussed in Section 2.2, ERA-Interim and consequently the surge model can underestimate hydrodynamic conditions due to the exclusion of tropical cyclones. Finally, the effect of an eroding or deforested mangrove area is reviewed in the concerned case studies.

[1] Google Earth
[2] Shuttle Radar Topography Mission (SRTM) 1 Arc-Second Global coverage
[3] Global Storm Surge Information System (GLOSSIS)
[4] AVISO, Satellite Altimetry Data

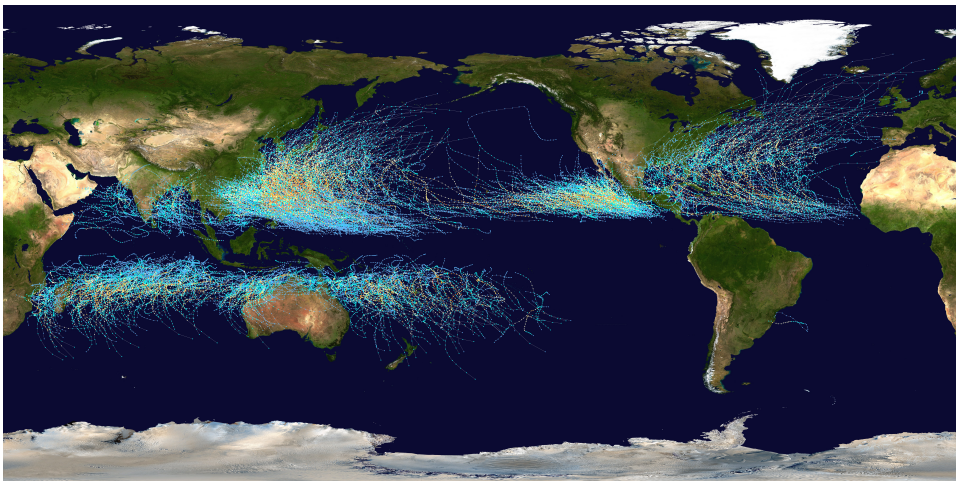

Figure 6.1: Global map of historical cyclone tracks (Brooks, 2008)

6.1. Andaman Sea

This location represents the study sites of Horstman et al. (2014). The location is at the coast of southern Thailand, facing the Andaman Sea at the west (Figure 6.2). This area is characterized by numerous embayments, islands and inlets. Due to the resulting mild wave conditions, this area is excellent for mangroves to grow in. The first study site in this area, from now on referred as 'Kantang', is situated in the estuary of the Mae Nam Trang and Khlong Palian rivers. The other site is located more southwards, in the Palian River estuary, and is named 'Palian'. The shrimp industry in Kantang and Palian is a large source of income, covering large (near-) coastal zones.

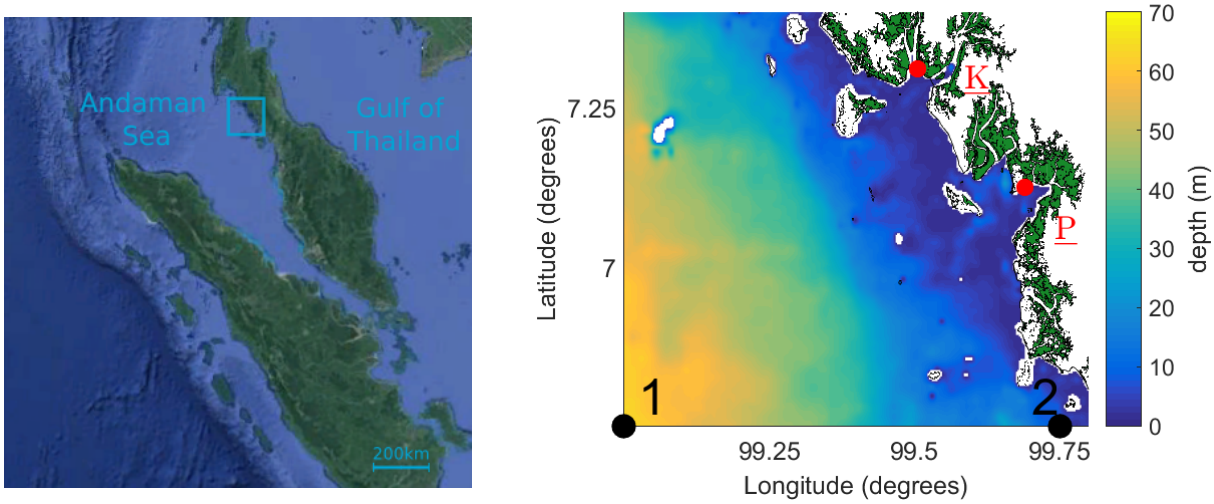

Figure 6.2: Location Andaman Sea case study location (left) and SWAN model area with mangroves and black-dotted ERA-I boundary conditions (right). K=Kantang and P=Palian

6.1.1. Hydrodynamics

In 2004, the coast was struck by a tsunami, but most likely due to the shelter and many islands, this area remained relatively unharmed (Horstman et al., 2014). Hence, it can be expected that the wave conditions in and after the forest are relatively mild. The low wave heights in the comparison of Section 5.1 confirms this.

Both the Kantang and Palian study sites can be reviewed in one SWAN model set-up due to their close mutual proximity (Figure 6.2). Two ERA-I points are located on the south of the domain. The representative storm wave conditions for a certain return period follows from the POT analysis (see Appendix B.3) and are presented in Table 6.1.

Table 6.1: Offshore wave conditions for the Andaman Sea's ERA-I points. RP = return period, ERA-I number can be observed in Figure 6.2 (right), *MWD* = mean wave direction, *WS* = wind speed, *MWiD* = mean wind direction and Δh = surge level

RP	ERA-I	H_s (m)	T_p (s)	*MWD* (°N)	*WS* (m s^{-1})	*MWiD* (°N)	Δh (m+MSL)
1	1	1.7	6.3	253	11.9	254	1.85
	2	1.1	5.6	262	7.0	264	1.85
10	1	2.1	6.9	253	15.8	254	1.93
	2	1.5	6.5	262	7.2	264	1.93
100	1	2.6	7.5	253	20.4	254	2.01
	2	1.8	7.0	262	7.4	264	2.01

The surge level differs only 8 cm between the different return periods, which is relatively low for estuary areas like Kantang and Palian. The exclusion of tropical cyclones might be the reason for this low difference. Due to this possible underestimation of ERA-I and subsequently also the surge heights (see Section 2.2.5), the wave height at the end of a mangrove forest can be underrated. Hence the wave and water level conditions can be scaled with factors, which are determined in Appendix B.2, compensating for the exclusion of tropical cyclones in the data. Due to lack of a viable substantiation for this approach, the potential underestimation of TC's is neglected.

A grid size of 275×275 m is applied in the SWAN model. The output location are positions near the study sites, where the water depth is sufficiently deep such that waves are not completely broken. This can suddenly change with bordering grid cells due to the relatively large grid size and corresponding abrupt depth change. The results (Table 6.2) are used as the boundary conditions in XBeach.

Table 6.2: Nearshore wave conditions for the Andaman Sea's study sites: Kantang (7.2950°N;99.5150°E) and Palian (7.1225°N;99.6950°E)

RP	Location	H_s (m)	T_p (s)	h (m)
1	Kantang	0.7	3.4	2.8
	Palian	0.6	3.7	4.3
10	Kantang	0.9	3.7	2.9
	Palian	0.8	4.1	4.4
100	Kantang	1.1	4.1	3.0
	Palian	1.0	4.6	4.5

6.1.2. Hazard model

The grid of the Kantang and Palian XBeach models can be divided into two distinct areas. In the first area is the bathymetry of Horstman et al. (2014) used. At the offshore boundary of this transect the SWAN output is imposed. This area is divided into a mudflat, Black mangrove and Red mangrove zone. Because it is expected that this Red mangrove area covers the coast to where the tide reaches, this Red zone is extended beyond the measurement area. The slope in this extended area is assumed to be the same gradient as in the Horstman-transect (from mudflat to end), which are 1:320 and 1:165 for Kantang and Palian respectively. The tidal range is around 2 m, implying that the length of this sloped extension is 280 m in Kantang en 120 in Palian. Furthermore, the mangrove area behind this sloped extension, which corresponds with the zone that is not reached by the tide, is assumed to be horizontal and covered with Black mangroves (similar as in Section 5.2.1). The Horstman-transect and extended profile together results in 1750 and 1256 non-equidistant grid locations for Kantang and Palian respectively. Additionally, the same model settings as in Section 5.2 are used: the layered medium mangrove sets, XBeach stationary mode with wave breaking and friction factor f_w=0.1. The result of the simulations are given in Figures 6.4 and 6.5.

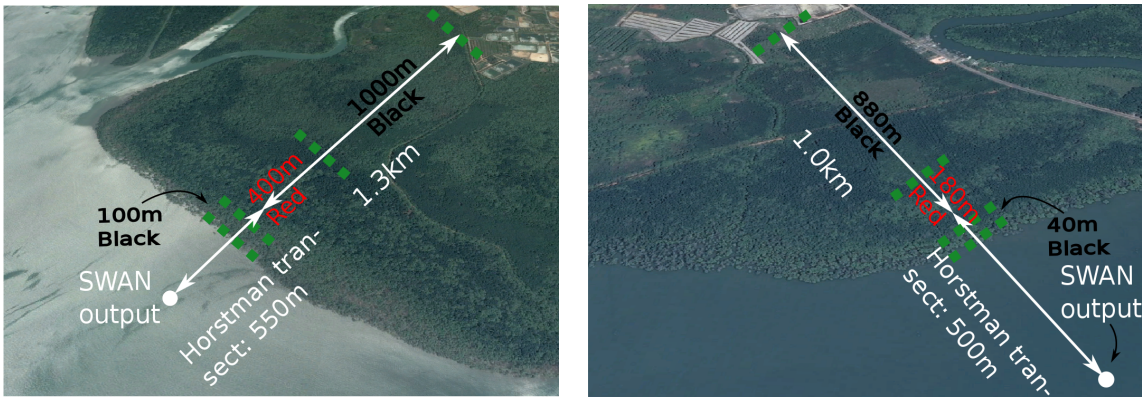

Figure 6.3: Kantang (left) and Palian (right) transects. Note the transition of forests and the fish ponds in the North

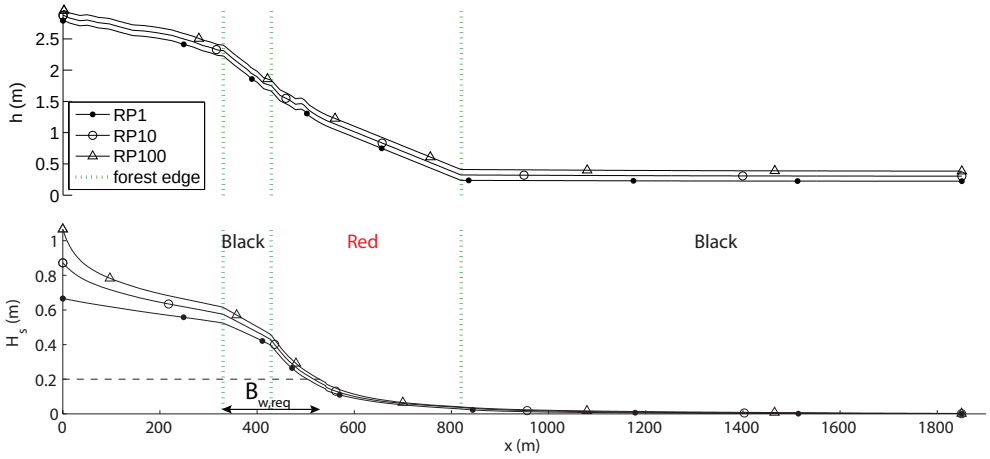

Figure 6.4: Water depth (upper) and wave height (lower) over the Kantang transect for different return periods

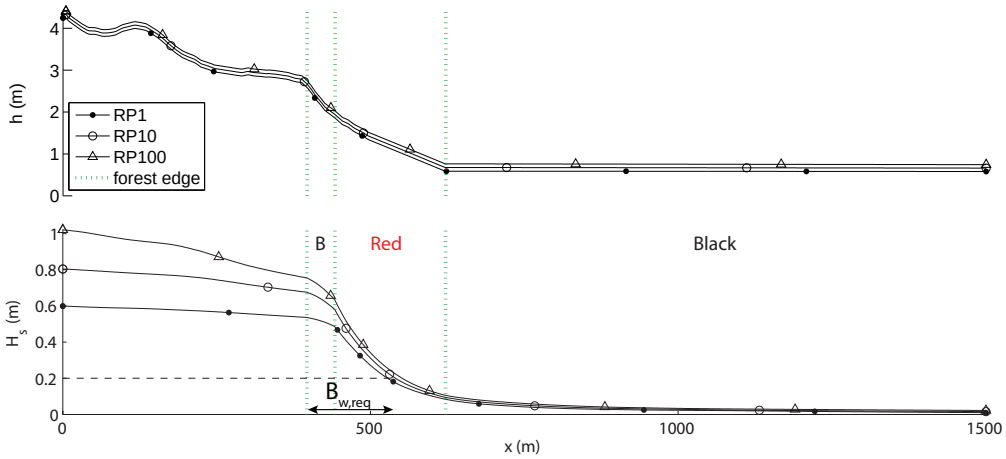

Figure 6.5: Water depth (upper) and wave height (lower) over the Palian transect for different return periods

The waves in front of the mangrove forest already dissipate due to breaking and friction for both locations. The attenuation in the Black mangrove area thereafter is also significant, which is probably

because of the strong depth variation as result of increasing bed slope. The wave reduction in the Red mangrove area even increases more, such that before the waves reach the extended Black mangrove area, they are almost completely dissipated. This holds for all the return periods, which do not differ much among each other, because of the limited differences in hydrodynamic conditions. The required forest width in Kantang for all return periods is around 170-200 m, while this is 130-150 m in Palian.

Effect of expanding aquaculture

The wide mangrove areas at the two location currently seem to provide sufficient protection against flood hazard by waves. Hence, the expansion of shrimp farms and fish ponds at the expense of the forest is not implausible. In both Kantang and Palian are already shrimp, fish or paddy cultivations present at the end of the forest (see Figure 6.3. Because of this potential landward loss of forest, the greenbelt policies discussed in Section 2.1.3 are applied. These are minimum width of 100 m, 200 m and a width based on the tidal range, which is $3 \cdot 130$=390 m (see Eq. 2.1). Only the simulations for Kantang are given in Figure 6.6, whereas the policies for Palian can be found in Appendix C.1.2.

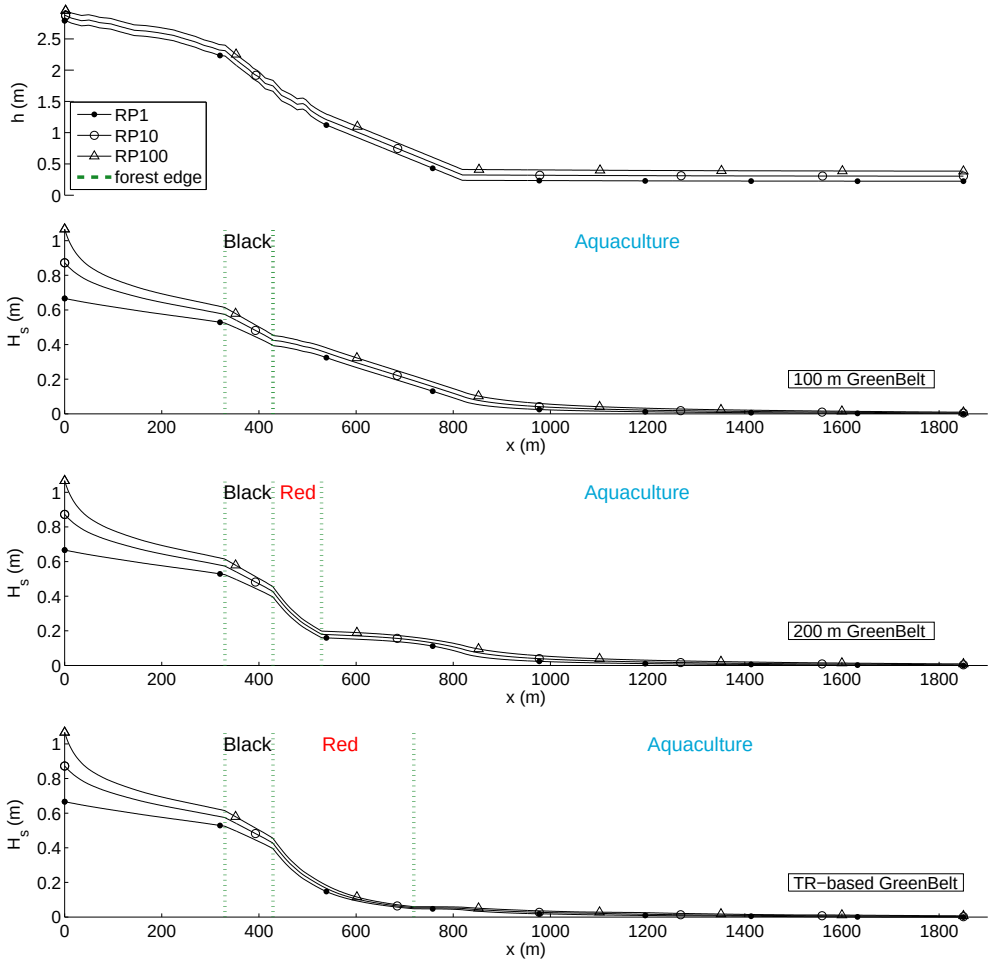

Figure 6.6: Water depth (upper) and wave height (lower) over the Kantang transect for different return periods and greenbelt policies

If the wave height directly behind the forest, i.e. in the aquaculture area approaches or exceeds 0.2 m, the area is considered to be exposed to an unacceptable hazard. This is the case for the 100 m and 200 m greenbelt policies in Kantang. The tidal range-based greenbelt seems to provide sufficient protection. For Palian, both the 200 m and tidal-range based greenbelt policies seem to enough. A 100 m policy is considered to be too low, because waves higher around 0.5 m can remain.

6.2. Singkawang

The city Singkawang, populated by almost 200,000 people, is located on the Indonesian island Borneo. The bay of Singkawang, which can be characterized as a headland bay (similar as Monterey Bay, see Section 3.1.5) is facing the Strait of Karimata on the west and the Chinese Sea on the north (Figure 6.7). The location is characterized by its small mangrove width in front of the city. Although the width over the coast length differs from place to place, it is expected that some mangrove areas provide insufficient protection for the Singkawang. It is confirmed that the area is susceptible for floods, even though accessible information hints more to extensive rainfall rather than high wave impacts. Nonetheless, this area is interesting to investigate.

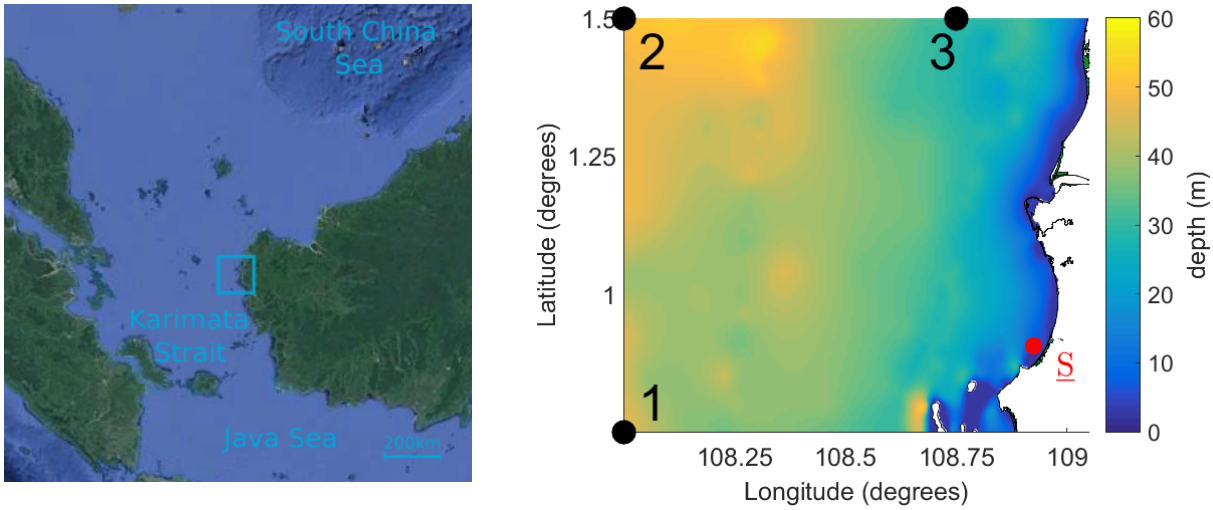

Figure 6.7: Location Singkawang case study location (left) and SWAN model area with mangroves and black-dotted ERA-I boundary conditions (right). S=Singkawang

6.2.1. Hydrodynamics

Three ERA-I points are used to simulate the nearshore conditions in the headland bay ('S' in left Figure 6.7), presented in Table 6.3. It can be observed that the conditions of ERA-I point two are the largest, because of its location far offshore. This in contrary to point 3, which is more nearshore.

Table 6.3: Offshore wave conditions for Singkawang's ERA-I points. RP = return period, ERA-I number can be observed in Figure 6.7 (right), *MWD* = mean wave direction, *WS* = wind speed, *MWiD* = mean wind direction and Δh = surge level

RP	ERA-I	H_s (m)	T_p (s)	*MWD* (° N)	*WS* (m s^{-1})	*MWiD* (° N)	Δh (m+MSL)
1	1	1.8	6.1	143	11.6	163	1.16
	2	1.9	6.4	108	14.2	129	1.16
	3	1.5	6.7	130	8.3	142	1.16
10	1	2.4	7.0	143	17.2	163	1.30
	2	2.7	7.4	108	17.6	129	1.30
	3	2.1	7.5	130	15.5	142	1.30
100	1	3.1	7.8	143	25.4	163	1.54
	2	3.6	8.2	108	25.4	129	1.54
	3	2.8	8.2	130	24.1	142	1.54

Not many tropical cyclones have been observed in the area (Figure 6.1), implying that the expected underestimation of the ERA-I data is limited. Hence, no possible scaling is conducted for this, although a possible range of wave conditions are given in Appendix 6. The eventual nearshore wave and water level, which provide the boundary condition for the XBeach input are presented in Table 6.4.

Table 6.4: Nearshore wave conditions for Singkawang study site (0.895°N;108.945°E)

RP	H_s (m)	T_p (s)	h (m)
1	0.14	1.3	3.7
10	0.24	1.6	3.9
100	0.41	1.9	4.1

6.2.2. Hazard model

At this location, no accurate bathymetry was available as was the case in Kantang and Palian. Therefore assumptions need to be made for the transect profile. The simulation domain consists of two parts, similar as in Section 5.2. The first is a sloped section over which the length is determined by the present tidal range, which is 0.85 m. Additionally, a clear transition in forest type is visible around 100 m, which might indicate the reachable level of the tide. Hence, the slope in this transect is assumed to be located from the SWAN output location (in some kind of mudflat) to the end of this forest, resulting in a slope of 1:470. Based on found photo's in the area, this front forest is most likely a young pioneer (dense) forest. Behind the pioneer trees a sparse forest is present, which is represented by the Black vegetation set. After 700 m of these Black mangroves, no vegetation seem to be present, stretching 600 m before reaching houses of the city (Figure 6.8). A grid size of 1 m is used, meaning that the grid consists of 1701 grid locations.

Figure 6.8: Singkawang transects used in XBeach

Figure 6.9: Mangrove rehabilitation in Singkawang (photo by Oi Dream Singkawang)

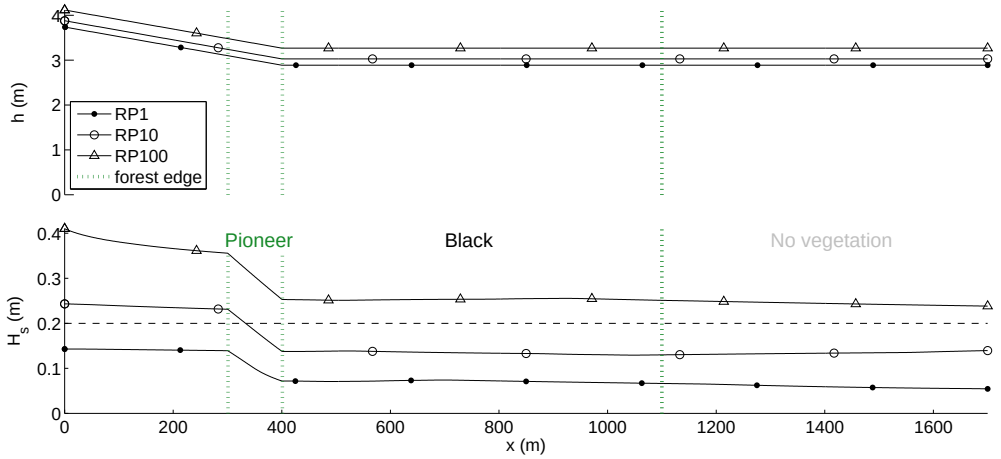

Figure 6.10: Water depth (upper) and wave height (lower) over the Singkawang transect for different return periods

In contrary to the Andaman Sea, there is a clear distinction in the required forest width for each return period (Figure 6.10). A storm with a return period once a year seem not to cause any damage, while a larger storm requires a small mangrove belt (30 m). According to the model, an once in the hundred year storm can even cause damage for the city of Singkawang, Increasing the pioneer forest can considerably reduce the hazard of a 1/100 year storm. Some mangrove rehabilitation projects are going on in Singkawang, which is considered to be a good solution for the city (Figure 6.9) in order to reduce the risk it is exposed to.

Effect of an eroding coast

Shoreline changes induced by erosion are both the consequence of human interventions and natural processes taken place over large range time scales. Even though mangroves are known for their accretion enhancing capabilities, these trees can also not always keep up with rising sea level, land subsidence or changing wave conditions. Additionally, human activities as land reclamation, port development and deforestation often exacerbate coastal erosion. In Asian countries, e.g. Indonesia the magnitude of the problem increases, especially when mangroves are removed from the coastal zone. Therefore the problem of an eroding front forest is simulated in Singkawang in which a 100 m mangrove forest is eroded.

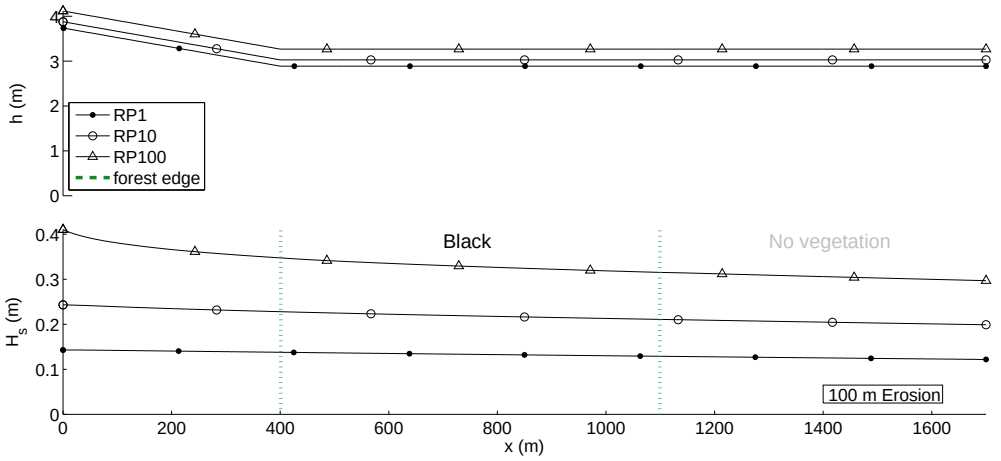

Figure 6.11: Water depth (upper) and wave height (lower) over the Singkawang transect for different return periods and 100 m erosion

It can be observed in Figure 6.11 that a loss of 100 m forest, erodes the complete dissipative pioneers. Hence, hardly any dissipation takes in de transect, significantly increasing the hazard in the city. Therefore, as already mentioned, the mangrove width in front the city should be preserved and preferably extended.

6.3. San Miguel Bay

The Philippines is the most exposed country in the world to tropical cyclones. The last devastating cyclone which made landfall in the Philippines is Typhoon Yolanda. In combination with the absence of resilient flood protection, this typhoon devastated around 70-80% of everything that came in its path. Also the San Miguel Bay was exposed to the damaging effect of Typhoon Yolanda. Although this bay is relatively sheltered by the surrounding land and mangroves are present in the area, some villages around the bay were still flooded. The San Miguel Bay is facing the Philippine Sea and located around 250 km west of Manilla, the capital of the Philippines. The reviewed location is Mercedes, a small city with a mangrove vegetated foreshore (Figure 6.12, right)

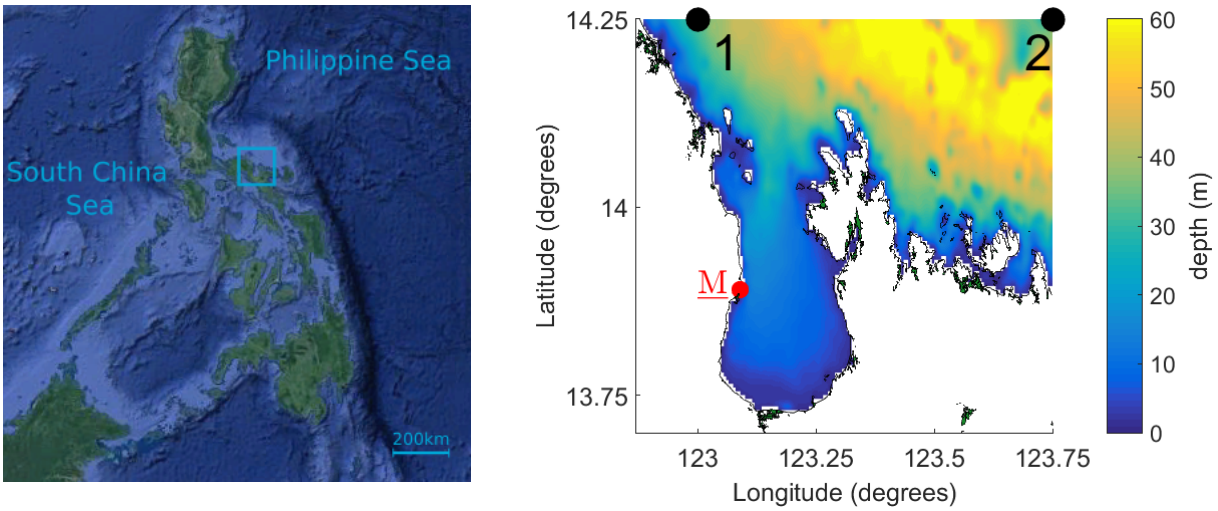

Figure 6.12: Location San Miguel Bay case study location (left) and SWAN model area with mangroves and black-dotted ERA-I boundary conditions (right). M=Mercedes

6.3.1. Hydrodynamics

The San Miguel Bay is interesting to investigate due to large differences in conditions between return periods. In addition, the hydrodynamic conditions in the area are extreme compared to the other case studies (Table 6.5).

Table 6.5: Offshore wave conditions for San Miguel Bay's ERA-I points. RP = return period, ERA-I number can be observed in Figure 6.12 (right), *MWD* = mean wave direction, *WS* = wind speed, *MWiD* = mean wind direction and Δh = surge level

RP	ERA-I	H_s (m)	T_p (s)	*MWD* (° N)	*WS* (m s^{-1})	*MWiD* (° N)	Δh (m)
1	1	3.3	8.4	53	15.6	71	1.5
	2	4.2	9.3	52	17.1	81	1.5
10	1	4.2	9.1	53	18.8	71	2.4
	2	5.2	10.1	52	21.5	81	2.4
100	1	4.9	9.5	53	21.3	71	3.3
	2	6.0	10.5	52	25.9	81	3.3

The city of Mercedes is located on the western side of the bay (Figure 6.12 right). The output of the SWAN model for a nearshore location at Mercedes is given in Table 6.6.

Table 6.6: Nearshore wave conditions for San Miguel Bay study site, the village Mercedes (123.09°N;13.875°E)

RP	H_s (m)	T_p (s)	h (m)
1	1.7	5.1	4.8
10	2.2	5.2	5.7
100	2.4	5.7	6.6

6.3.2. Hazard model

Unfortunately no bathymetry data is available for the area. Based on the characteristics on (satellite) images, assumptions are made considering the profile in the area. The distance between SWAN output position and location of the beach is around 100 m (Figure 6.13). This is a locally steep beach, consisting of large cobblestones (Figure 6.14 left).

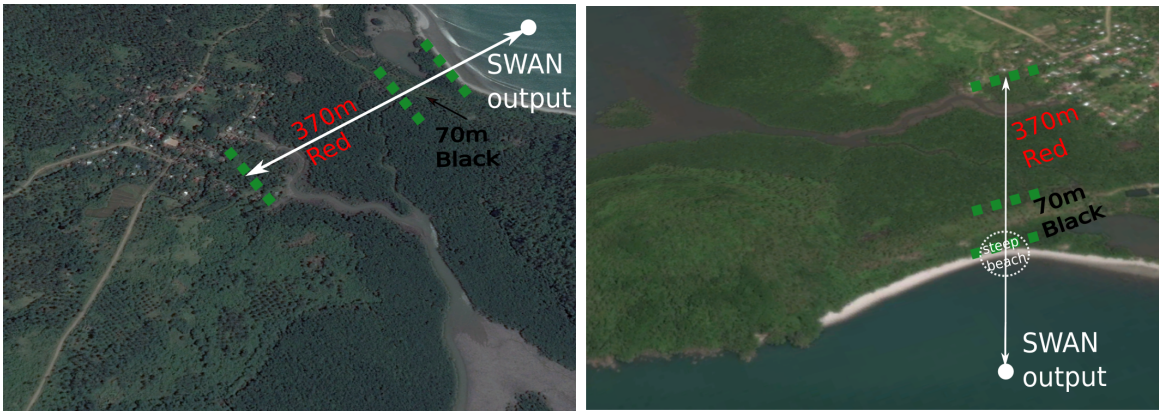

Figure 6.13: Mercedes transect for during ebb (left) and during flood period (right) seen from different angles

Figure 6.14: Left: Steep beach in front of Mercedes village. Right: mangrove reforestation in San Miguel Bay (both from Panoramio)

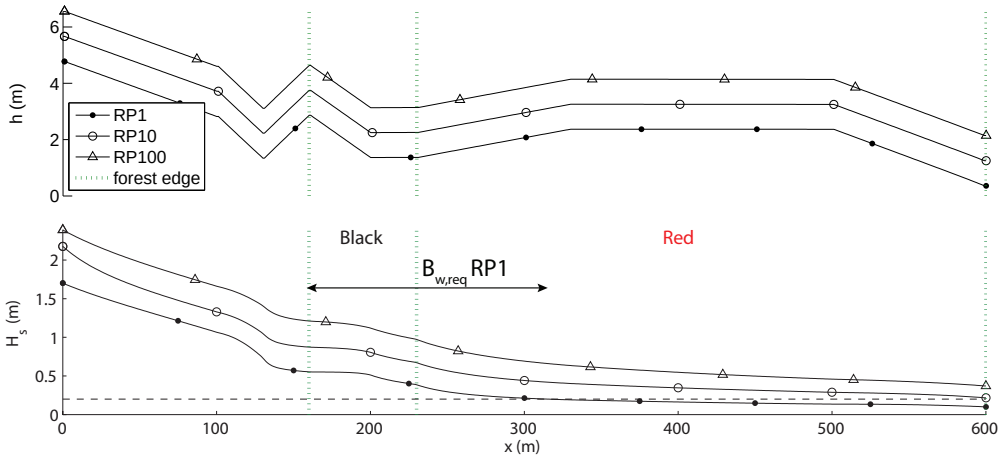

Figure 6.15: Water depth (upper) and wave height (lower) over the Mercedes transect for different return periods

Behind the steep front beach, it is expected that elevation rapidly decreases again. The reason for this is the healthy looking mangroves directly behind the beach, which have to be submerged by the tide under normal conditions and hence are located lower. Further land inward the forest is rapidly decreasing in density, which might indicate that this area is higher compared to its surroundings. This can clearly be observed in the right illustration of Figure 6.13, in which a sparse strip of mangroves is present. Behind this sparse stretch of forest, a denser forest is present, which is thus assumed to be located lower and hence more often flooded (by the rivers). The river is considered to be almost dry around ebb tide and filled during flood, in which the surrounding forest is provided by water and nutrients. A typical Indo-Pacific zonation is assumed, meaning that Black mangroves cover the front and Red mangroves the back forest. At the end of the transect, the elevation is expected to be higher, because otherwise the Mercedes villages would be flooded twice a day.

The large differences in storm conditions between the different return periods causes a yearly storm to be unable to pose large hazards, while larger storms can endanger the hinterland considerably. For the yearly storm a 200 m large forest might be able to dissipate the waves to 0.2 m and hence results in a save situation. However, the current 440 m is possibly insufficient for the protection against larger storms, especially the one-in-hundred year storm.

Effect of expanding aquaculture

Protection by large storms and cyclones is paramount for protection of the people and their small-scale fishery. Externally-assisted mangrove projects have been launched by the national government in order to replant mangroves to obtain natural solutions against floods.

Also the regions around San Miguel Bay are highly dependant on the income of fishery. The Philippine government maintains a relatively low greenbelt policy (see Section 2.1.3). Around 50-100 m of coastal mangroves is often used as default. In the Philippines are many mangrove rehabilitation projects going on to restore the mangroves from storm impact and obtain the adequate buffer zone width. Based on the observations from the current forest width in Figure 6.15, it is evident that a 50 or 100 m policy is most likely insufficient to protect the Mercedes village (Figure 6.16), because it would lead to wave heights of 0.8-1.1 for a one-in-hundred year storm.

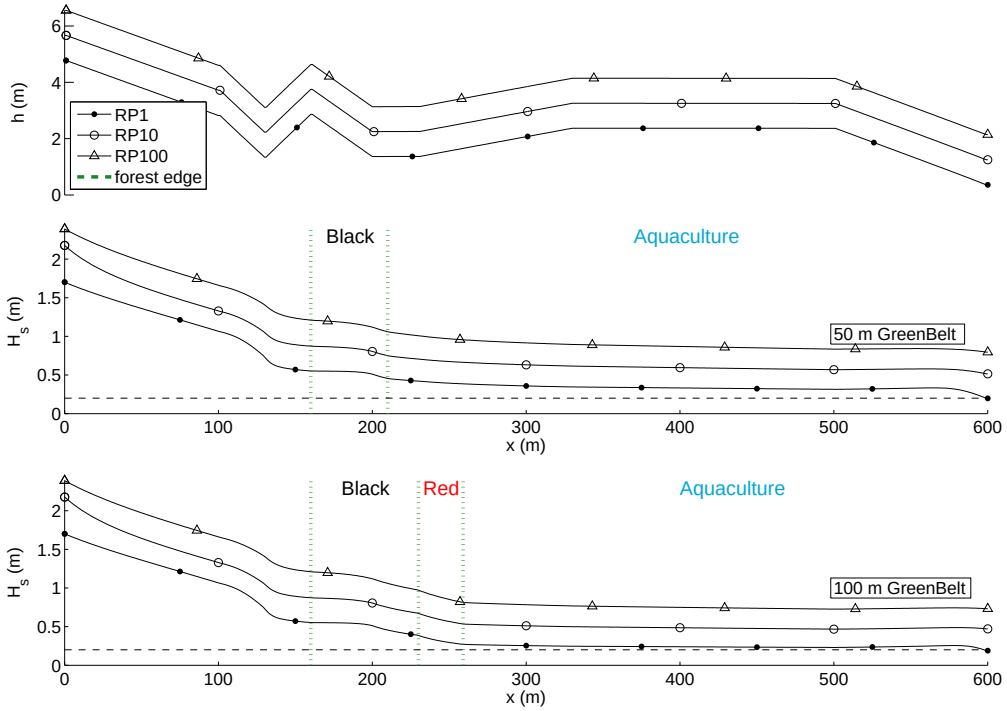

Figure 6.16: Water depth (upper) and wave height (middle and lower) over the Mercedes transect for different return periods and greenbelt policies

7

Discussion

In this research a globally applicable method was developed for determining the influence of mangroves on wave attenuation. This involved:

1. The development of a procedure to describe nearshore storm conditions for mangrove coasts.
2. Modelling the wave attenuation in a mangrove forest for a broad range of conditions.
3. Evaluation of required forest widths, current greenbelt policies and the influence of erosion.

This research was focussing on a global applicability of a tool for determining flood hazards in mangrove forests. Hence, global databases were used to calculate the representative wave conditions in front of such forests. In combination with the numerical model SWAN, the offshore located wave data was transformed to nearshore wave conditions. Prior to application in the hazard model, the global data and SWAN procedure were validated for four buoy locations. The transformation significantly improved the description of wave characteristics for sheltered conditions, like embayments, barrier islands and estuaries, although there were some differences between simulation and buoy measurements. Deviations are due to the large equidistant grid, inaccuracies of ERA-I or the rough bathymetry. For deep and exposed coasts, ERA-I often already provides acceptable results (±5-15%), which is in accordance with Shanas and Kumar (2015). Although ERA-I seems to be a promising basis for a global wave tool, it does not properly describe tropical cyclones. A deviation of around 30% was measured in this study (B.2), similar as was found by Kumar and Naseef (2015). A better description of this in ERA-I would require the inclusion of historical cyclone paths and/or reducing the ERA-I grid size. This is however outside the scope of this research. Hence no adjustment was made for this effect, implying a potential underestimation of hazard for cyclone susceptible coasts might exist.

One might argue that even a faster tool is to assume that the waves in the shallow water around mangroves are depth limited, and a depth-induced breaking formulation might be sufficient for the high level of uncertainty in this research. Such an approach was tested and considered to deviate too much from buoy measurements. Additionally, it does not provide wave periods, whereas SWAN does. However, the verification method was not conducted in very shallow water, because these buoys are difficult to find.

The water level and wave conditions determination for certain storm return periods are applied at the SWAN boundaries, resulting in the extreme nearshore conditions used in the mangrove model. Potential inaccuracies in this approach are the extreme-value analysis on the offshore boundaries instead of nearshore, the assumption that waves and surges simultaneously occur for a certain storm return period and the determination of wave period and direction by relating it with the wave height.

Although the method is applied under many assumptions, it is considered to improve the prediction of nearshore wave conditions compared to current datasets. The procedure can be valuable for engineering purposes in data scarce areas or for quick services which ”support (nature-based) shoreline protection against flooding and erosion”[1].

[1] After: the Foreshore Assessment Using Space Technology project (FAST)

Various sources were used find representative sets of vegetation parameters, used in the numerical model XBeach, which is able to describe wave attenuation by vegetation based on the formulation of Mendez and Losada (2004). The diversity in mangrove properties was even higher than expected, despite a classification was made for two root types and various densities. An argumentation for this is the combination of riverine and coastal mangroves in the classification, which significantly differ in dimensions. Also the techniques to measure mangroves are not all according to the standards given in Kauffman and Donato (2012). Finally, linearly increasing relations between the physical mangrove characteristics were found, implying that denser forests also coincide with thicker and higher trees, which is not necessarily true. Based on data of Horstman et al. (2014) and initial model results, the found sparse and dense variants were considered to be too low and high respectively. Hence the medium vegetation set was applied in further simulations.

Narayan (2009), Phan et al. (2014) and Burger (2005) use two or tree layers to represent the roots, stems and canopy of a mangrove tree. In this research it was assumed that this number is insufficient to represent the vertical variation of a mangrove tree. Additionally, the strong dependency of wave attenuation on small depth changes is reduced, while it does not increase the computation time in XBeach. The increase of layers seem to correspond better with measurements. However, the many uncertainties in both measurements and model inputs were too large to conclude that the vertical layering is a direct improvement of the model.

The non-physical parameter in the Mendez and Losada (2004) description, the bulk drag coefficient $\tilde{C}_D$, is determined for two different methods. The first method focusses on the aforementioned medium vegetation set and a relation between wave height, water depth and root/stem density (Suzuki et al., 2012) for $\tilde{C}_D$. In Method two, local measured data and a calibration relation for the bulk drag coefficient (Hendriks, 2014) were used. Due to the significant lower values of the physical parameters of Method 2, it was expected and confirmed that the bulk drag coefficient would be much higher than in Method 1. The approach of local measurements in combination with a calibrated bulk drag coefficient is considered to be a viable and good solution for local studies, because site-specific data is used and the many uncertainties are included in one factor. On the other hand does Method 1 coincided slightly better with the measurements, uses the physical background of $\tilde{C}_D$ and is canopy data included. The latter was not implemented in Method 2, although the uncertainty in canopy characteristics of Method 1 is still very high.

By determining $\tilde{C}_D$ in advance, the possibility to compare the model with a field study by tuning it with bottom friction (f_w) was enabled. The combination of a layered medium set mangroves, f_w=0.1 and the stationary mode of XBeach was considered to be accurate enough. The friction factor was determined by comparison with measurements and a reference study for sandy beaches, in which f_w=0.06 was applied Van Dongeren et al. (2012). However, the choice of bottom friction has a large impact on the eventual wave attenuation, while this parameter lacks background in this research. Hence, inaccuracies in the friction factor can eventually lead to over- or underestimation of flood hazard.

From a sensitivity analysis it followed that a steeper slope, smaller tidal range, lower water depth and smaller incoming wave height results in less required forest width. Large assumption is the imposition of the criterion of 0.2 m to be the transition between hazard and no hazard. However, the conceptual model is broadly applicable, and for case-specific applications, a sharper criterion can be applied.

From multiple models for a landward (deforestation) and seaward (erosion) loss of forest, it was observed that the wave height on a sloped profile increased more in case of deforestation than for erosion. However, the model does not take impact of larger hydrodynamic conditions on mangroves into account. Namely, the trees are more susceptible to breaking and uprooting in extremer conditions. Hence, dissipation in the erosion case would have been smaller, if this was included. Experiments have been conducted regarding the stability of trees under extreme wind conditions (Gardiner et al., 1997), which can potentially serve the initial implementation of similar behaviour under hydrodynamic conditions in numerical models.

The modelling was conducted with Xbeach stationary. Although this mode efficiently solves the wave action balance, it does not take long waves into account. Horstman et al. (2014) found an increase in mean wave periods as the waves propagate further into a mangrove forest. This is a result of a more efficient dissipation of short period waves (i.e. frequencies >0.1 Hz) than for long period waves. Hence, the importance of gaining knowledge of the behaviour of long period waves in mangrove forests can be important. Surfbeat does include long waves, but not the evolution of the wave period. Hence, a phase resolving model like SWASH or XBeach in non-hydrostatic mode can be used to simulate the wave period. However, first-mentioned does not include the Mendez and Losada (2004) or a similar formulation for the dissipation by vegetation.

8

Conclusions and recommendations

In this research a wave attenuation model for mangroves is set up, based on global data and mangrove field studies. First the conclusions drawn from the hydrodynamics, mangroves and model settings are presented, followed by the recommendations.

8.1. Conclusions

How can global representative hydrodynamic conditions for mangrove areas be determined?
Mangroves are often located in sheltered areas like embayments, estuaries and behind barrier islands, which causes the waves to be relatively mild. An offshore global wave database in combination with global bathymetry (open source) and surge models, ERA-Interim, SRTM and GTSR respectively, were used in the wave transformation numerical model SWAN to describe the sheltered nearshore wave conditions. The procedure resulted in a significant improvement for wave heights (RMSE reduction of 1.7-3.7) and periods (3.6-4.8) compared to the direct use of the wave data of ERA-Interim for the sheltered mangrove locations. A similar procedure for exposed and deep coasts did not improve the wave height nor period estimations.

What is the magnitude of wave related mangrove parameters, are there relations between them and what is their influence on wave attenuation?
The most important wave-related characteristics are the vegetation factor V_{fac} (diameter times density), vegetation height (h_v) and bulk drag coefficient ($\tilde{C}_D$), divided into high stilt rooted mangroves (Red), low aerial rooted mangroves (Black) and young pioneer trees. The diameter, density and vegetation height were determined based on literature and linear relations between them and the bulk drag coefficient using the relation proposed by Suzuki and Arikawa (2010), see Table 8.1.

Table 8.1: Vegetation parameters for Red (stilt roots), Black (pencil-shaped roots) and pioneer mangroves, in which the range represents sparse, small trees and dense, large trees.

	Root			Stem			Canopy		
	V_{fac} (m^{-1})	h_v (m)	$\tilde{C}_D$ (-)	V_{fac} (m^{-1})	h_v (m)	$\tilde{C}_D$ (-)	V_{fac} (m^{-1})	h_v (m)	$\tilde{C}_D$ (-)
Red	0.2-2.1	0.3-1	0.6-1.0	0.1-0.7	2-8	0.6-1.0	0.4-4.5	10-12	0.5
Black	0.2-1.2	0.15-0.8	0.6-1.0	0.01-0.8	1-8	0.6-1.0	0.5	9-13	0.5
Pioneer	2	1	0.6-1.0	-	-	-	1	2	0.5

The density of a forest, i.e. type and age of trees largely determined the wave attenuation in a forest. The pioneers dissipate the most, followed by Red and lastly Black mangroves. In order to better represent the vertical variation of a mangrove tree, more layers than in the initial three-layered schematization were used. This reduces the large dependency on depth and does not increase the computation time. A smaller depth, steeper slope and lower incoming wave resulted in lower wave heights at the end of a mangrove forest.

How does the mangrove forest, as function of its width, contribute to flood hazard reduction?
In here also the main research question is answered: ”How wide should mangrove areas be to contribute to flood hazard reduction under diverging boundary conditions”.

A tidal range of 1.5-2.5 m and a slope between 1:250 and 1:500 are commonly found in mangrove forests. Typical storm conditions are a storm surge height of 1-1.5 m and 0.5-1.0 m incoming wave height. In addition, a significant wave height of 0.2 m was assumed to be representative for damaging low-quality walls. This combined resulted in a required forest width of around 100-450 m. In unfavourable conditions, i.e. high waves, large depth, sparse forest, this width can even be 900 m. A dense pioneer forest can be 4 times smaller than an sparse forest for similar conditions and same attenuation. Higher wave heights are more strongly dissipated than lower wave heights. Additionally, wave heights are higher at the seaward edge of a forest than at the landward side. Hence, on a sloping coast, the effect of an landward loss of forest was more clearly visible than erosion of the coast over the same distance.

Some governments maintain a greenbelt policy to protect their mangrove ecosystems and hence obtain protection against floods. Currently not or hardly any local conditions are considered in such policies to determine the required forest widths. Nationally maintained greenbelt policies were simulated for two case studies. Whether these provided safe situations, differed between the various locations. In contrary, the use of global (open source) data, SWAN-2D and XBeach-1D (stationary) provided a (quick) tool to assess the flood hazard a location is facing.

8.2. Recommendations

The following topics are recommended for further research and model implementations:

Hydrodynamics

- Use of SWAN in combination with open source bathymetry and ERA-Interim to quickly assess nearshore conditions in embayments, estuaries and behind barrier islands in data scarse areas, rather than using solely ERA-Interim.
- A proper implementation of tropical cyclone paths into the ERA-Interim-SWAN model.

Mangrove modelling

- In case local mangrove measurements are lacking, the found values of Table 8.1 can be used, although this data need to be improved by means of a validation with measurements.
- For accurate (risk) assessments, is it recommended to use local data and a calibrated bulk drag coefficient rather than the large range of parameters given in Table 8.1.
- More knowledge into canopy characteristics of mangroves. The large spread in these values (Table 8.1) underlines the great uncertainty in representative values, while the canopy layers can significantly influence wave attenuation.
- Investigation of a better determination of the friction coefficient for the muddy and leaf-littered soil, which appeared to influence the wave attenuation in case of extreme conditions significantly.
- Obtain good bathymetry data, because the depth largely determines dissipation by wave breaking, friction and vegetation.
- Implementation of breaking and uprooting of mangroves under extreme conditions into model.

Hazard reduction

- Required forest widths for flood hazard reduction should be determined locally. Some (inter)national-wide policies are too rough for mangrove coastal zone management, because they do not take local conditions into account. Additionally, these policies do not always require sufficient greenbelt for the protection of their hinterland.
- Upgrade framework to risk assessment, because risk also includes exposure and vulnerability of a coastal area compared to a hazard assessment. A better understanding of the risk at which a mangrove vegetated foreshore is exposed to, is a more helpful tool for the implementation of flood reductive measures.

- Due to the importance of the wave period in flood hazard (or risk) assessments and the difficulties of mangroves to dissipate longer waves, the use of a phase-resolving model is recommended. Xbeach non-hydrostatic is able to do this and uses the formulation of Mendez and Losada (2004) for vegetation.

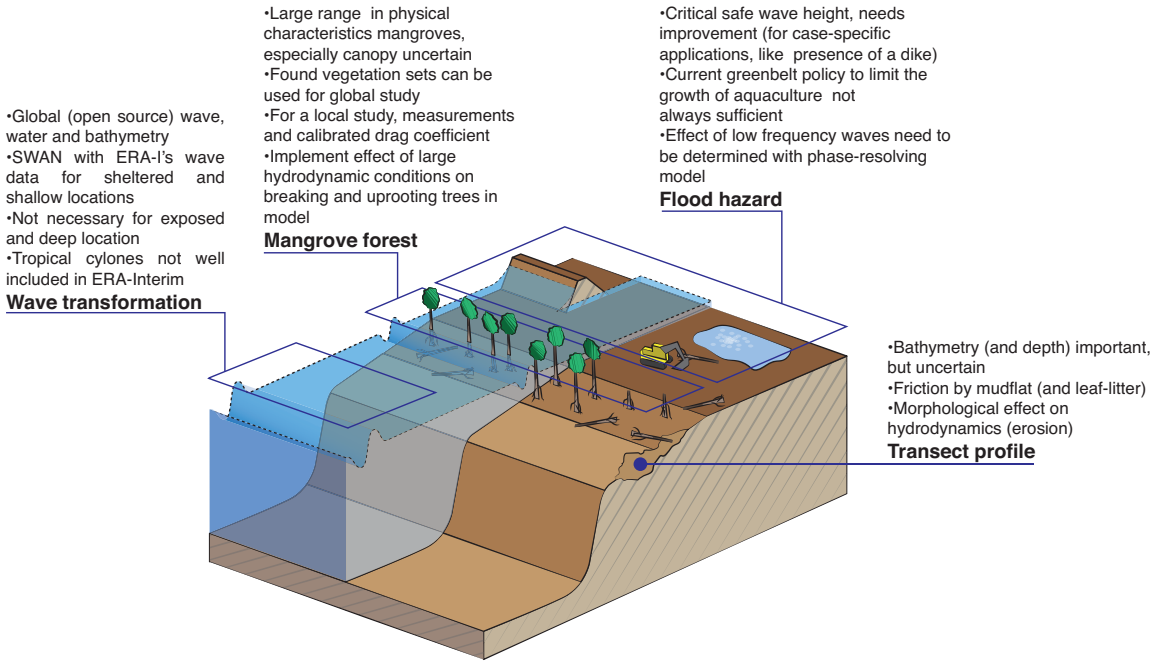

Figure 8.1: Most important methods, observations and recommendations

Bibliography

Alongi, D. M. Present state and future of the world's mangrove forests. *Environmental conservation*, 29(03):331–349, 2002.

Appelquist, L. R. and Halsnæs, K. The coastal hazard wheel system for coastal multi-hazard assessment & management in a changing climate. *Journal of Coastal Conservation*, pages 1–23, 2015.

Avila, L. A. and Cangialosi, J. Tropical cyclone report: Hurricane irene. *National Hurricane Center*, 2011.

Bao, T. Q. Effect of mangrove forest structures on wave attenuation in coastal vietnam. *Oceanologia*, 53(3):807–818, 2011.

Bo, J. *A Study on Geometric and Material Properties of the Mangrove Root System in Singapore*. PhD thesis, TU Delft, Delft University of Technology, 2012.

Booij, N., Haagsma, I., Holthuijsen, L., Kieftenburg, A., Ris, R., Van Der Westhuysen, A., and Zijlema, M. Swan cycle iii version 40.41 user manual. *Delft University of Technology*, 115, 2004.

Brinkman, R. M., Massel, S. R., Ridd, P. V., Furukawa, K., et al. Surface wave attenuation in mangrove forests. In *Pacific Coasts and Ports' 97: Proceedings of the 13th Australasian Coastal and Ocean Engineering Conference and the 6th Australasian Port and Harbour Conference; Volume 2*, page 909. Centre for Advanced Engineering, University of Canterbury, 1997.

Brinkman, R. M. *Wave attenuation in mangrove forests: an investigation through field and theoretical studies*. PhD thesis, James Cook University, 2006.

Brooks, H. Extreme weather: Understanding the science of hurricanes, tornadoes, floods, heat waves, snow storms, global warming and other atmospheric disturbances. *Eos, Transactions American Geophysical Union*, 89(28):258–258, 2008.

Brown, B., Lewis, R., Coen, A., and Hooper, P. Resilience thinking applied to the mangroves of indonesia. *IUCN and Mangrove Action Project, Yogyakarta, Indonesia*, 2007.

Brunt, M. and Davies, J. *The Cayman Islands: natural history and biogeography*, volume 71. Springer Science & Business Media, 2012.

Burger, B. *Wave attenuation in mangrove forests*. PhD thesis, TU Delft, Delft University of Technology, 2005.

Caires, S. and van Os, J. met ocean data t ransformation classification and analysis guidelines: Orca. *Deltares*, 2012.

Caires, S., Groeneweg, J., and Sterl, A. Changes in the north sea extreme waves. In *Preprints of 9th international workshop on wave hindcasting and forecasting*, 2006.

Cole, T. G., Ewel, K. C., and Devoe, N. N. Structure of mangrove trees and forests in micronesia. *Forest Ecology and Management*, 117(1):95–109, 1999.

Dahdouh-Guebas, F., Kairo, J. G., De Bondt, R., and Koedam, N. Pneumatophore height and density in relation to micro-topography in the grey mangrove avicennia marina. *Belgian journal of botany*, 140(2):213–221, 2007.

Dalrymple, R. A., Kirby, J. T., and Hwang, P. A. Wave diffraction due to areas of energy dissipation. *Journal of Waterway, Port, Coastal, and Ocean Engineering*, 110(1):67–79, 1984.

Das, S. C., Iimura, K., and Tanaka, N. Effects of coastal vegetaion species and ground slope on storm surge disaster mitigation. *Coastal Engineering Proceedings*, 1(32):24, 2011.

de Vos, W.-J. *Wave attenuation in mangrove wetlands. Red River Delta, Vietnam*. PhD thesis, TU Delft, Delft University of Technology, 2004.

Deltares. Xbeach manual. *Deltares*, 2015.

Feller, I. C. and Sitnik, M. Mangrove ecology: a manual for a field course. *Smithsonian Institution, Washington, DC*, 1996.

Furukawa, K. and Wolanski, E. Sedimentation in mangrove forests. *Mangroves and salt marshes*, 1 (1):3–10, 1996.

Gardiner, B., Stacey, G., Belcher, R., and Wood, C. Field and wind tunnel assessments of the implications of respacing and thinning for tree stability. *Forestry*, 70(3):233–252, 1997.

Giri, C., Ochieng, E., Tieszen, L. L., Zhu, Z., Singh, A., Loveland, T., Masek, J., and Duke, N. Status and distribution of mangrove forests of the world using earth observation satellite data. *Global Ecology and Biogeography*, 20(1):154–159, 2011.

Hendriks, J. Wave dissipation in mangroves: Parameterization of the drag coefficient based on field data., 2014.

Hinkel, J. and Klein, R. J. Integrating knowledge to assess coastal vulnerability to sea-level rise: The development of the diva tool. *Global Environmental Change*, 19(3):384–395, 2009.

Holthuijsen, L. H. *Waves in oceanic and coastal waters*. Cambridge University Press, 2010.

Horstman, E., Dohmen-Janssen, C., Narra, P., van den Berg, N., Siemerink, M., and Hulscher, S. Wave attenuation in mangroves: A quantitative approach to field observations. *Coastal engineering*, 94:47–62, 2014.

Horstman, E., Dohmen-Janssen, M., Narra, P., van den Berg, N.-J., Siemerink, M., Balke, T., Bouma, T., and Hulscher, S. Wave attenuation in mangrove forests; field data obtained in trang, thailand. *Coastal Engineering Proceedings*, 1(33):waves–40, 2012.

Husrin, S., Strusińska, A., and Oumeraci, H. Experimental study on tsunami attenuation by mangrove forest. *Earth, planets and space*, 64(10):973–989, 2012.

Hutchison, J., Manica, A., Swetnam, R., Balmford, A., and Spalding, M. Predicting global patterns in mangrove forest biomass. *Conservation Letters*, 7(3):233–240, 2014.

ISO. Iec 31010—risk management: Risk assessment techniques. *International Organization for Standardization*, 2009.

Journèe, J. M. and Massie, W. Offshore hydrodynamics. *Delft University of Technology*, 4:38, 2001.

Kathiresan, K. and Rajendran, N. Coastal mangrove forests mitigated tsunami. *Estuarine, Coastal and Shelf Science*, 65(3):601–606, 2005.

Kauffman, J. B. and Donato, D. Protocols for the measurement, monitoring and reporting of structure, biomass and carbon stocks in mangrove forests. Technical report, Center for International Forestry Research (CIFOR), Bogor, Indonesia, 2012.

Kobayashi, N., Raichle, A. W., and Asano, T. Wave attenuation by vegetation. *Journal of Waterway, Port, Coastal, and Ocean Engineering*, 119(1):30–48, 1993.

Komen, G. J., Cavaleri, L., Donelan, M., Hasselmann, K., Hasselmann, S., and Janssen, P. *Dynamics and modelling of ocean waves*. Cambridge university press, 1996.

Krauss, K., Allen, J. A., and Cahoon, D. Differential rates of vertical accretion and elevation change among aerial root types in micronesian mangrove forests. *Estuarine, Coastal and Shelf Science*, 56 (2):251–259, 2003.

Kumar, S. V. and Naseef, M. T. Performance of era-interim wave data in the nearshore waters around india*. *Journal of Atmospheric and Oceanic Technology*, 32(6):1257–1269, 2015.

Mazda, Y., Magi, M., Kogo, M., and Hong, P. N. Mangroves as a coastal protection from waves in the tong king delta, vietnam. *Mangroves and Salt marshes*, 1(2):127–135, 1997a.

Mazda, Y., Wolanski, E., King, B., Sase, A., Ohtsuka, D., and Magi, M. Drag force due to vegetation in mangrove swamps. *Mangroves and Salt Marshes*, 1(3):193–199, 1997b.

Mazda, Y., Magi, M., Ikeda, Y., Kurokawa, T., and Asano, T. Wave reduction in a mangrove forest dominated by sonneratia sp. *Wetlands Ecology and Management*, 14(4):365–378, 2006.

Mendez, F. J. and Losada, I. J. An empirical model to estimate the propagation of random breaking and nonbreaking waves over vegetation fields. *Coastal Engineering*, 51(2):103–118, 2004.

Méndez, F. J., Losada, I. J., and Losada, M. A. Hydrodynamics induced by wind waves in a vegetation field. *Journal of Geophysical Research: Oceans*, 104(C8):18383–18396, 1999.

Muis, S., Verlaan, M., Winsemius, H., Aerts, J. C., and Ward, P. J. The first global-scale hindcast of extreme sea levels. *IAHR*, 2007.

Muis, S., Verlaan, M., Winsemius, H., Aerts, J. C., and Ward, P. J. A global reanalysis of storm surges and extreme sea levels. *Nature Communications*, 7(11969), 2016.

Narayan, S. *The effectiveness of mangroves in attenuating cyclone-induced waves*. PhD thesis, TU Delft, 2009.

Nepf, H. Drag, turbulence, and diffusion in flow through emergent vegetation. *Water resources research*, 35(2):479–489, 1999.

Phan, L. K., van Thiel de Vries, J. S., and Stive, M. J. Coastal mangrove squeeze in the mekong delta. *Journal of Coastal Research*, 31(2):233–243, 2014.

Primavera, J. H. Mangroves and aquaculture in southeast asia. 2005.

Quartel, S., Kroon, A., Augustinus, P., Van Santen, P., and Tri, N. Wave attenuation in coastal mangroves in the red river delta, vietnam. *Journal of Asian Earth Sciences*, 29(4):576–584, 2007.

Reimann, S., Husrin, S., Strusińska, A., and Oumeraci, H. Damping tsunami and storm waves by coastal forests - parameterisation and hydrualic model tests. In *FZK-Kolloquium'Potenziale für die Maritime Wirtschaft', Han-nover*, 2009.

Shanas, P. R. and Kumar, V. S. Trends in surface wind speed and significant wave height as revealed by era-interim wind wave hindcast in the central bay of bengal. *International Journal of Climatology*, 35(9):2654–2663, 2015.

Soerianegara, I. The width of mangrove green belt as coastal zone protection forest. In *Proceedings of the Symposium on New Perspectives in Research and Management of Mangrove Ecosystems, Colombo, Sri Lanka*, pages 227–229, 1986.

Spalding, M., McIvor, A., Tonneijck, F., Tol, S., and van Eijk, P. Mangroves for coastal defence, guidelines for coastal managers and policy makers. Technical report, Wetlands International and The Nature Conservancy, 2014.

Suzuki, T. and Arikawa, T. Numerical analysis of bulk drag coefficient in dense vegetation by immersed boundary method. In *Proceedings of the 32nd International Conference on Coastal Engineering, ICCE 2010, June/July, Shanghai*, 2010.

Suzuki, T., Zijlema, M., Burger, B., Meijer, M. C., and Narayan, S. Wave dissipation by vegetation with layer schematization in swan. *Coastal Engineering*, 59(1):64–71, 2012.

Tomlinson, P. The botany of mangroves. cambridge tropical biology series, 1986.

Tung, C., Kasal, B., Rogers, S., and Yeh, S. Behavior of breakaway wall subjected to wave forces: Analytical and experimental studies. *Federal Emergency Management Agency, Washington, DC*, 1999.

Tusinski, A. *The role of mangroves in the design of coastal dikes: Hydrodynamic and cost related aspects*. PhD thesis, TU Delft, Delft University of Technology, 2012.

UNISDR. Terminology on disaster risk reduction. *United Nations International Strategy for Disaster Reduction*, 2009.

Vafeidis, A. T., Nicholls, R. J., McFadden, L., Tol, R. S., Hinkel, J., Spencer, T., Grashoff, P. S., Boot, G., and Klein, R. J. A new global coastal database for impact and vulnerability analysis to sea-level rise. *Journal of Coastal Research*, pages 917–924, 2008.

Van Dongeren, A., Lowe, R., Pomeroy, A., Duong, T. M., Roelvink, D., Symonds, G., and Ranasinghe, R. Modelling infragravity waves and currents across a fringing coral reef. *Coastal Engineering Proceedings*, 1(33):29, 2012.

Vo-Luong, P. and Massel, S. Energy dissipation in non-uniform mangrove forests of arbitrary depth. *Journal of Marine Systems*, 74(1):603–622, 2008.

Xiaofeng, Z. *An investigation on the root system of mangroves and its influence on current flow*. PhD thesis, 2014.

A

Mangroves

A.1. Method 1

A.1.1. Assumptions

Table A.1: Mangrove species for the different studies

Type	Species	Source
Red	Lumnitzera littorea	Cole et al. (1999)
	Xylocarpus granatum	Cole et al. (1999)
	Bruguiera gymnorrhiza	Cole et al. (1999)
	'Rhizophora sp.'	Krauss et al. (2003), Horstman et al. (2012)
	Rhizophora mucronata	Cole et al. (1999), Narayan (2009)
	Rhizophora apiculata	Cole et al. (1999)
	Rhizophora stylosa	Mazda et al. (1997b), Brinkman (2006), Xiaofeng (2014)
Black	Avicennia marina	Dahdouh-Guebas et al. (2007), Horstman et al. (2012)
	Xylocarpus	Cole et al. (1999)
	Sonneratia alba	Cole et al. (1999), Krauss et al. (2003), Mazda et al. (2006), Narayan (2009), Bo (2012), Xiaofeng (2014)

- Mazda et al. (1997b). The upper and lower limit are determined by the minimum and maximum respectively of the 'Nakama-Gawa' and 'Coral Creek'.
- Krauss et al. (2003). The upper and lower limit are determined by the minimum and maximum respectively found in the table for both 'prop roots' and 'pneumotophores'.
- de Vos (2004). Results from the measurement campaign are used.
- Brinkman (2006). Max. and min. vegetation values from the model sensitivity analysis are used.
- Mazda et al. (2006). Average values found plus and minus standard deviation given.
- Dahdouh-Guebas et al. (2007). For the density of the roots the lowest and highest values are used. For the root height, an estimation based on the provided figures is made.
- Narayan (2009). The values from page 36 in this research are taken.
- Reimann et al. (2009). The dimensions are taken from the mid age and mature growth stage of the Rhizophora apiculata. C_D is from the range of experimental values of different model types. The ratio of different dimensions are also used to adjust values of Cole et al. (1999), Tusinski (2012) and Horstman et al. (2014).
- Tusinski (2012). The "various sources" are used. Depending whether prop roots or pneumatophores were present, the tree is considered Red or Black respectively. C_D is determined from the range of values which are used in the sensitivity analysis.
- Bo (2012). The average root density within 1 meter from tree trunk is taken.
- Xiaofeng (2014), page 168 and 169 provides a summary of vegetation observations

Table A.2: Upper and lower limits of vegetation parameters, where Red represent prop rooted mangroves and Black pneumathophores based mangroves

		Layer 1				Layer 2			
		b_v (m)	N (roots/m^2)	C_D (-)	h_v (m)	b_v (m)	N (roots/m^2)	C_D (-)	h_v (m)
Red mangroves	Mazda et al. (1997b)	0.036-0.037	72-152	0.4-10	0.182-0.255	0.057-0.086	0.8-1.0	0.4-10	-
	Cole et al. (1999)	-	-	-	1.2-2.4	0.184-0.245	-	-	2.3-4.9
	Krauss et al. (2003)	0.0269-0.0276	39-52	-	-	-	-	-	-
	Brinkman (2006)	0.02-0.08	9-49	0.7-1.2	0.75	-	-	0.7-1.2	-
	Narayan (2009)	0.05-0.1	1-130	1	-	0.15-0.4	0.5-1.7	1	5-8
	Husrin et al. (2012)	0.02-0.08	-	1-10	1-2	0.05-0.20	-	1-10	1-4
	Tusinski (2012)	-	6-50	0.12-1	1.1-3.3	0.4-0.9	0.35-0.59	0.7-1.0	2.1-6.7
	Bo (2012)	0.02-0.04	-	-	-	-	-	-	-
	Xiaofeng (2014)	0.03-0.05	16-233	1.2-1.8	0.114	-	-	-	-
	Horstman et al. (2014)	0.019-0.033	16-26	-	1.3-2.7	0.16-0.46	0.06-0.15	-	2.7-5.3
	Number of inputs	8	7	6	7	6	4	5	5
	Low	0.019	1	0.12	0.114	0.05	0.06	0.4	1
	Average	0.042	58.29	2.45	1.15	0.27	0.64	1.77	4.2
	High	0.1	233	10	3.3	0.9	1.7	10	8
Black mangroves	Cole et al. (1999)	-	-	-	-	0.258-0.453	-	-	5.2-9.2
	Krauss et al. (2003)	0.0114-0.044	45-51	-	-	-	-	-	-
	de Vos (2004)	-	9-130	-	0.1-0.28	-	-	-	-
	Mazda et al. (2006)	0.003-0.012	131	-	0.03-0.246	0.071-0.163	0.08	-	-
	Dahdouh-Guebas et al. (2007)	-	4-1950	-	0.11-0.25	-	-	-	-
	Narayan (2009)	0.01-0.04	4-100	1	0.3-0.8	0.2-0.5	0.5-1.7	1	3-15
	Tusinski (2012)	0.004-0.006	-	0.12-1	0.1-0.45	-	-	0.7-1.0	2.4-4.8
	Bo (2012)	-	120	-	0.146	0.4-0.9	0.2-1.7	-	-
	Xiaofeng (2014)	0.006-0.02	70-160	0.5-1.5	0.08-0.3	-	-	-	-
	Horstman et al. (2014)	0.004-0.006	28-2000	-	0.025-0.055	0.057-0.75	0.32-0.47	-	0.7-8
	Number of inputs	6	8	3	8	5	4	2	4
	Low	0.003	4	0.12	0.025	0.057	0.08	0.7	0.7
	Average	0.014	303.8	2.04	0.21	0.38	0.64	0.93	6.04
	High	0.044	2000	1.5	0.8	0.9	1.7	1	15

Boxplots

The values of representative densities, given in Table 4.3, are determine from Figure 4.2 as follows. If the average value is within the 25th and 75th percentiles, these boundaries will represent the minimum and maximum values respectively and the median is considered to be the most viable 'average' value. In case the real average is outside the mentioned boundaries, this average will represent the minimum or maximum value and the 25th or 75th percentile the other minimum or maximum respectively. The boxplots for vegetation height, vegetation factor and drag coefficient are illustrated below. However, these are not directly used in the analysis.

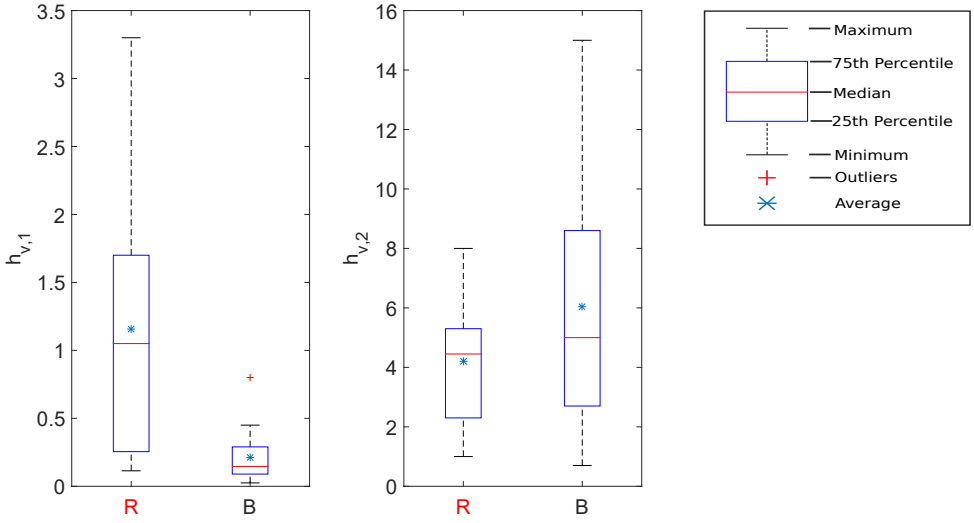

Figure A.1.1: Boxplot for vegetation height of layer 1 (left) and layer 2 (right) for Red (=R) and Black (=B) mangroves according to different sources (see Table A.2)

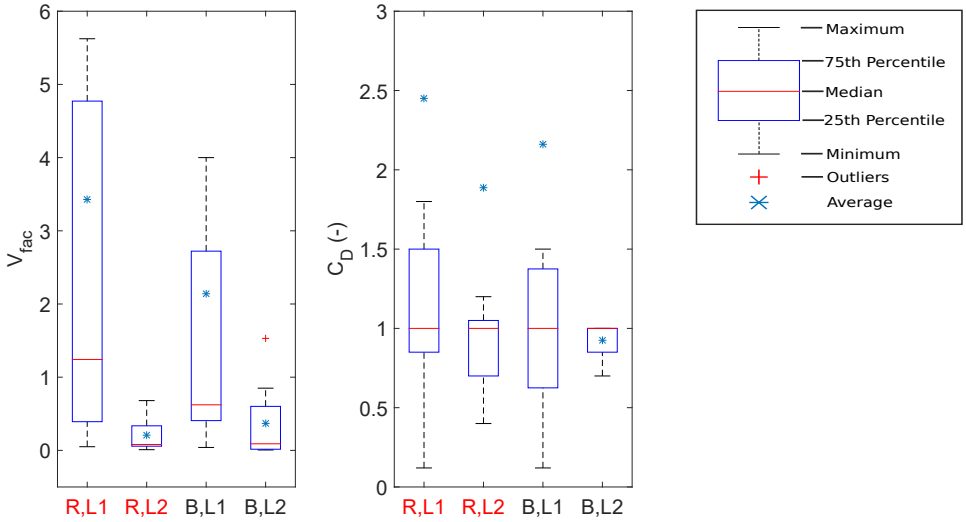

Figure A.1.2: Left: boxplot for vegetation factor (Eq. 4.2) and right: boxplot for drag coefficient according to different sources (see Table A.2). R=Red mangroves, B=Black mangroves, L1=layer 1, i.e. root layer and L2=layer 2, i.e. stem layer

Canopy characteristics

This includes the determination of the canopy values presented in Table 4.3. The parameters are determined in the following sequence: height, biomass, vegetation factor and bulk drag coefficient.

Volume equations were constructed in order to estimate the biomass of mangrove trees in Cole et al. (1999). Multiple equations are given for different areas, which required a separate analysis. Most likely 'height' is defined as the total height of a mangrove tree and not only the stem (i.e. layer 2). In the study two volume equations are given based on statistical analysis: one with and one without the height included. This is done for several locations where other mangrove species are present. Comparing both equations and average them resulted in Figure A.1.3. By using the diameters of layer 2 (Table 4.3), the total tree height is determined. The subdivision for Red and Black mangroves is based on Table A.1. The result is given in Table A.3

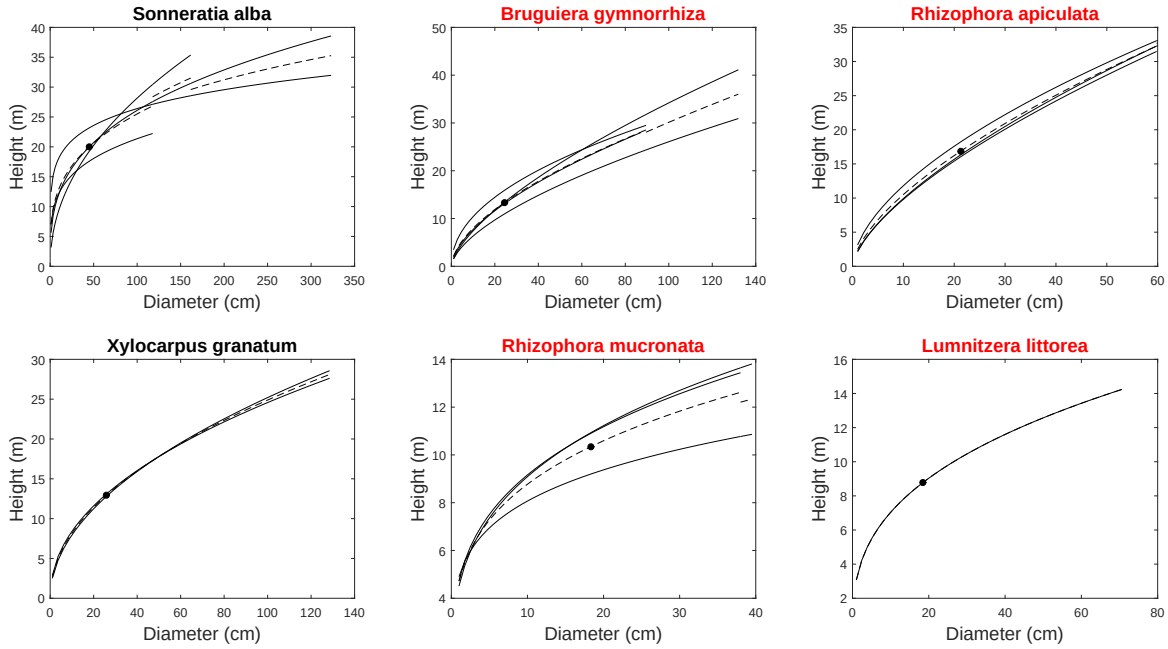

Figure A.1.3: Relation height and diameter (DBH) for different mangrove species, after Cole et al. (1999). Solid lines represent relations for different study sites, dashed lines the average of these locations and the dots the average based on found characteristics.

Table A.3: Total vegetation heights in meter according to Figure A.1.3 for four Red mangrove and two Black mangrove types. S=sparse, M=medium and D=dense

	BG	RA	LL	RM	XG	SA
S	13.7	18.7	11.3	9.8	17.3	13.2
M	17.2	23.9	12.5	11.4	19.9	17.0
D	19.9	28.3	12.3	12.4	23.3	21.5

The vegetation factor for layer 3, i.e. (Eq. 4.2) $V_{\text{fac},3}$ is determined using the biomass relation, given in Eq. 4.1. The made assumption is that a large summed biomass for layer 1 and layer 2, corresponds with a large biomass of layer 3. The maximum assumed BM_3 for a certain vegetation set is 100 (Narayan, 2009). Therefore the scaling is presented as:

$$BM_{fac,3} = \frac{BM_{fac,1} + BM_{fac,2}}{max(BM_{fac,1} + BM_{fac,2})} \cdot 100 \tag{A.1}$$

Apparently has the dense variant of Red mangroves the maximum biomass, implying that BM_3=100 is assigned to this variant. Based on this, the canopy biomass of the other variants is determined (Table A.4). The vegetation factor for layer 3 is subsequently determined by dividing the biomass factor by the found $h_{v,3}$ (Table 4.3). Finally, the bulk drag coefficient is assumed to be 0.5, because it is considered to be lower than stem and root layer, which can minimal reach the value of 0.6.

Table A.4: Biomass factors for all layers, vegetation factor and bulk drag coefficient of layer 3 for all six variants. S=sparse, M=medium, D=dense and br=branches

		BM_1	BM_2	BM_3	$V_{fac,3}$	$\tilde{C}_{D,3}$
Red	S	0.05	0.14	1.3	0.1	0.50
	M	0.45	1.35	12.8	1.1	0.50
	D	2.10	5.51	54.3	4.5	0.50
Black	S	0.03	0.01	0.3	0.1	0.50
	M	0.48	0.30	5.6	0.5	0.50
	D	7.68	6.34	100	7.7	0.50

A.1.2. Vertical layering

The distribution of vegetation factors is changed, but not its maximum values. This means that the same vegetation factor for root, stem and canopy is applied, but the transitions towards this values is more spread out. The method for quantifying the vegetation parameters of the different layers is as follows:

1. Determine if the tree is Red, Black or pioneer
2. Find amount of added layers n per root, stem or canopy based on the ratio in vegetation factor between root and stem layer. For canopy this is set to 3, because this layer is less frequently submerged and thus do not need an increase in accuracy.
3. Linearly decrease/increase the vegetation factor with ΔV_{fac}, which is defined as the difference between bordering vegetation factors divided by the number of added layers.

The following exceptions are made:

- The layering of the Red root layer continues till 1/3 of the stem layer height, because this layer is relatively small, implying that ΔV_{fac} would be too large. Additionally, it is assumed to better represent a Red mangrove tree.
- No layering of Black mangrove roots is added, because the pneumatophores are assumed to be around the same height.
- The layering of the canopy layer consist of a part from stem to halfway canopy height and a part from canopy to top of the tree
- Also no layering is for the root layer of the pioneer type is conducted, because insufficient data is available. Additionally, only an upper canopy is presented, because no stem layer is present.

Table A.5: Increasing number of layers to n for different vegetation sets

	Root			Lower canopy			Upper canopy		
	n	ΔV_{fac}	Δh_v (m)	n	ΔV_{fac}	Δh_v (m)	n	ΔV_{fac}	Δh_v (m)
Red	4	0.16	0.5	3	0.24	1.7	3	0.33	1.7
Black	1	-	-	3	0.3	1.7	3	0.33	1.7
Pioneer	1	-	-	-	-	-	3	0.36	0.7

The bulk drag coefficients for each non-canopy layer is determined according to the method described in Section 4.1.4. This means that the density of root and stem layer need to be preserved. Therefore the density for all the layers remains the same as the initial 3-layered model and thus can the vertical layering be seen as an adjustment of solely diameter. The effect of this vertical layering is presented in Figure 5.3.

A.2. Method 2

This is the only used dataset, provided by Horstman et al. (2014). The set gives measurements of diameters of Rhizophora sp. and Avicennia sp. and height of pneumatophores, determined at different heights above the ground. The data is analysed using the same approach elaborated in Section 4.1.1, i.e. make a boxplot, calculate the average and determine range (Figure A.2.4). The stem heights are also given, but indicate a guess rather than a measurement. The determination of the stem height in this analysis is based on the ratio approach, also applied in Cole et al. (1999) analysis above.

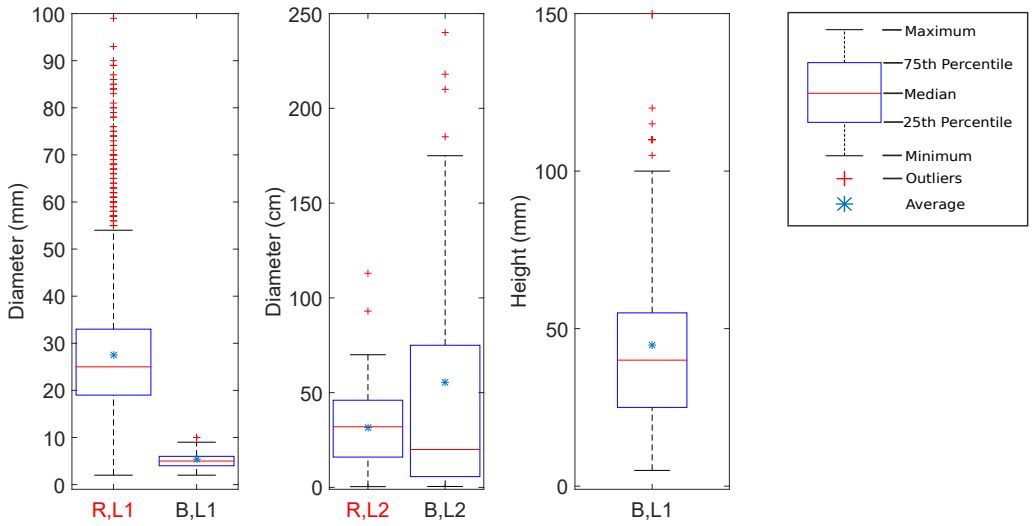

Figure A.2.4: Boxplot for diameter (left and middle figures) and height (right figure), after Horstman et al. (2014)

Whether certain parts of the tree contribute to the Mazda length scale depends on the local depth. Namely, for a water depth of 2.00 m, the projected surface area and mangrove volume per unit width are given by:

$$A_p = \sum_{i=1}^{5} b_{v,i} N_i h_{v,i} \qquad \text{(A.2)}$$

$$V_M = \sum_{i=1}^{5} \frac{1}{4} \pi b_{v,i}^2 N_i h_{v,i} \qquad \text{(A.3)}$$

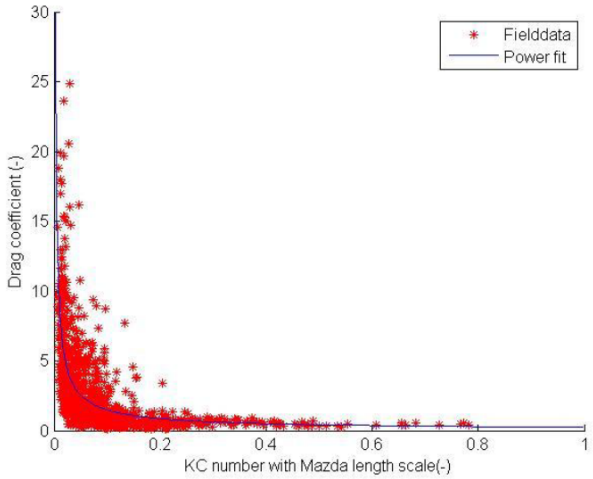

Figure A.2.5: Calibrated bulk drag coefficients as function of the Keulegan-Carpenter number with included Mazda length scale from Hendriks (2014). The blue line represents Eq. 4.6

B

Hydrodynamics

B.1. SWAN

B.1.1. Case study locations (stationary)

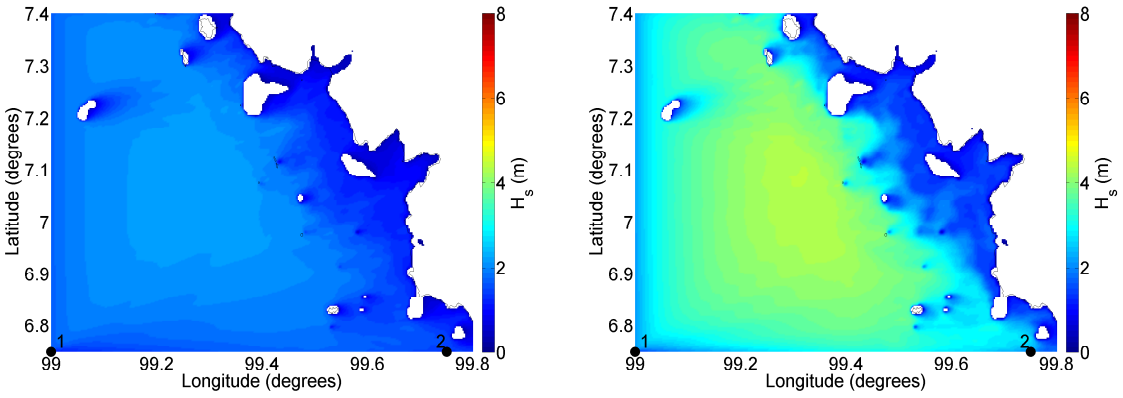

Figure B.1.1: Wave height 1 yr^{-1} return period Andaman Sea for the non-scaled (left) and cyclone-scaled (right) simulations

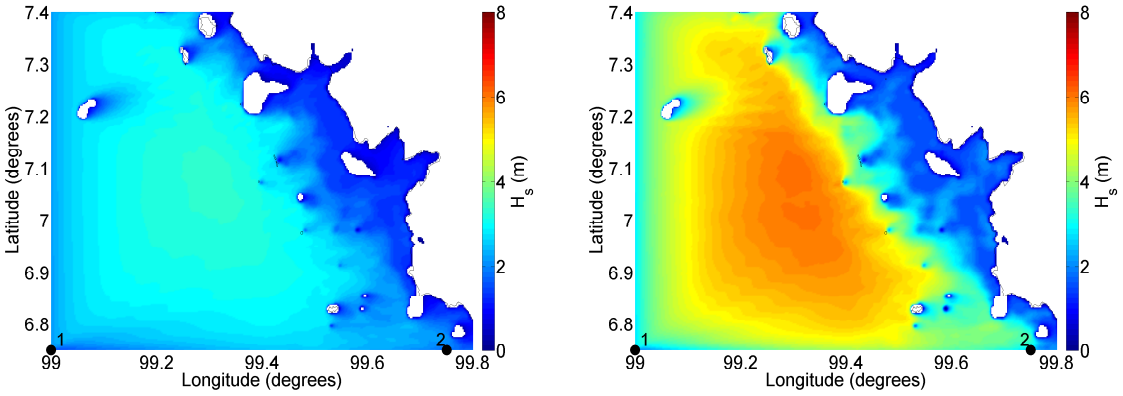

Figure B.1.2: Wave height 10 yr^{-1} return period Andaman Sea for the non-scaled (left) and cyclone-scaled (right) simulations

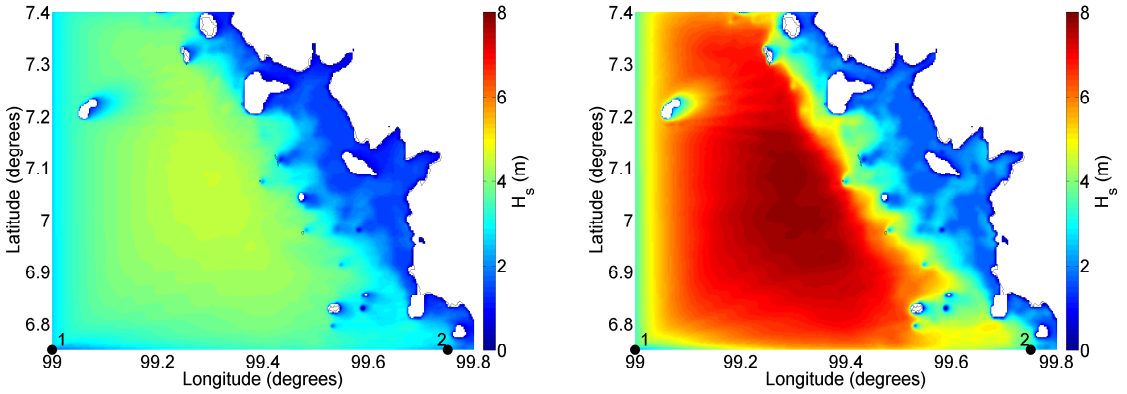

Figure B.1.3: Wave height 100 yr^{-1} return period Andaman Sea for the non-scaled (left) and cyclone-scaled (right) simulations

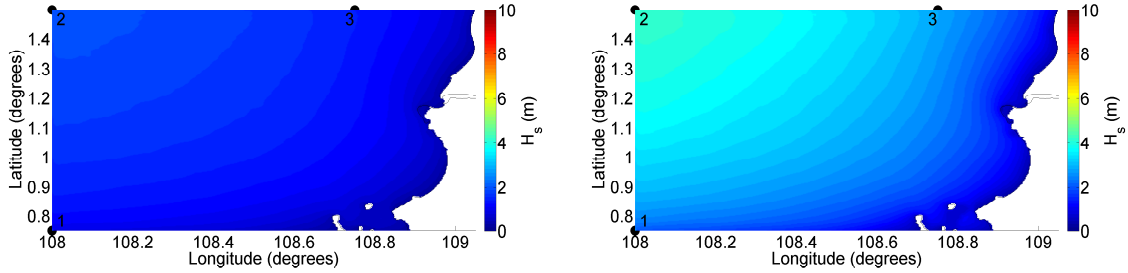

Figure B.1.4: Wave height 1 yr^{-1} return period Singkawang for the non-scaled (left) and cyclone-scaled (right) simulations

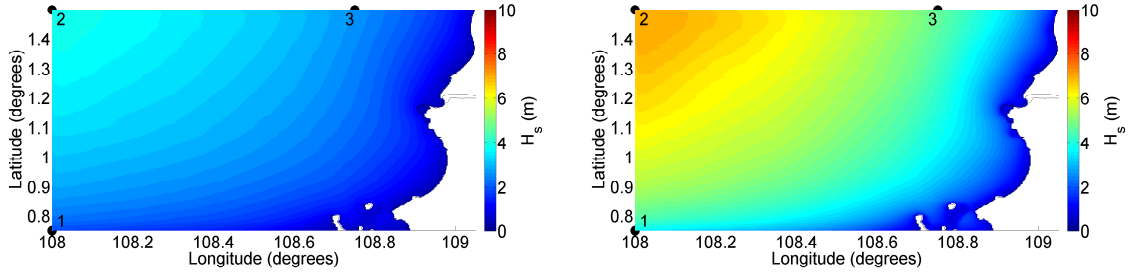

Figure B.1.5: Wave height 10 yr^{-1} return period Singkawang for the non-scaled (left) and cyclone-scaled (right) simulations

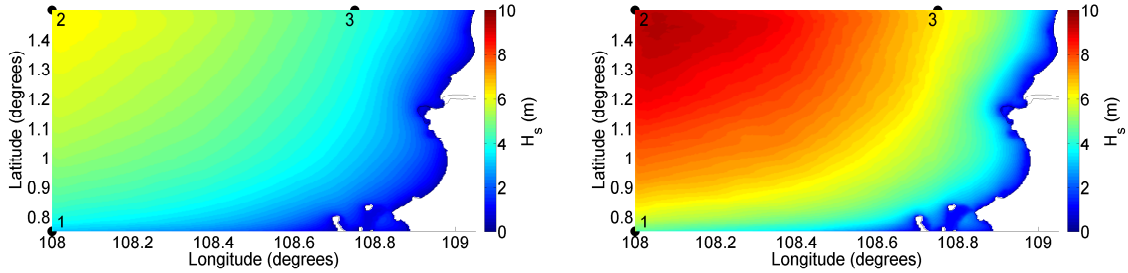

Figure B.1.6: Wave height 100 yr^{-1} return period Singkawang for the non-scaled (left) and cyclone-scaled (right) simulations

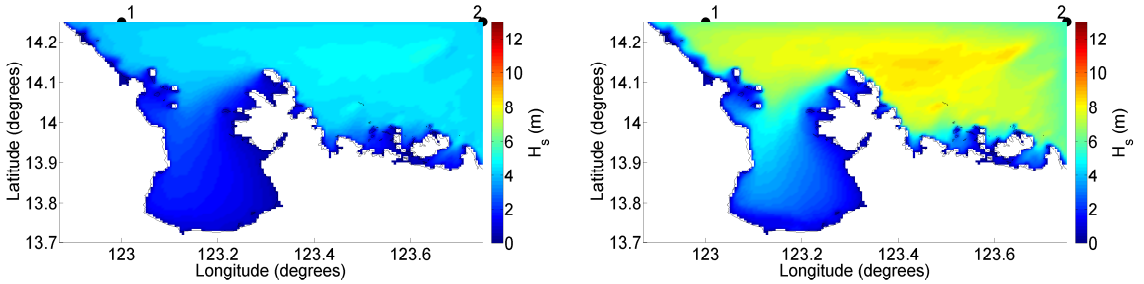

Figure B.1.7: Wave height 1 yr^{-1} return period San Miguel Bay for the non-scaled (left) and cyclone-scaled (right) simulations

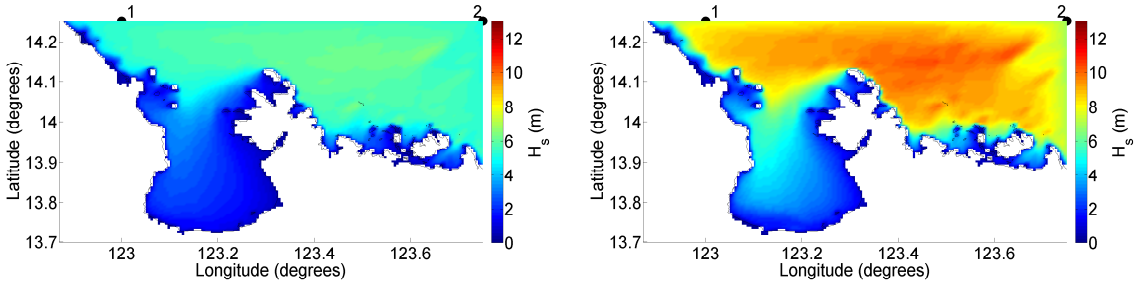

Figure B.1.8: Wave height 10 yr^{-1} return period San Miguel Bay for the non-scaled (left) and cyclone-scaled (right) simulations

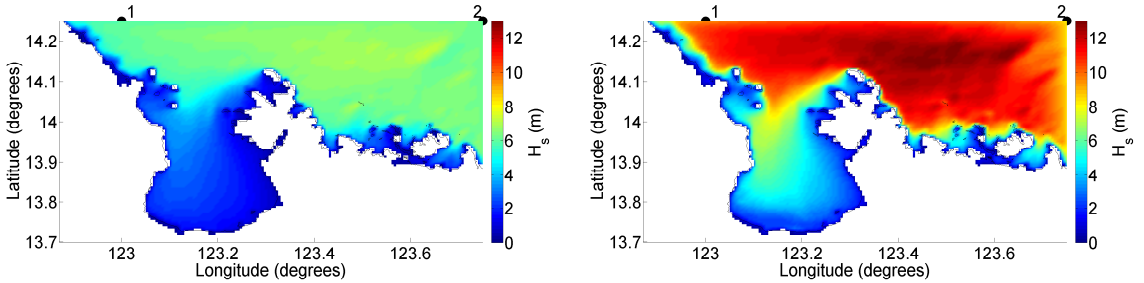

Figure B.1.9: Wave height 100 yr^{-1} return period San Miguel Bay for the non-scaled (left) and cyclone-scaled (right) simulations

B.1.2. Hydrodynamic study locations (non-stationary)

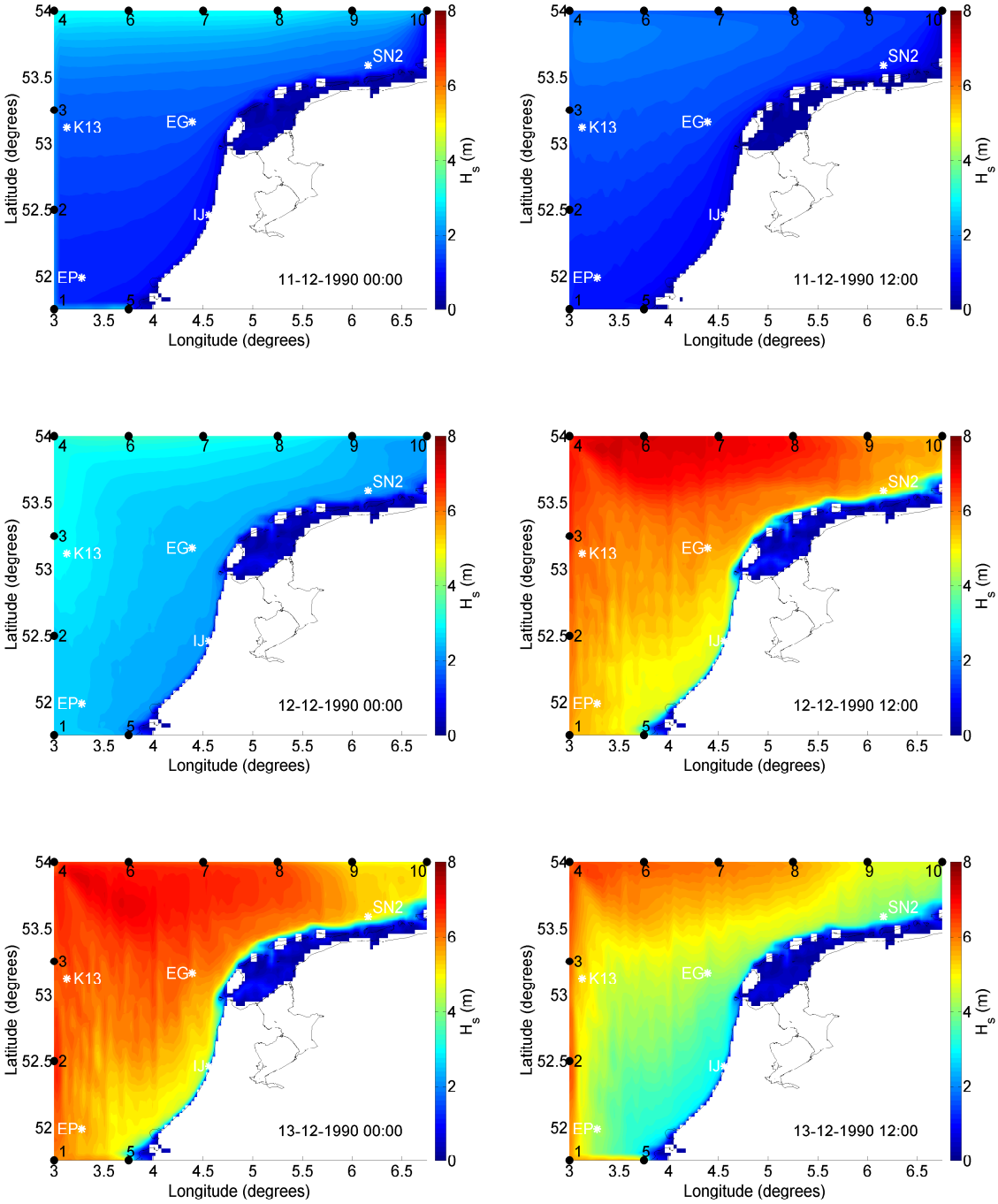

Figure B.1.10: December 1990 storm simulation North Sea with ERA-I points (black dots) and wave buoys (white stars)

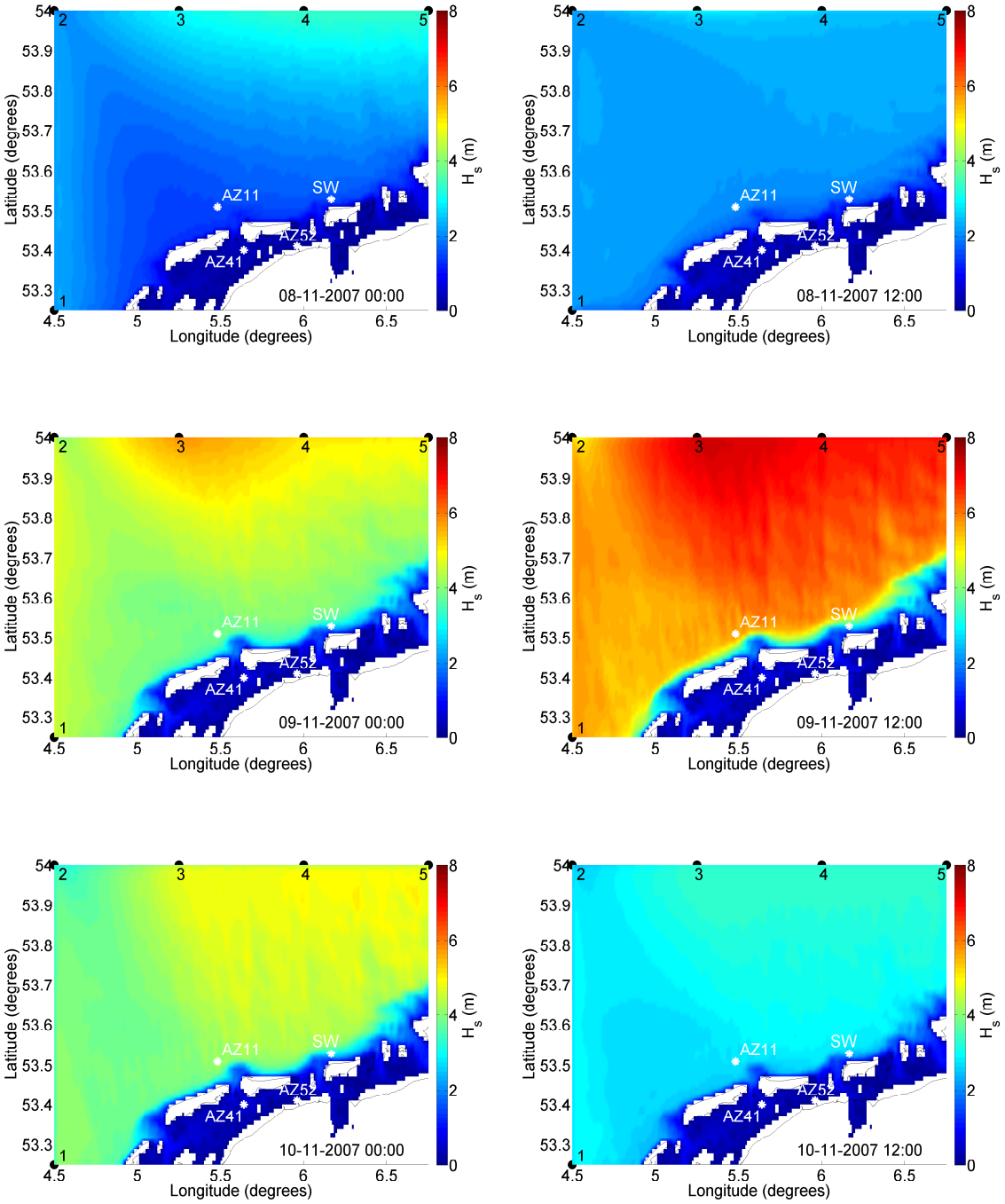

Figure B.1.11: November 2007 storm simulation Wadden Sea with ERA-I points (black dots) and wave buoys (white stars)

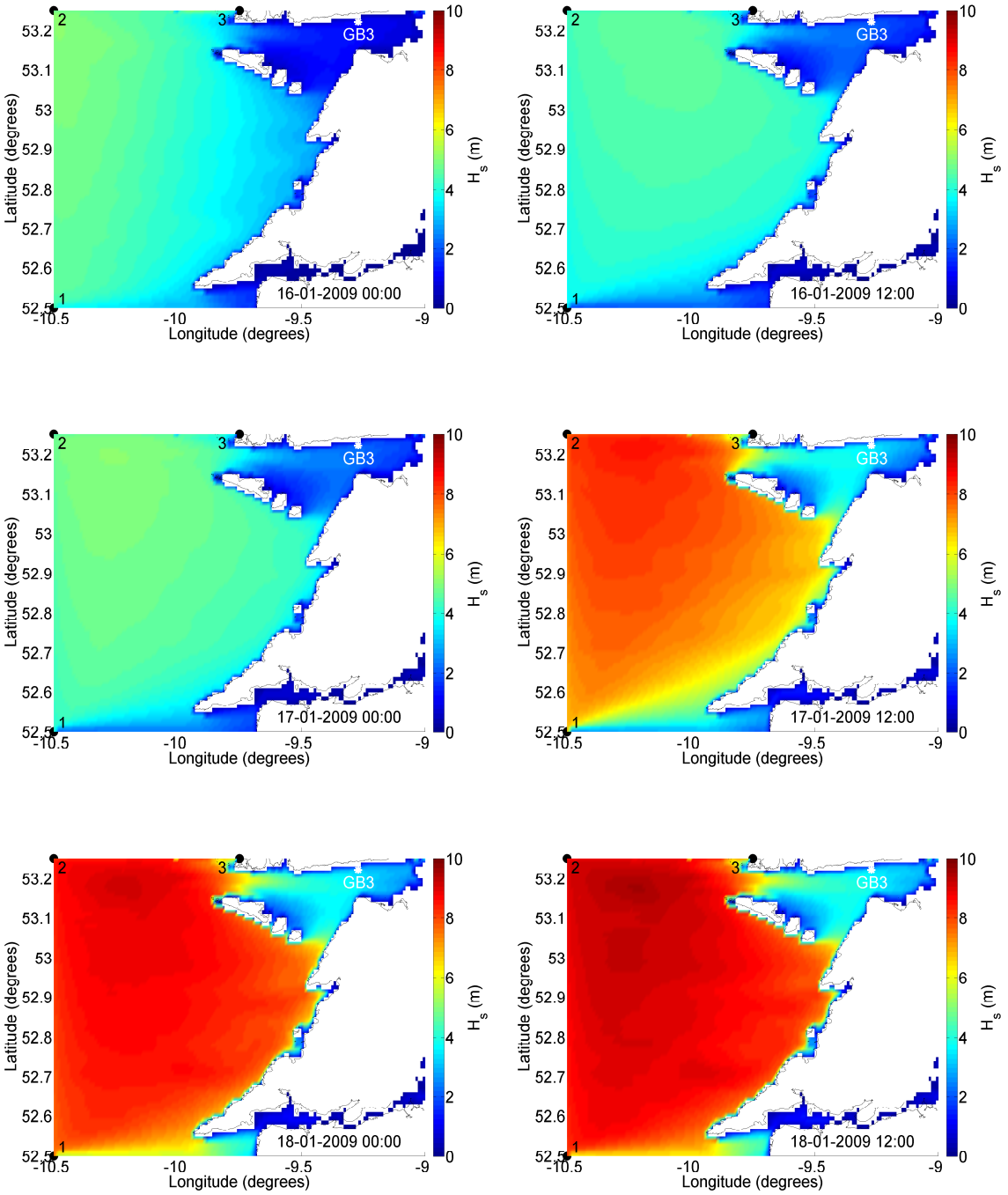

Figure B.1.12: January 2009 storm simulation Galway Bay with ERA-I points (black dots) and wave buoy (white star)

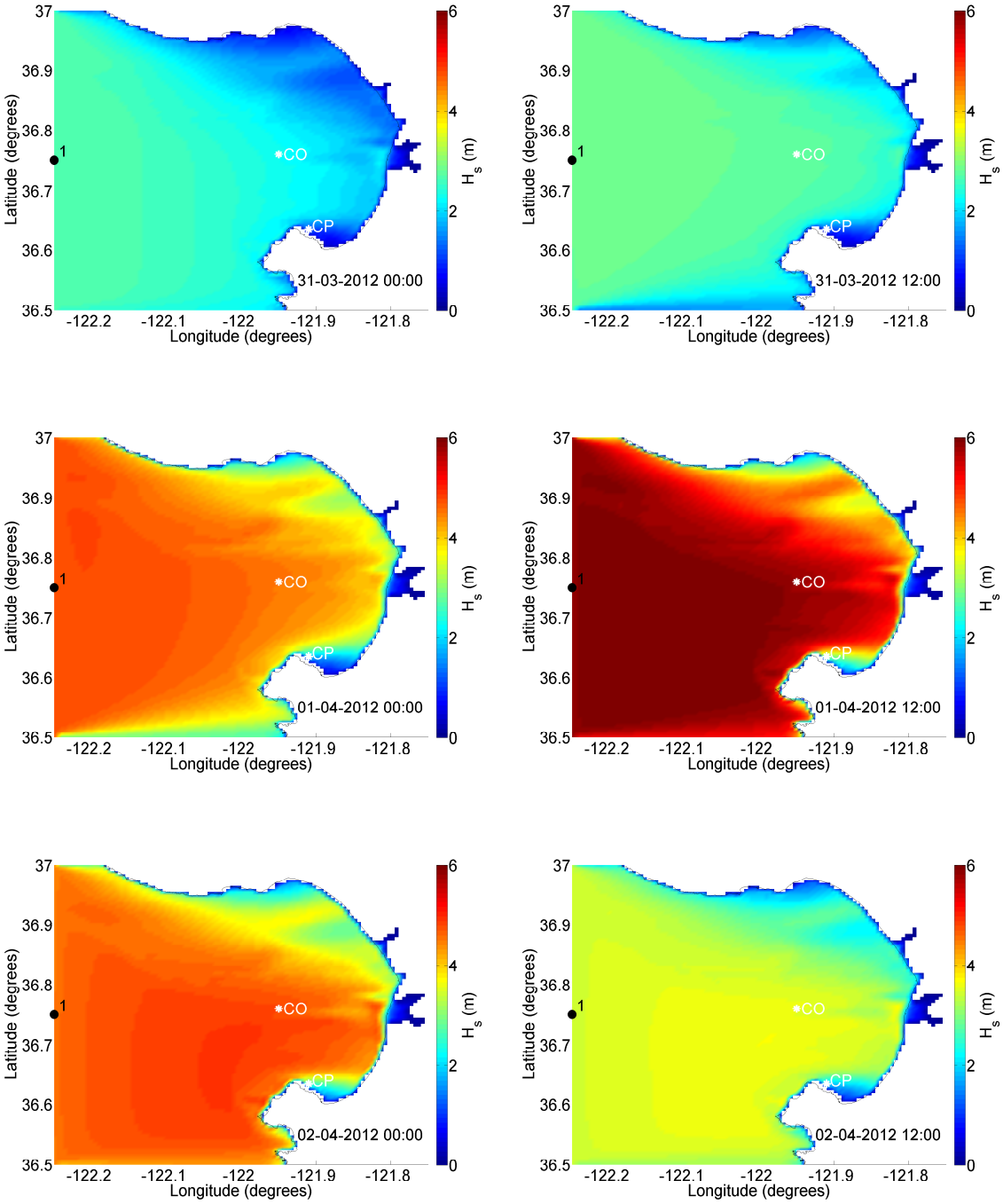

Figure B.1.13: March 2012 storm simulation Monterey Bay with ERA-I point (black dot) and wave buoys (white stars)

B.1.3. Buoy validation

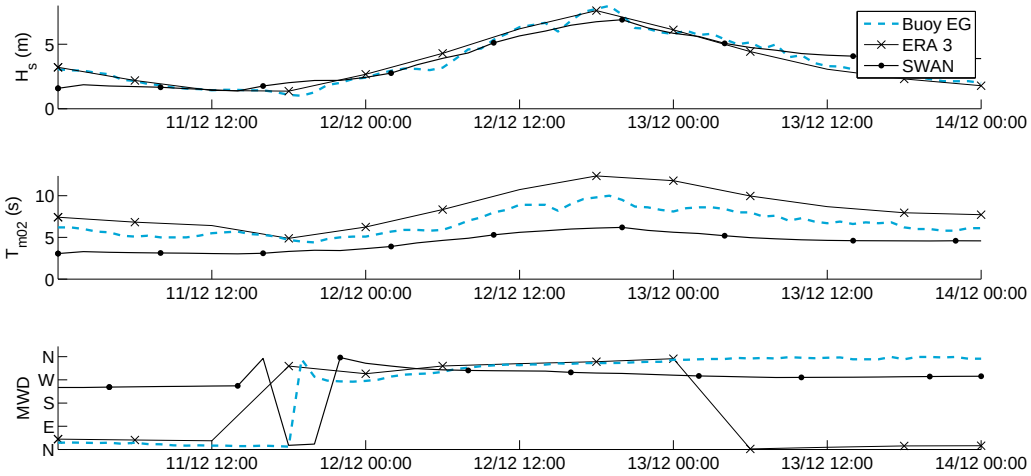

Figure B.1.14: SWAN validation for Eierlandse Gat buoy. ERA-I point 3 is the closest boundary point to Eierlandse Gat.

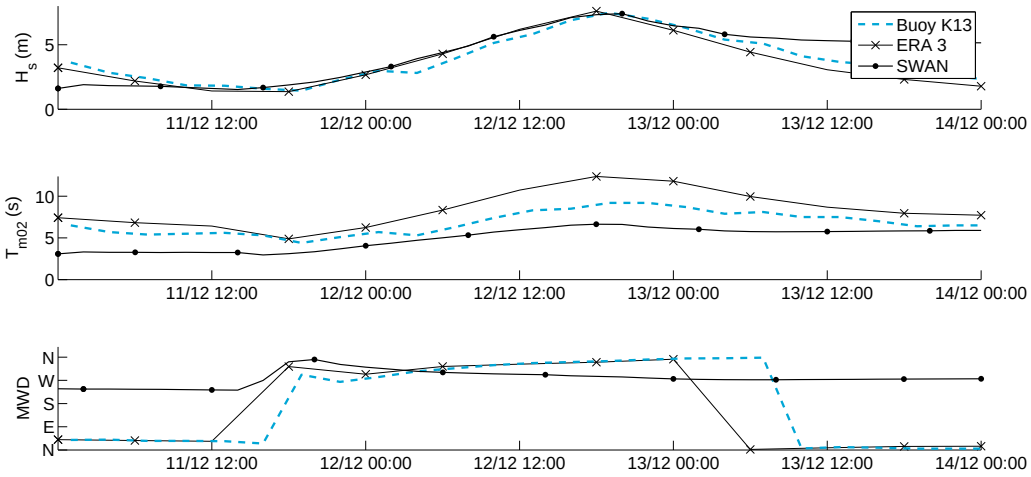

Figure B.1.15: SWAN validation for K13 buoy. ERA-I point 3 is the closest boundary point to K13.

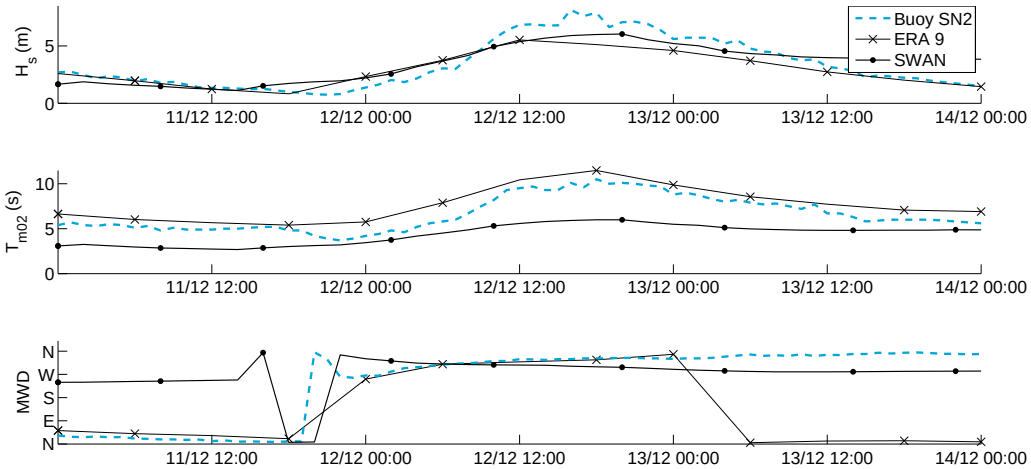

Figure B.1.16: SWAN validation for Schiermonnikoog Noord 2 buoy. ERA-I point 9 is the closest boundary point to Schiermonnikoog Noord 2.

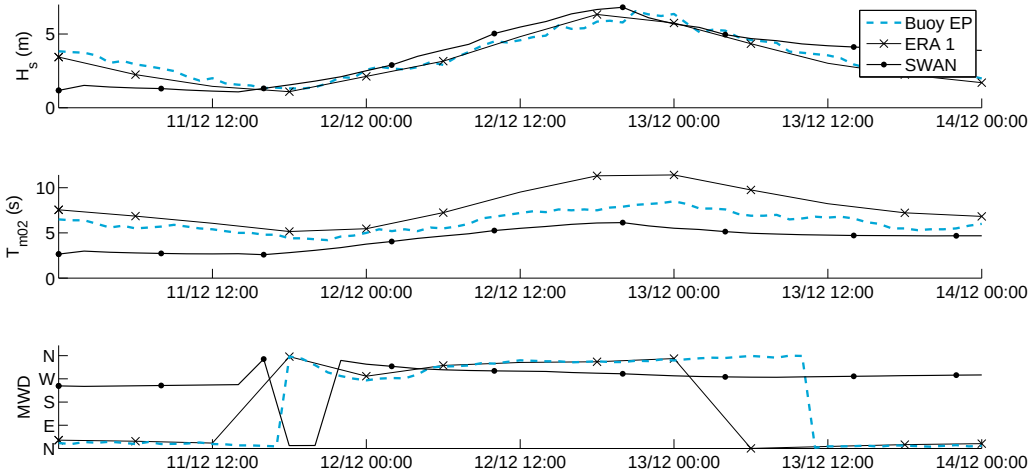

Figure B.1.17: SWAN validation for Europlatform buoy. ERA-I point 1 is the closest boundary point to Europlatform.

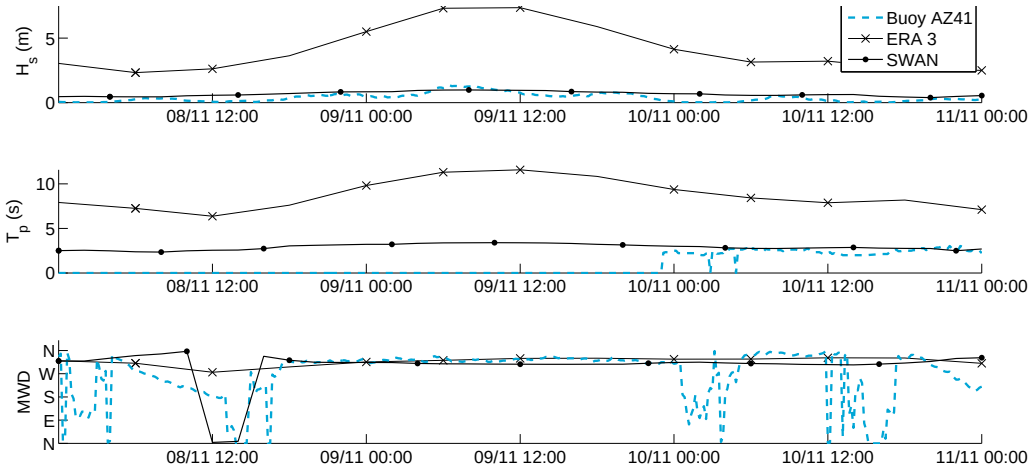

Figure B.1.18: SWAN validation for Amelander Zeegat 4.1 buoy. ERA-I point 3 is the closest boundary point to Amelander Zeegat 4.1.

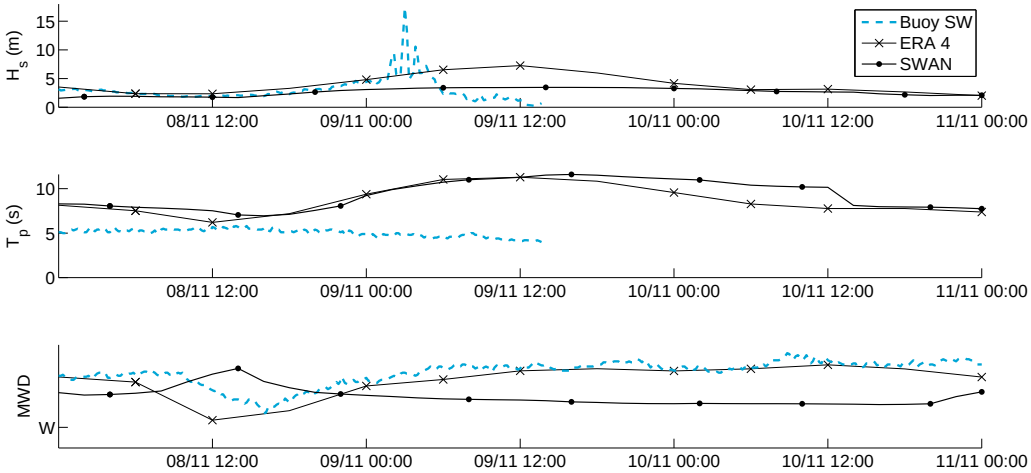

Figure B.1.19: SWAN validation for Schiermonnikoog Westgat buoy. ERA-I point 4 is the closest boundary point to Schiermonnikoog Westgat.

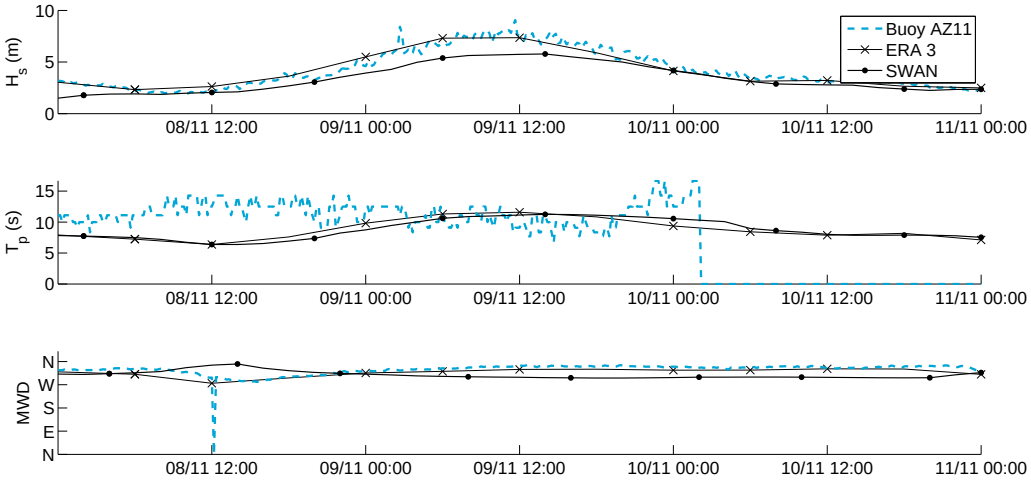

Figure B.1.20: SWAN validation for Amelander Zeegat 1.1 buoy. ERA-I point 3 is the closest boundary point to Amelander Zeegat 1.1.

B.1.4. Comparison

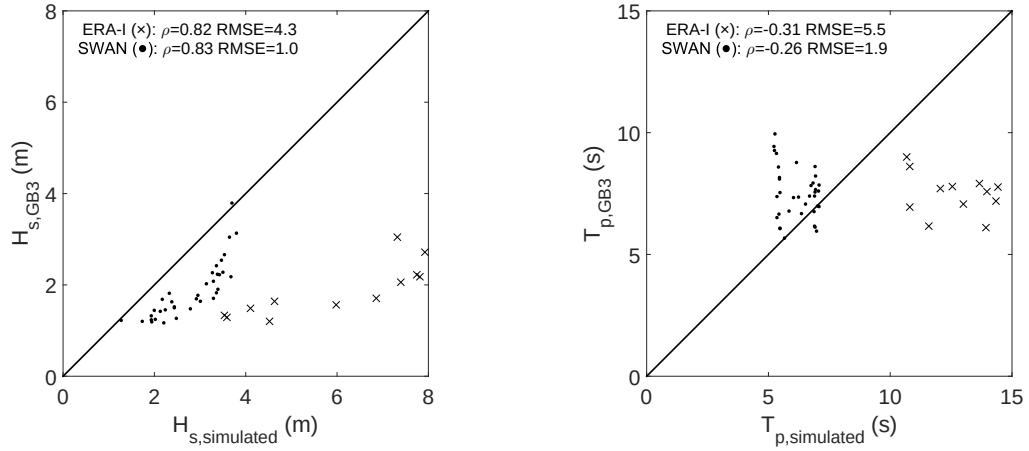

Figure B.1.21: Comparison of the Galway Bay 3 buoy with simulated wave heights (left) and periods (right) of ERA-I and SWAN.

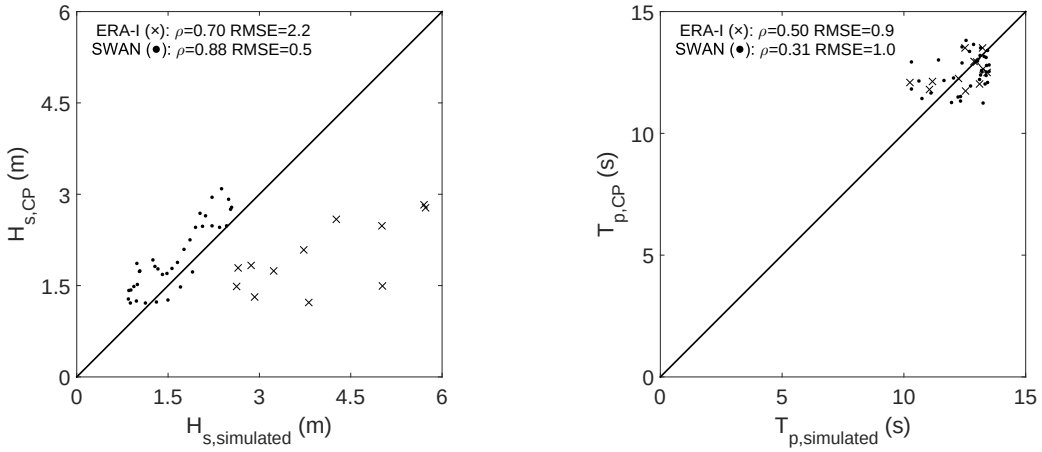

Figure B.1.22: Comparison of the Cabrillo Point buoy with simulated wave heights (left) and periods (right) of ERA-I and SWAN.

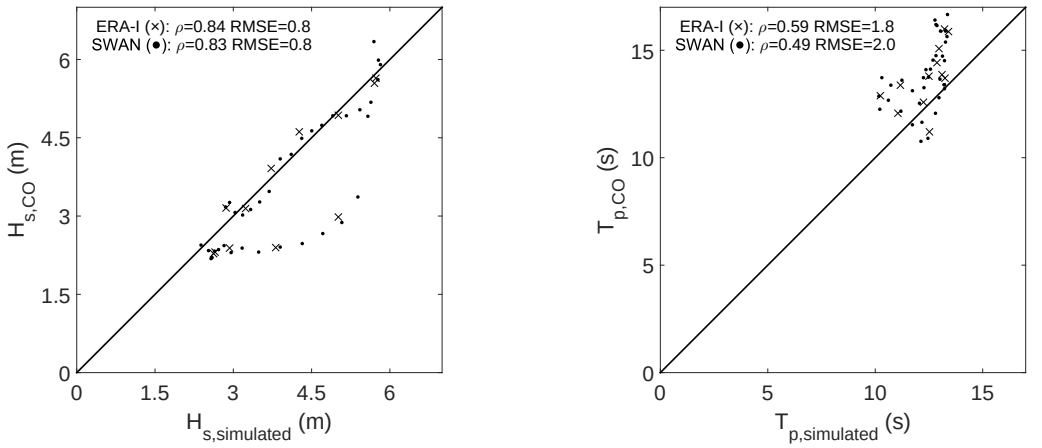

Figure B.1.23: Comparison of the Canyon Outer buoy with simulated wave heights (left) and periods (right) of ERA-I and SWAN.

B.2. Tropical cyclone scaling

The best way to determine the influence of the cyclone parameters on wave height, is to analyse the most common cyclone paths and their respective intensity for different areas. This data is however often lacking for the mangrove related areas. Additionally, as already mentioned, tropical cyclones (TC's) are not included in ERA-I. Although the potential inaccuracy of tropical cyclones is neglected in this research, a potential method is given in which the mismatch can be determined.

The scaling is done by comparing the wave and wind conditions of ERA-I with wave buoys, which measured during a tropical cyclone, for two locations along the US coast. The approach is very simplified, but at least gives an method to compensate for the missing TC-values in ERA-I. Due to the changing hurricane position in time, the scaling interval for an individual wave buoy is performed at the moment the hurricane is at the buoy location, plus and minus 18 hours in order to take the hurricane diameter into account. This means that the scaling factor is highly dependant on the time interval chosen. The 36 hour interval is however considered to be sufficient, especially because it is also based on the observations from the wave buoys.

The scaling is performed for the data in which the buoy was able to measure. This implies that for gaps in the data, no adjustment is applied. The scaling factor for an individual buoy and its ERA-I is given as follows:

$$S_j = \frac{j_{buoy}}{j_{ERA-I}} \tag{B.1}$$

in which j represents the wave height, wave period, wave direction and wind speed. The scaling results are given at the end of this section.

B.2.1. Gulf of Mexico - Hurricane Ike

This large ocean basin is often exposed to hurricanes. An example of such a TC was in September 2008, where hurricane Ike came ashore in Texas and Cuba (Figure B.2.24). Due to its large size, Ike was the costliest TC, seriously affecting infrastructure and agriculture. Ike strengthened to a category 4 hurricane at its peak. This is considered to be a 'catastrophic damaging' storm on the scale of Saffir-Simpson.

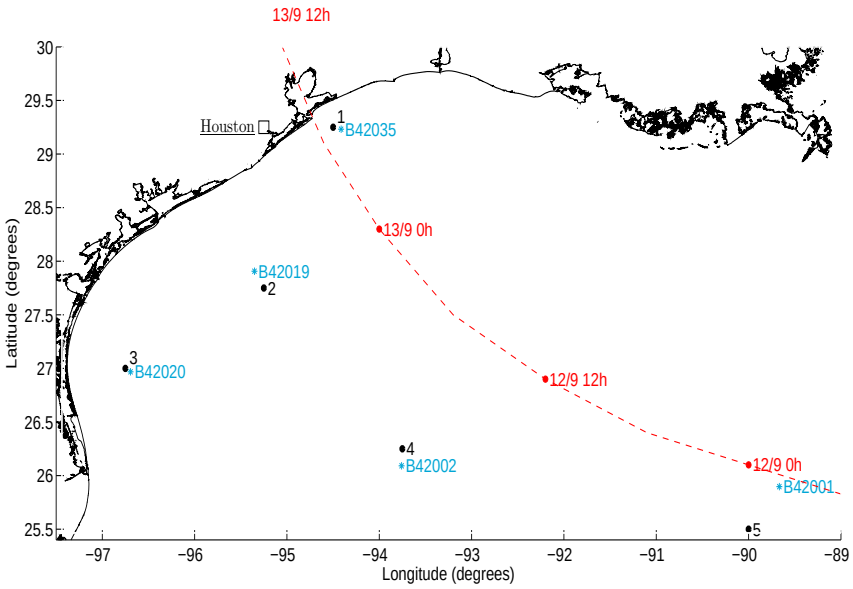

Figure B.2.24: Track, date and time of center of hurricane Ike (red dotted line), wave buoys (blue stars) and their nearest ERA-I points (black dots).

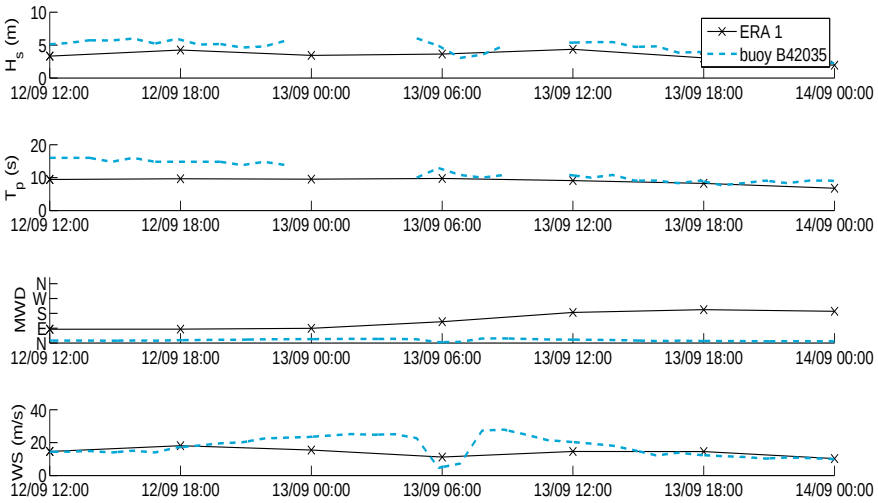

Figure B.2.25: Wave height, wave peak period, mean wave direction and wind speed from top to bottom for both buoy B42035 and ERA-I point 1 (see Figure B.2.24).

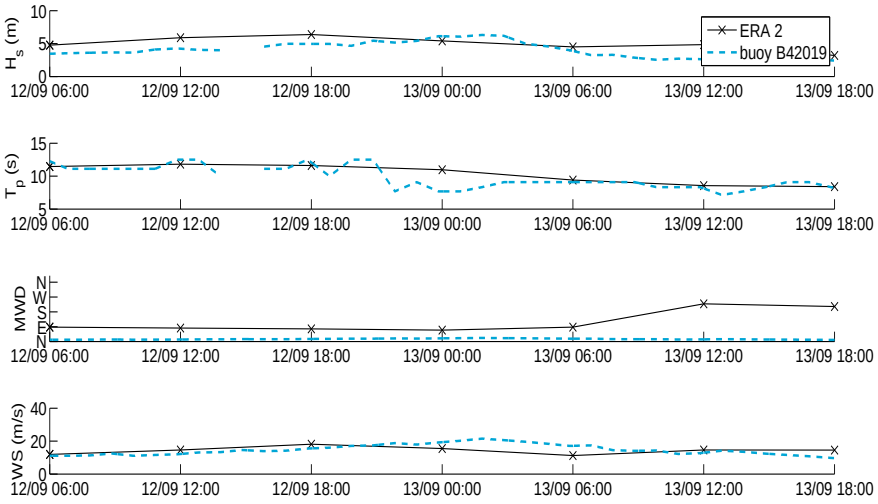

Figure B.2.26: Wave height, wave peak period, mean wave direction and wind speed from top to bottom for both buoy B42019 and ERA-I point 2 (see Figure B.2.24).

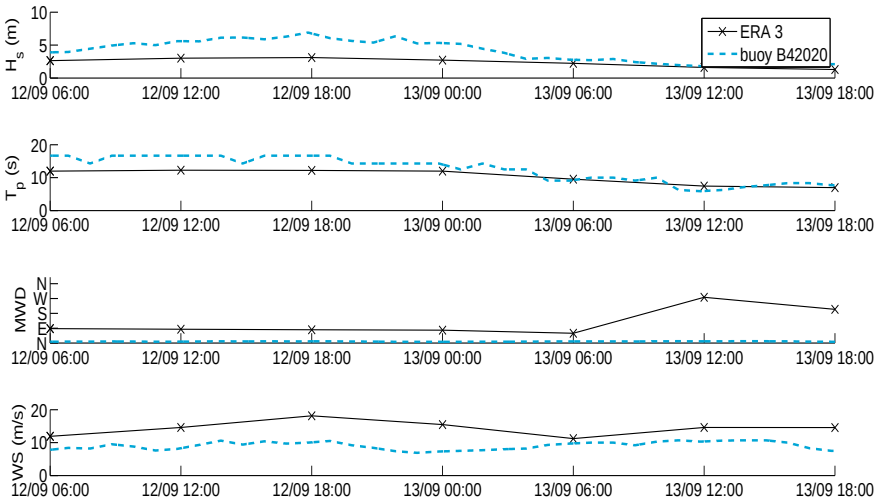

Figure B.2.27: Wave height, wave peak period, mean wave direction and wind speed from top to bottom for both buoy B42019 and ERA-I point 3 (see Figure B.2.24).

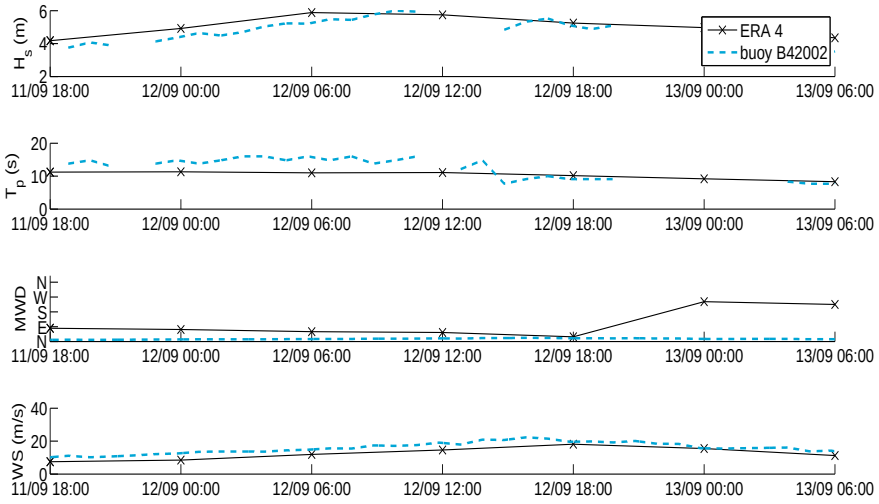

Figure B.2.28: Wave height, wave peak period, mean wave direction and wind speed from top to bottom for both buoy B42002 and ERA-I point 4 (see Figure B.2.24).

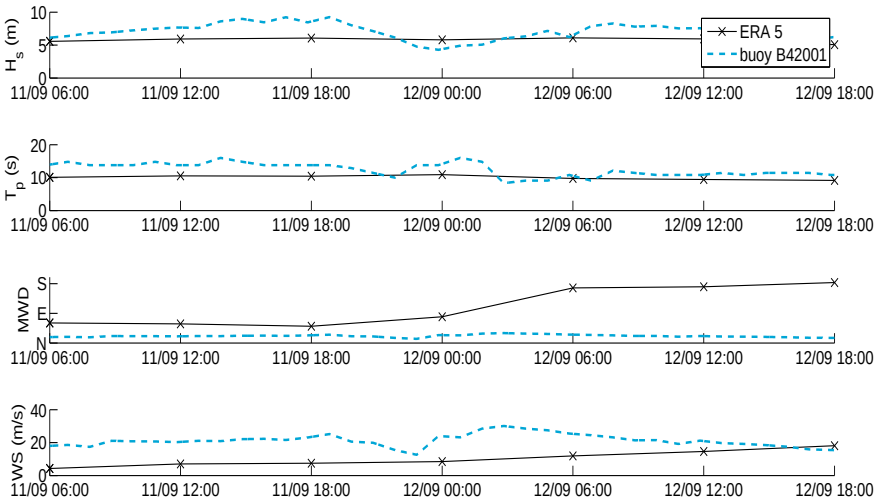

Figure B.2.29: Wave height, wave peak period, mean wave direction and wind speed from top to bottom for both buoy B42001 and ERA-I point 5 (see Figure B.2.24).

B.2.2. East Coast US - Hurricane Irene

In August 2011 hurricane Irene affected large parts of the Carribean and the East Coast of the US (Figure B.2.30). Shortly before making landfalls, Irene peaked at a category 3 (’devastating damage will occur’) hurricane. Damage was estimated to be near $15.6 billion (Avila and Cangialosi, 2011).

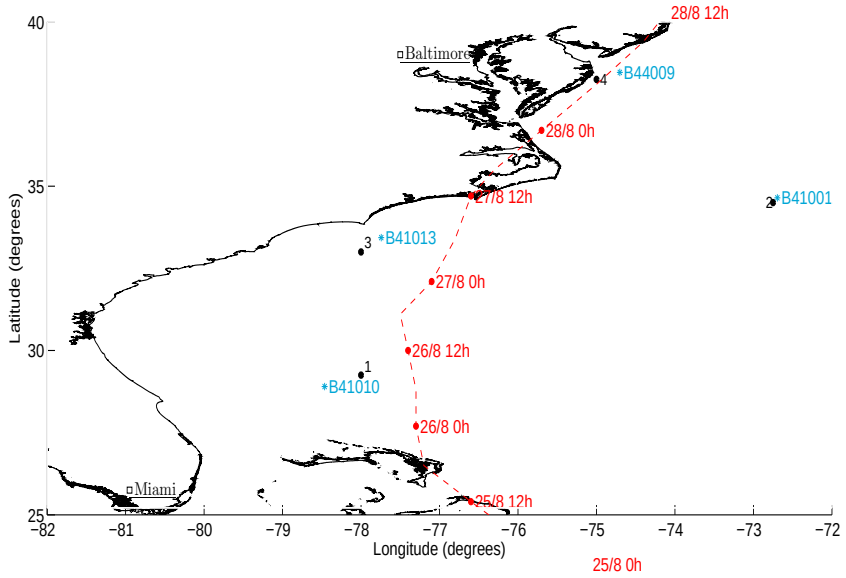

Figure B.2.30: Track, date and time of center of hurricane Irene (red dotted line), wave buoys (blue stars) and their nearest ERA-I points (black dots).

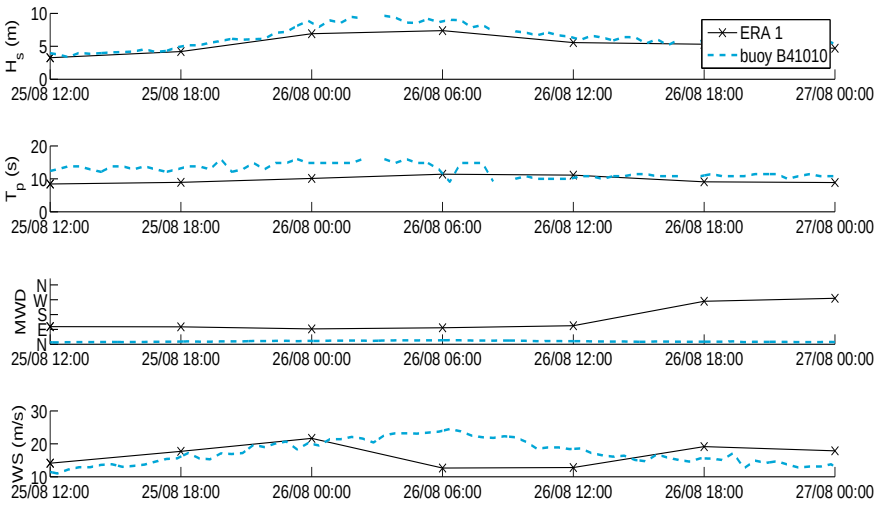

Figure B.2.31: Wave height, wave peak period, mean wave direction and wind speed from top to bottom for both buoy B41010 and ERA-I point 1 (see Figure B.2.30).

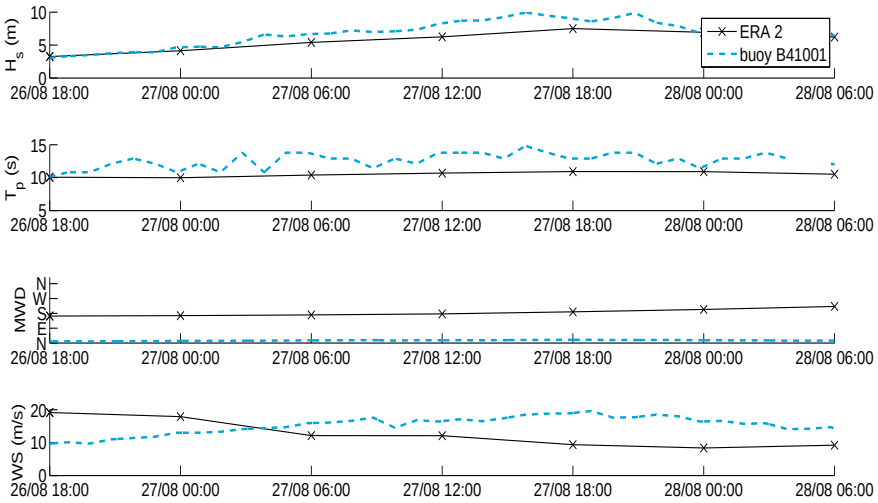

Figure B.2.32: Wave height, wave peak period, mean wave direction and wind speed from top to bottom for both buoy B41001 and ERA-I point 1 (see Figure B.2.30).

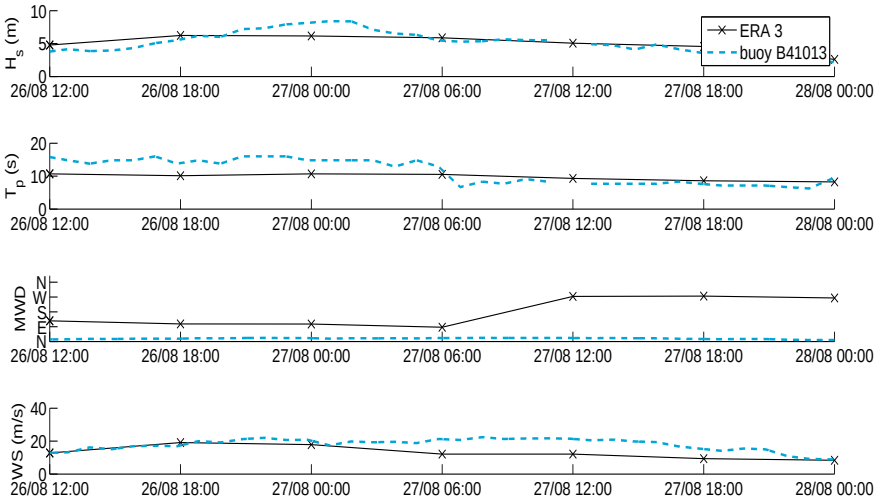

Figure B.2.33: Wave height, wave peak period, mean wave direction and wind speed from top to bottom for both buoy B41013 and ERA-I point 3 (see Figure B.2.30).

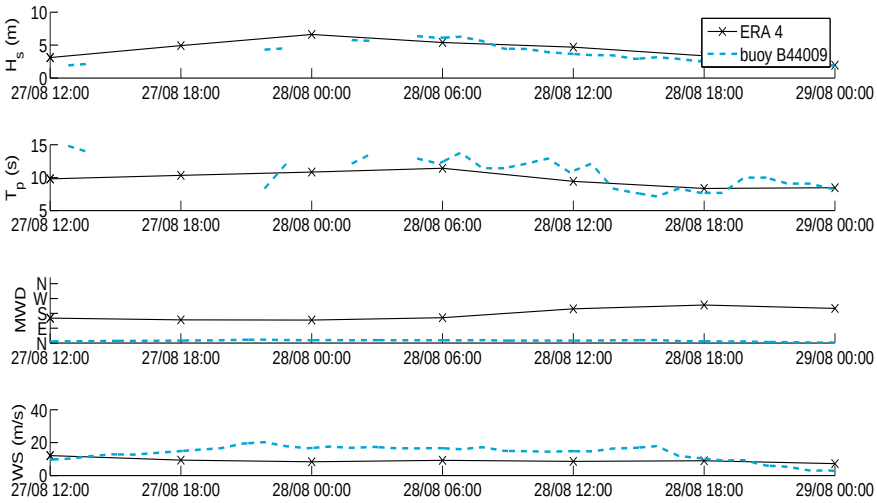

Figure B.2.34: Wave height, wave peak period, mean wave direction and wind speed from top to bottom for both buoy B44009 and ERA-I point 4 (see Figure B.2.30).

B.2.3. Comparison

The buoy records are compared with the ERA-I data. This is only done for a 38 hour interval, which is specified for the location of the respective buoy. Subsequently the values are averaged, resulting in representative scale factors for the parameters j. If the ERA-I data overestimates the buoy data, no scale factor is calculated (Table B.1).

Table B.1: Result of scaling factor analysis (Eq. B.1) for hurricane Ike and Irene, Figures B.2.24 and B.2.30 respectively. First digit represents ERA-I number and last two digits are last buoy numbers.

	Ike					Irene				
	1-35	2-19	3-20	4-02	5-01	1-10	2-01	3-13	4-09	Average
S_{H_s} (-)	1.3	1.1	1.6	-	1.2	1.2	1.2	1.3	1.1	1.3
S_{T_p} (-)	1.4	1.1	1.3	1.4	1.3	1.3	1.2	1.3	1.1	1.3
S_{MWD} (-)	4.7	1.2	2.1	7.4	12.9	8.7	5.6	1.8	6.1	5.6
S_{WS} (-)	1.5	1.4	-	1.3	2.8	1.7	1.7	1.5	1.7	1.7

From the above conducted analysis and the obtained results, the following is observed:

- On average there consist an underestimation of ERA-Interim's wave height, although also overestimations are observed. The scaled values seem to coincide with Kumar and Naseef (2015). See also Section 2.2.2.
- ERA-I seems to really underestimate the wave periods during a TC.
- The wave directions during a TC is very random due to its rotating character, resulting in inaccurate measurements of wave buoys. This can also be observed in Table B.1. Therefore, the initial MWD of ERA-I is used in the determination of representative wave conditions.
- The wind speeds in a hurricane can reach to 70 m/s. These are considered to be gust winds, but nonetheless the average values from both wave buoys and ERA-I are considerably low. No adjustment for this is made due to a lack proper argumentation.

B.3. Peak-over-threshold

Due to the determination of hazard reduction in this research, representative values for certain storms are required. The probability of occurrence of certain extreme wind and wave conditions are often expressed in terms of return periods (RP). The conditions during a 1/10 yr^{-1} (RP10) are lower than those in a 1/100 yr^{-1} (RP100) year storm. A way to determine the representative wave conditions for a certain RP is a peak-over-threshold (Section 2.2.4). This method is applied using the ORCA toolbox (Section 2.2.4).

1. Determine model area and the respective ERA-I boundary conditions.
2. Conduct peak-over-threshold (POT) method in order to determine wind and wave conditions accompanied to a return period. The ORCA toolbox is used for this step .
3. Find representative surge levels from the surge model of Muis et al. (2016).
4. Run SWAN model using the wave conditions from ERA-I and the found waterlevels to determine nearshore hydrodynamic conditions for RP1, RP10 and RP100.

The sequence of this approach is faster than running models with the complete ERA-I database and subsequently conduct a POT (Section 2.2.3). It however probably goes at the expense of the accuracy, although this missing accuracy is considered to be a fraction of the many assumptions made in this hydrodynamic analysis. The background of the individual procedure steps can be found in Section 2.2 and the result at the vegetation study locations is given in Chapter 5.

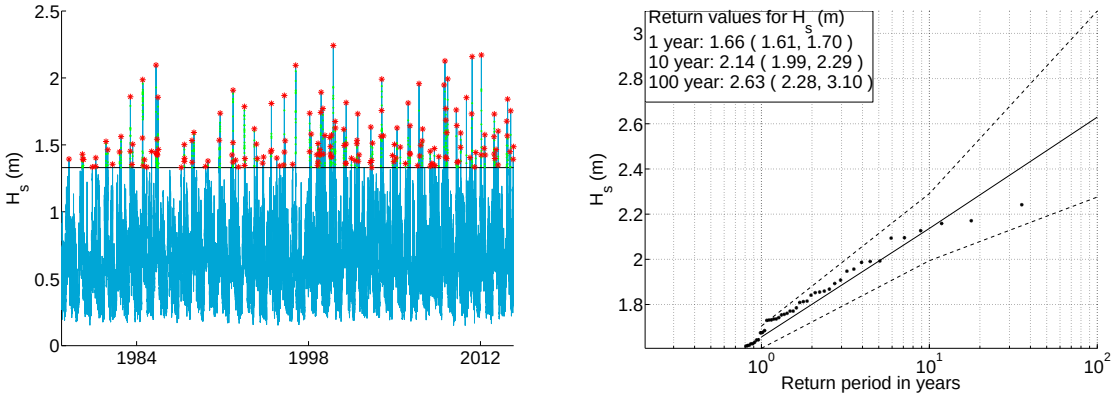

Figure B.3.35: Peak-over-threshold analysis (left) and extreme-value analysis (right) for Andaman Sea ERA-I point 1

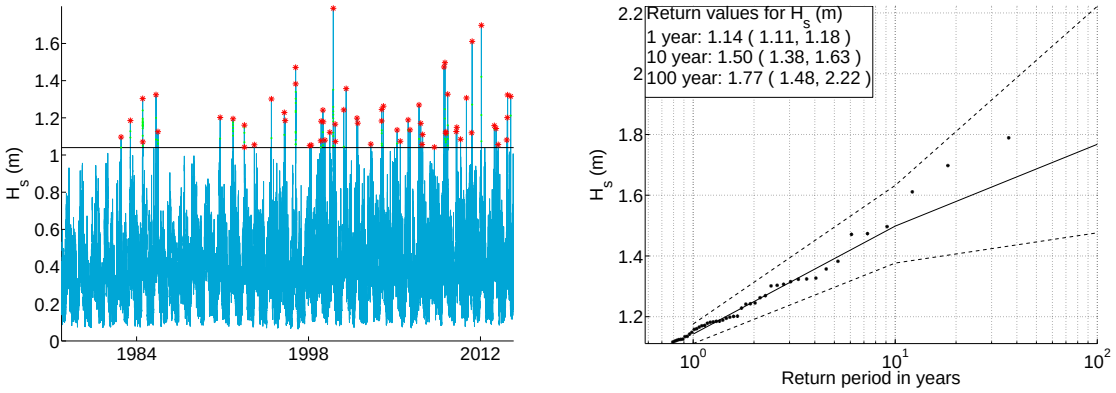

Figure B.3.36: Peak-over-threshold analysis (left) and extreme-value analysis (right) for Andaman Sea ERA-I point 2

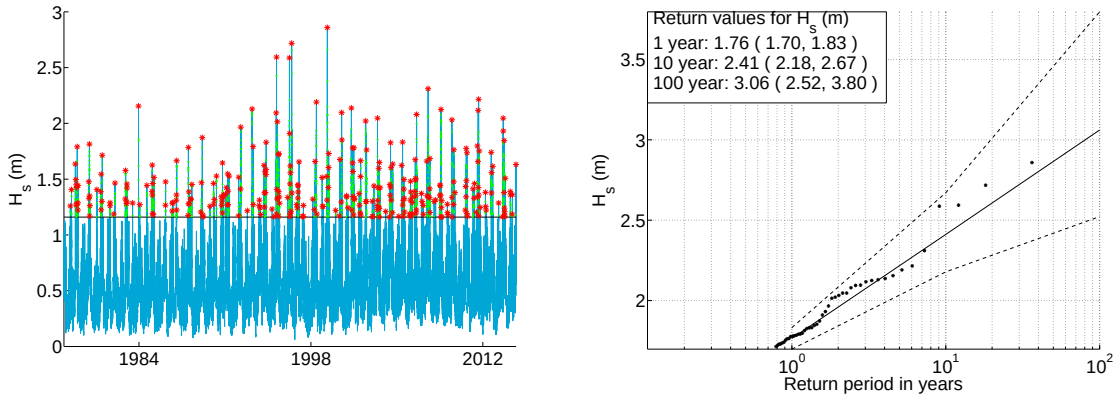

Figure B.3.37: Peak-over-threshold analysis (left) and extreme-value analysis (right) for Singkawang ERA-I point 1

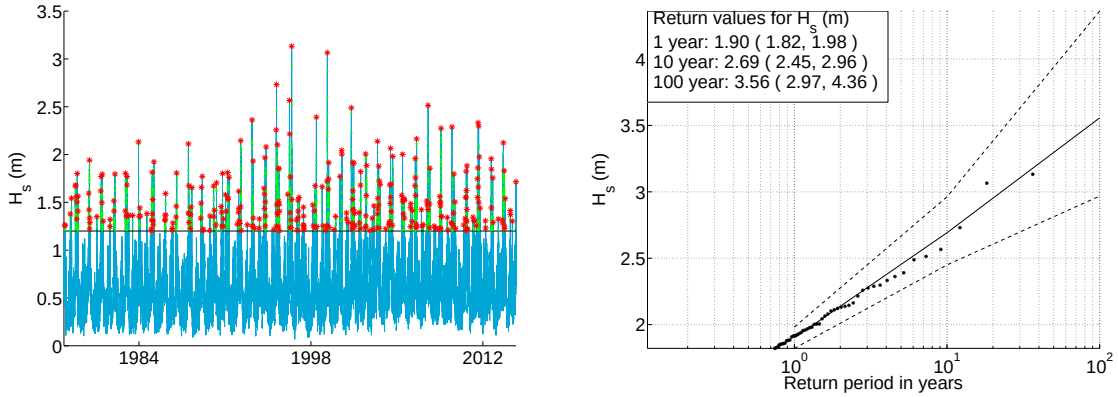

Figure B.3.38: Peak-over-threshold analysis (left) and extreme-value analysis (right) for Singkawang ERA-I point 2

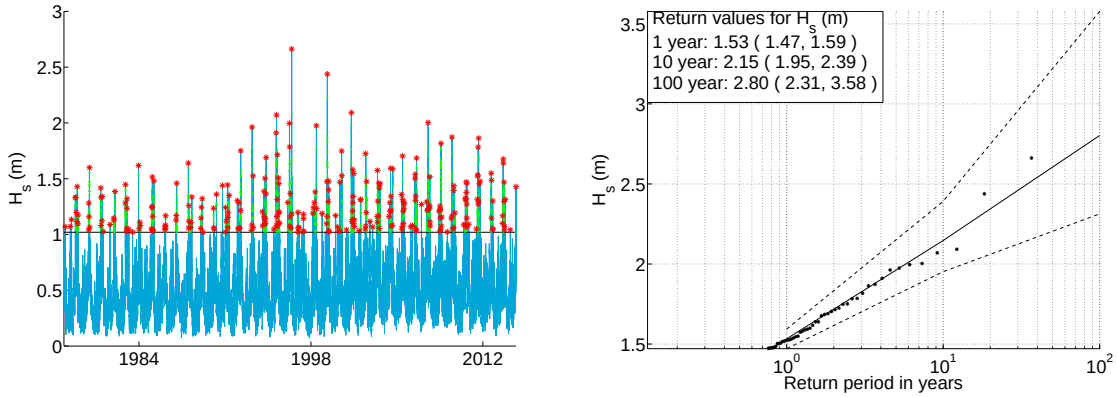

Figure B.3.39: Peak-over-threshold analysis (left) and extreme-value analysis (right) for Singkawang ERA-I point 3

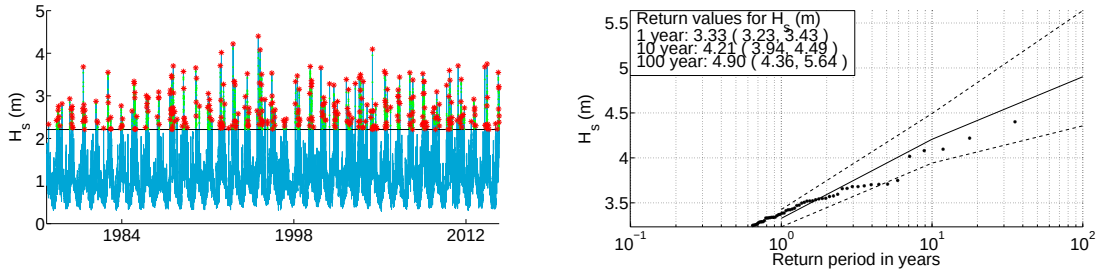

Figure B.3.40: Peak-over-threshold analysis (left) and extreme-value analysis (right) for San Miguel Bay ERA-I point 1

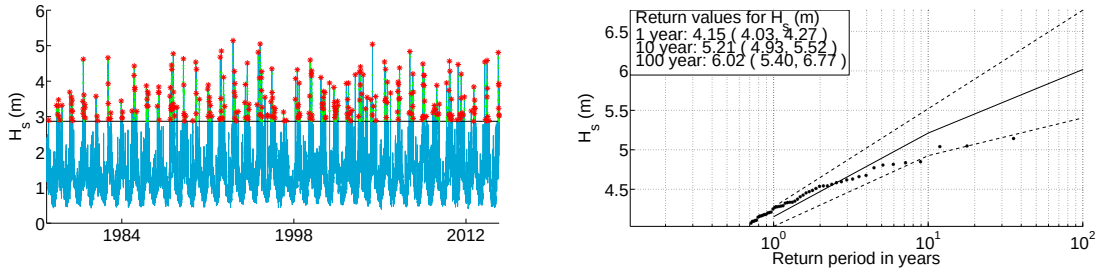

Figure B.3.41: Peak-over-threshold analysis (left) and extreme-value analysis (right) for San Miguel Bay ERA-I point 2

B.4. Ranges

The ranges for the tide and surge height for the mangroves is presented in this section. The used data sets are from AVISO (Satellite Altimetry Data) and the Global Storm Surge Information System (GLOSSIS) respectively. These provide data world wide, but due to the focus on mangroves area, this data is filtered between 25° north and 25° south (Figure B.4.42).

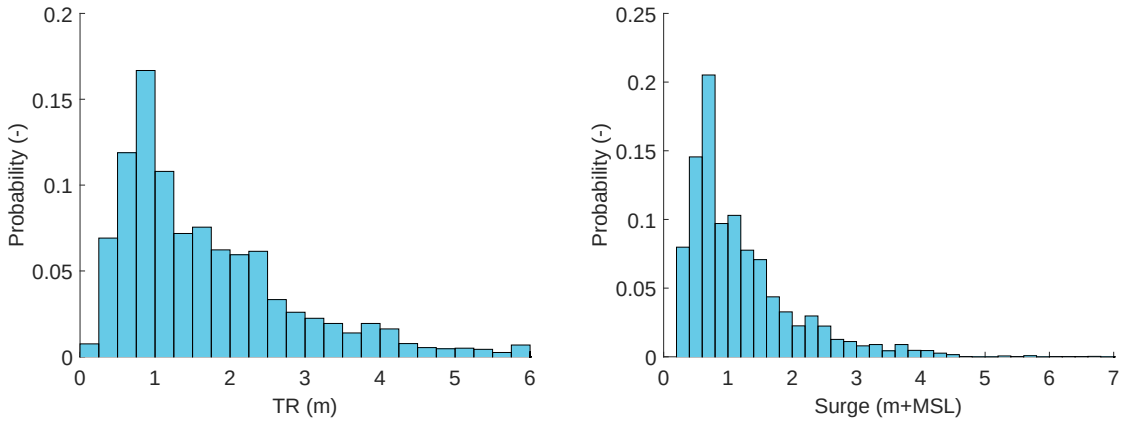

Figure B.4.42: Occurrence of tidal range (left) and surge (right) between 25° north and 25° south

C

XBeach

C.1. Palian

C.1.1. Comparison

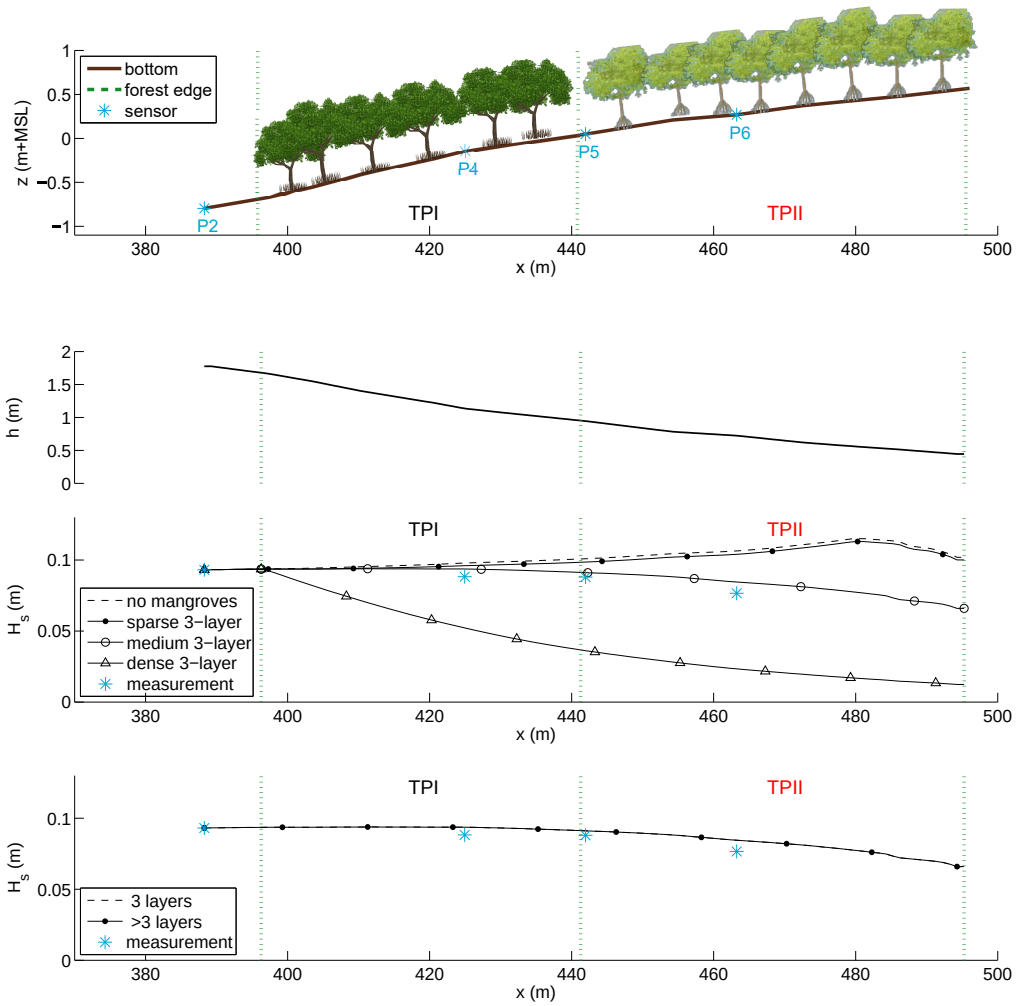

Figure C.1.1: Profile (top), water depth (2nd from top), wave height initial layers (3th from top) and wave height after vertical layering (bottom) over Palian transect.

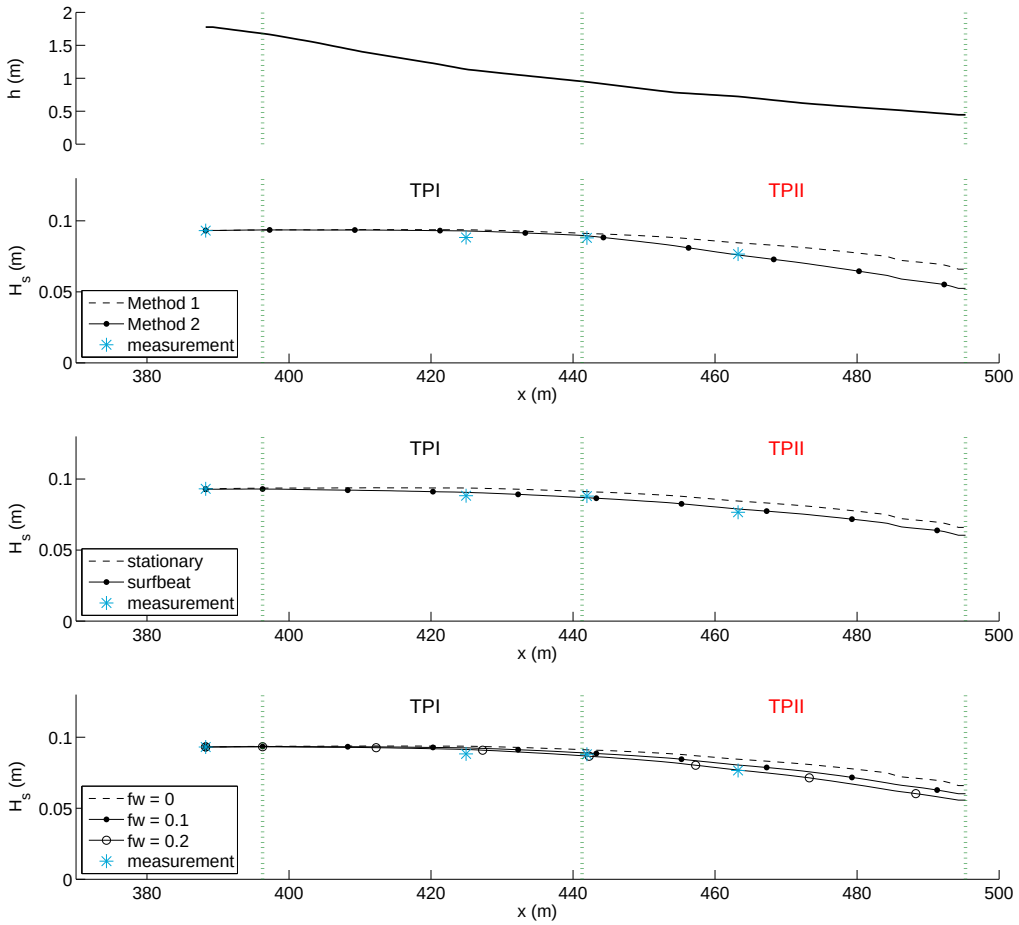

Figure C.1.2: Water depth (top), wave height mangrove methods (2nd from top), wave height XBeach mode (3th from top) and wave height with different friction coefficients (bottom) over Palian transect.

C.1.2. Greenbelt policy

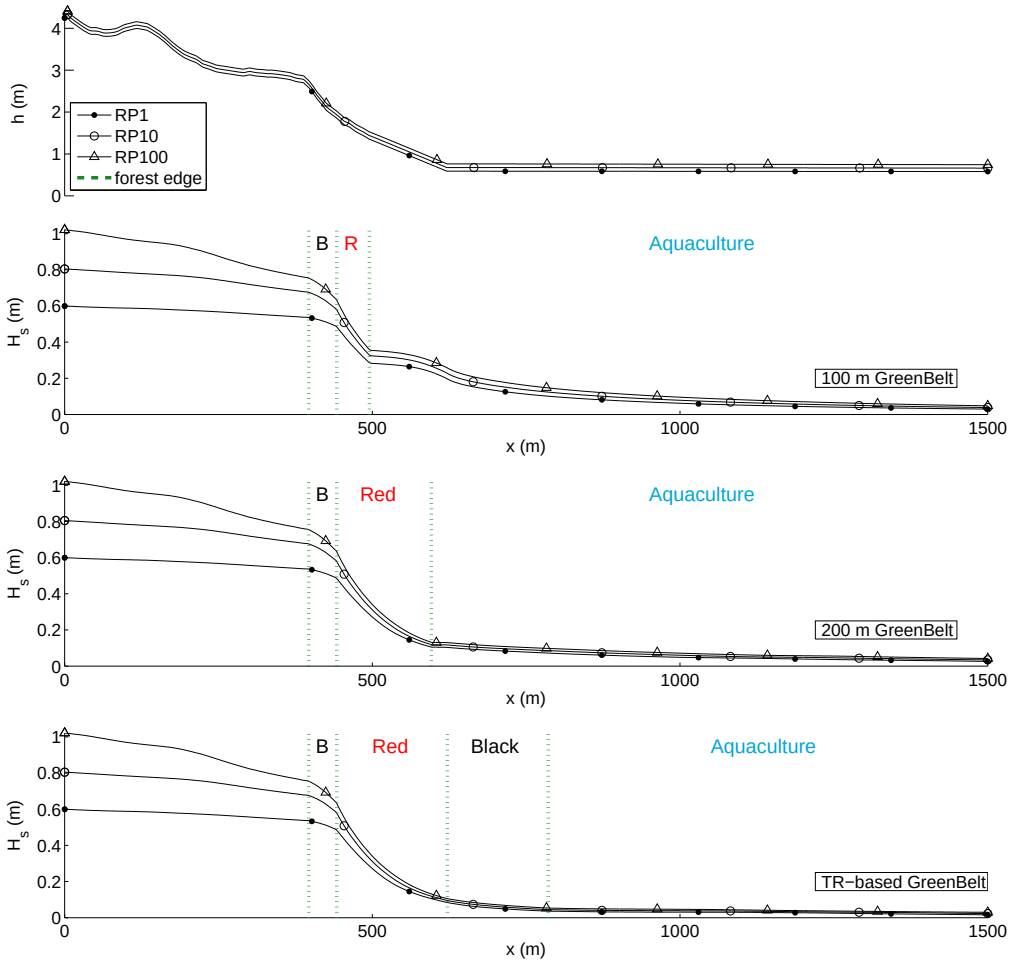

Figure C.1.3: Water depth (upper) and wave height (lower) over the Palian transect for different return periods and greenbelt policies

C.2. Hazard runs

Table C.1: Percentages increased wave height (%) as a result of 20% mangrove deforestation (=D) and erosion (=E) for different parameters and forest types

i_b (-)	1:250								1:500							
TR (m)	1.5				2.5				1.5				2.5			
Δh (m)	1		1.5		1		1.5		1		1.5		1		1.5	
H_0 (m)	0.5	1	0.5	1	0.5	1	0.5	1	0.5	1	0.5	1	0.5	1	0.5	1
D, FT1	16	21	16	22	17	24	18	25	14	20	14	19	15	21	16	22
D, FT2	38	48	32	44	43	58	39	55	28	44	35	46	36	58	39	55
E, FT1	13	14	13	16	11	15	10	14	13	16	13	16	12	16	11	16
E, FT2	3	2	2	2	2	2	2	2	5	3	4	4	4	4	3	4